INVESTIGATION OF THE ROTOR SPEED IMPACT ON THE EFFICIENCY OF ROTARY HEAT RECOVERY VENTILATION DEVICES

A Thesis Submitted to
the Graduate School of Engineering and Sciences of
Izmir Institute of Technology
in Partial Fulfillment of the Requirements for the Degree of

MASTER OF SCIENCE

in Energy Engineering

by
Mustafa DİLŞEN

July, 2018
İZMİR

We approve the thesis of **Mustafa DİLŞEN**

Examining Committee Members:

Dr. Kasım TOPRAK
Department of Mechanical Engineering, Izmir Institute of Technology

Prof. Dr. Macit TOKSOY
Eneko Havalandırma A.Ş.

Prof. Dr. Tahsin BAŞARAN
Department of Architecture, Izmir Institute of Technology

Assoc. Prof. Dr. Orhan EKREN
Solar Energy Institute, Ege University

Dr. Ziya Haktan KARADENİZ
Department of Mechanical Engineering, Izmir Katip Celebi University

09 July 2018

Dr. Kasım TOPRAK
Supervisor, Department of Mechanical Engineering, Izmir Institute of Technology

Prof. Dr. Macit TOKSOY
Co-Supervisor,
Eneko Havalandırma A.Ş.

Prof. Dr. Gülden GÖKÇEN
Head of the Department of Energy System Engineering, Izmir Institute of Technology

Prof. Dr. Aysun SOFUOĞLU
Dean of the Graduate School of Engineering and Science

ACKNOWLEDGEMENTS

I first would like to thank my thesis supervisor Assistant Dr. Kasım TOPRAK of the Department of Mechanical Engineering at Izmir Institute of Technology and co-supervisor Professor Dr. Macit TOKSOY of Eneko Havalandırma. The doors to Prof. TOKSOY and Dr. TOPRAK office were always open whenever I ran into a trouble spot or had a question about my research or writing.

I would also like to acknowledge Prof. Tahsin BAŞARAN of the Department of Architecture at Izmir Institute of Technology, Assoc. Prof. Dr. Orhan EKREN of the Solar Energy Institute at Ege University, Dr. Ziya Haktan KARADENİZ of the Department of Mechanical Engineering at Izmir Katip Celebi University who were the examining committee members of this thesis, for their valuable comments, recommendations and infinite support. I would also like to thank Serap OZANSOY and Sinan AKTAKKA as the second readers of this thesis, and I am gratefully indebted to them for their very important comments on this thesis.

Finally, I must express my very profound gratitude to my parents and to my friends; Ahmet Gökçer BEKLERGÜL, Göknil AĞAR, Huriye OĞUZ, Ramazan YAYLA, Aslı BULUKLU and Mehmet Doğukan KOCABAŞI for providing me with unfailing support and continuous encouragement throughout my years of study and through the process of researching and writing this thesis. I would also like to thank the company of ENEKO HAVALANDIRMA A.Ş. for reserving the Eneko EnergyLab® to the experiments of this thesis and granting a ventilation device for the study.

This accomplishment would not have been possible without them. Thank you.

ABSTRACT

INVESTIGATION OF THE ROTOR SPEED IMPACT ON THE EFFICIENCY OF ROTARY HEAT RECOVERY VENTILATION DEVICES

In this study, the thermal efficiency of the rotary (regenerative) heat exchanger has been experimentally investigated in a heat recovery mechanical ventilation device. Beside impact of the same variable on pressure drop of the heat exchanger has been researched. Experiments have been carried out in a laboratory which belongs to a company manufactures heat recovery ventilation devices. The rotor has been tested within a commercial ventilation device rather than being tested alone in order to realize the actual conditions.

Test results have also been compared with mathematical model results calculated with respect to the equations according to the literature research. NTU (number of transfer units) method has been used to calculate the thermal efficiency by using the various relevant equations which had been previously proposed by various researchers. The efficiency equation, which had a good agreement with the experimental results, has been determined by evaluating this comparison as a conclusion.

Keywords and Phrases: heat transfer, heat recovery, energy recovery, ventilation, mechanical ventilation, regenerative heat exchanger, rotary heat exchanger (rotary wheel), thermal efficiency, thermal effectiveness, pressure drop

ÖZET

ROTORLU (ISI TEKERLEKLİ) ISI GERİ KAZANIMLI HAVALANDIRMA CİHAZLARINDA ROTOR DEVİR SAYISININ CİHAZ VERİMİNE ETKİSİNİN BELİRLENMESİ

Bu çalışmada, rotorlu ısı geri kazanımlı mekanik havalandırma cihazlarında verimlilik araştırılmıştır. Rotorlu ısı değiştiricisinin hızının (devir sayısının), rotorun sıcaklık verimine etkisi deneysel olarak araştırılmıştır. Ayrıca aynı parametrenin, ısı değiştiricisinin kendi basınç düşümüne etkisi olup olmadığı da araştırılmıştır. Deneyler, ısı geri kazanımlı havalandırma cihazı üretimi yapan bir firmanın cihazlarının performans testlerinin gerçekleştirildiği laboratuvarda yapılmıştır. Rotor tek başına test edilmemiş olup, ticari tip bir havalandırma cihazının içerisinde gerçeğe en yakın haliyle test edilmiştir.

Yapılan deneyler sonucunda elde edilen test sonuçları aynı zamanda literatür araştırmalarından elde edilen matematiksel modelleri ile de kontrol edilmiş ve kıyaslanmıştır. Hesaplamalarda NTU metodu kullanılmış ve daha önce yapılan benzer çalışmalarda önerilen farklı denklemler kullanılmıştır. Bu zamana kadar önerilen eşanjör verimi denklemlerinin sonuçları ile test sonuçları karşılaştırılmış ve sonrasında bu tez için en yakın sonuçları veren denklem belirlenmiştir.

Anahtar Kelimeler ve Deyimler: ısı transferi, ısı geri kazanımı, enerji geri kazanımı, havalandırma, mekanik havalandırma, ısı değiştirici (eşanjör), rejeneratif ısı değiştirici, rotorlu tip ısı değiştirici (ısı tekerleği), sıcaklık verimi, basınç düşümü

TABLE OF CONTENTS

LIST OF TABLES viii

LIST OF FIGURES ix

LIST OF SYMBOLS xii

CHAPTER 1. INTRODUCTION 1

1.1. Indoor Air Quality (IAQ) 3

1.2. Heat and Energy Recovery Ventilation 5

1.3. Air-to-Air Heat Recovery Methods 6

1.3.1. Plate Type Heat Exchangers (Recuperative Heat Recovery) 7

1.3.2. Rotary Heat Exchangers (Regenerative Heat Recovery) 8

1.3.3. Heat Recovery with Run-Around Coils 10

1.3.4. Heat Recovery with Heat Pipe 11

1.3.5. Heat Recovery with Heat Pump Systems 12

CHAPTER 2. LITERATURE SURVEY 13

CHAPTER 3. EXPERIMENTAL APPROACH 19

3.1. Description of the Test Unit 20

3.2. Description of Experiment Rig (Laboratory) 23

3.3. Measurement System 25

3.4. The Rotary Heat Exchanger 29

3.5. Experiment Parameters 32

CHAPTER 4. MATHEMATICAL MODEL 34

4.1. Dimensionless Parameters 34

4.2. Calculation of Pressure Drop 38

4.3. Calculation of Thermal Effectiveness 40

4.3.1. Calculation of NTU and $\boldsymbol{\varepsilon_o}$ 40

4.3.2. Calculation of Thermal Effectiveness of the Exchanger 44
4.4. Computer Codes 46

CHAPTER 5. RESULTS 48
5.1. Experimental Results 48
5.1.1. Rotational Speed vs. Pressure Drop 48
5.1.2. Rotational Speed vs. Thermal Efficiency 50
5.2. Mathematical Model Results 56

CHAPTER 6. CONCLUSION 64

CHAPTER 7. RECOMMENDATIONS FOR FUTURE WORK 66

CHAPTER 8. REFERENCES 68

APPENDICES
APPENDIX A. MATLAB CODES FOR THE MATHEMATICAL MODEL OF PRESSURE DROP CALCULATION
APPENDIX B. MATLAB CODES FOR THE MATHEMATICAL MODEL OF THERMAL EFFECTIVENESS CALCULATIONS
APPENDIX C. CALCULATION EXAMPLE OF THERMAL EFFECTIVENESS WITH RESPECT TO THE SEQUENCE ON MATLAB FOR ONE MEASUREMENT POINT
APPENDIX D. CALCULATION EXAMPLE OF PRESSURE DROP WITH RESPECT TO THE SEQUENCE ON MATLAB FOR ONE MEASUREMENT POINT

LIST OF TABLES

Table **Page**

Table 3.1. Physical and Thermodynamic Properties of the Exchanger 30

Table 3.2. List of the Experimental Measurement Points..... 32

Table 5.1. Volumetric Airflow Rates of Experimental Test Points for each Rotational Speed Given in Table 3.1 50

LIST OF FIGURES

Figure **Page**

Figure 1.1. Expected CO_2 Effects on Human Health 1
Figure 1.2. A Simple Scheme of a Heat Recovery Ventilation Unit 3
Figure 1.3. Some Elements Affected by Relative Humidity 4
Figure 1.4. Air-to-Air Heat Exchanger Types – Cross-flow, Counter-flow, Rotary Type 7
Figure 1.5. Airflow through the Cross-flow Heat Exchanger Channels..... 8
Figure 1.6. Rotary Heat Exchanger Airflow Directions 8
Figure 1.7. Purge Section on the Rotary Heat Exchanger 9
Figure 1.8. Run-around Coil Circuit..... 11
Figure 1.9. Heat Pipe Coil 11
Figure 1.10. Heat Recovery Ventilation with Heat Pump 12
Figure 3.1. Heat Recovery Ventilation Unit in Eneko EnergyLab® 19
Figure 3.2. Heat Recovery Ventilation Device..... 20
Figure 3.3. Components of the Heat Recovery Ventilation Device 21
Figure 3.4. Electric Motor and Speed Reducer (Gearbox) 22
Figure 3.5. Rotary Heat Exchanger (Rotary Wheel) – Electric Motor Pulley and Belt System 23
Figure 3.6. Eneko EnergyLab® Laboratory 23
Figure 3.7. Experiment Rig in the Laboratory..... 24
Figure 3.8. Conditioning System in Eneko EnergyLab® 25
Figure 3.9. Measurement Points on Experiment Rig..... 26
Figure 3.10. Measurement Duct 26
Figure 3.11. Thermocouple Locations in Measurement Ducts..... 27
Figure 3.12. Venturi Tube..... 28
Figure 3.13. Static Pressure Measurement Points on the Test Device 29
Figure 3.14. Heat Exchanger Matrix 30
Figure 3.15. Heat Exchanger Matrix Dimensions 31
Figure 3.16. Klingenburg Rotor Selection Software 31
Figure 4.1. Dimension Parameters of a Matrix of Rotary Heat Exchanger..... 34

Figure 4.2. Interface of MATLAB Parameter Input 47
Figure 5.1. Static Pressure Drop of Rotary Heat Exchanger with Respect to the Rotational Speed at Different Airflow Rates (Supply Stream) 49
Figure 5.2. Static Pressure Drop of Rotary Heat Exchanger with Respect to the Rotational Speed at Different Airflow Rates (Exhaust Air Stream) 49
Figure 5.3. Thermal Efficiency for 'a' Conditions on Table 5.1 (Outdoor Air Temperature: 0 °C – Return Air Temperature 25 °C) 51
Figure 5.4. Thermal Efficiency for 'b' Conditions on Table 5.1 (Outdoor Air Temperature: 5 °C – Return Air Temperature 25 °C 51
Figure 5.5. Thermal Efficiency for 'c' Conditions on Table 5.1 (Outdoor Air Temperature: 10 °C – Return Air Temperature 25 °C) 52
Figure 5.6. Thermal Efficiency for 'd' Conditions on Table 5.1 (Outdoor Air Temperature: 15 °C – Return Air Temperature 25 °C) 52
Figure 5.7. Thermal Efficiency for 'e' Conditions on Table 5.1 (Outdoor Air Temperature: 5 °C – Return Air Temperature 20 °C) 53
Figure 5.8. Thermal Efficiency Comparison between Experimental Results and Supplier Software Data for 'a' Conditions on Table 3.2 (Outdoor Air Temperature: 0 °C – Return Air Temperature 25 °C) 54
Figure 5.9. Thermal Efficiencies for all Conditions on Table 5.1 54
Figure 5.10. The Variation Ratio of Cp (a), Pr (b), and Nu (c) Parameters 55
Figure 5.11. Comparison of the Calculated Results with the Experimental Results (Outdoor Air Temperature: 5 °C – Return Air Temperature 25 °C – 1100 m³/h) 57
Figure 5.12. Comparison of the Calculated Results with the Experimental Results (Outdoor Air Temperature: 5 °C – Return Air Temperature 25 °C – 5975 m³/h) 58
Figure 5.13. Comparison of the Calculated Results with the Experimental Results (Outdoor Temperature: 0 °C, Return Air Temperature: 25 °C) 59
Figure 5.14. Comparison of the Calculated Results with the Experimental Results (Outdoor Temperature: 5 °C, Return Air Temperature: 25 °C) 60
Figure 5.15. Comparison of the Calculated Results with the Experimental Results (Outdoor Temperature: 10 °C, Return Air Temperature: 25 °C) 60

Figure 5.16. Comparison of the Calculated Results with the Experimental Results (Outdoor Temperature: 15 °C, Return Air Temperature: 25 °C)..... 61
Figure 5.17. Comparison of the Calculated Results with the Experimental Results (Outdoor Temperature: 5 °C, Return Air Temperature: 20 °C)..... 61
Figure 5.18. Comparison between the Software Output, the Experimental and the Calculated Results..... 62
Figure 5.19. Comparison of Thermal Efficiencies of the Software Output, the Calculated Results and the Experimental Results for Different Rotational Speeds..... 63

LIST OF SYMBOLS

A_c	Cross-section area of a unitary cell of rotary heat exchanger matrix
A_h	Cross-section area of a unitary cell due to the hydraulic diameter
A_r	Face area of rotary heat exchanger
Ar	Total heat transfer area of rotary heat exchanger
C	Heat capacity of air flow
C_{min}	Minimum heat capacity of air flow
C_{max}	Maximum heat capacity of air flow
C^*	Heat capacity ratio of minimum and maximum heat capacities
C_p	Specific heat capacity
C_r	Heat capacity due to rotary speed
C_{r_m}	Heat capacity due to rotary speed for Equation (2.7)
C_r^*	Heat capacity ratio due to rotary speed
d_h	Hydraulic diameter of a unitary cell
d_{max}	Maximum diameter of a circle inscribed in a unitary cell
$d*$	Dimensionless diameter
ΔP_r	Total pressure drop
ΔP_l	Pressure drop related with inlet and outlet of an exchanger
ΔP_{fr}	Frictional and incremental pressure drop
ΔP^*	Dimensionless pressure drop
f	Sine function
h	Convective heat transfer coefficient
H_c	Wave height of a unitary cell of rotary heat exchanger matrix
H_m	Distance between two foils of rotary heat exchanger
K	Additional pressure drop coefficient
K_l	Pressure drop number
L	Length of the rotary heat exchanger
l_{arc}	Arc length of a unitary cell
M	Mass
$\dot{M}$	Mass flow rate

n	Ratio of cross-section area with respect to hydraulic diameter and max diameter of a unitary cell
N	Rotational speed of the rotary heat exchanger
NTU	Number of transfer units
NTU_m	Number of transfer units for Equation (2.7)
NTU_∞	Number of transfer units for Z*⟶ ∞
Nu	Nusselt Number
Nu_∞	Nusselt Number for Z*⟶ ∞
P_c	Periphery of a unitary cell of rotary heat exchanger
Pr	Prandtl Number
Re	Reynolds Number
S_m	Foil thickness of rotary heat exchanger matrix
S	Surface area of a unitary cell of rotary heat exchanger
T	Temperature
u	Air velocity of air with respect to porosity
u_f	Air velocity of air
Q	Heat transfer
v	Kinematic viscosity
V_c	Volume of a unitary cell of rotary heat exchanger
W_c	Wave length of a unitary cell of rotary heat exchanger
$x*$	Dimensionless duct length
$z*$	Dimensionless coordinates

<u>Greek Letters</u>

Δ	Differential
ε_a	Thermal effectiveness of rotary heat exchanger
ε_r	Effectiveness parameter for Equation (2.4)
ε_o	Thermal effectiveness of recuperative heat exchanger
η_t	Thermal efficiency of the ventilation device
λ	Thermal conductivity

ρ	Density
σ	Porosity of exchanger matrix
φ_r	Correction factor of rotational speed
φ_c	Correction factor of purge section
φ	Shape factor
φ_∞	Shape factor (Infinite)
Φ	Heat transfer factor
ϕ	Heat transfer factor

<u>Subscripts and Superscripts</u>

$*$	Dimensionless
i, j	$i = 1$ fresh air stream, $i = 2$ exhaust air stream
	$j = 1$ inlet , $j = 2$ outlet

CHAPTER 1

INTRODUCTION

The need for clean and healthy air for residences, offices and commercial buildings -all important spaces for the human life- is increasing more than ever at this moment; as more and more people inhabitate the higher buildings with the booming industries. Mechanical ventilation systems in buildings became common as a reinforcement to natural ventilation or an alone system because of the developments of building industry, high air-tightness level of well-sealed buildings and automation demands. It can be also considered as more controllable than natural ventilation.

The effects of CO_2 level on human health have been depicted in Figure 1.1 according to Schell and Int-Hout (2001). The recommended limit to minimize health effects is 5000 ppm. A carbon dioxide level in excess of 1000 ppm should be considered an indicator of inadequate makeup air in a building according to ASHRAE (2012).

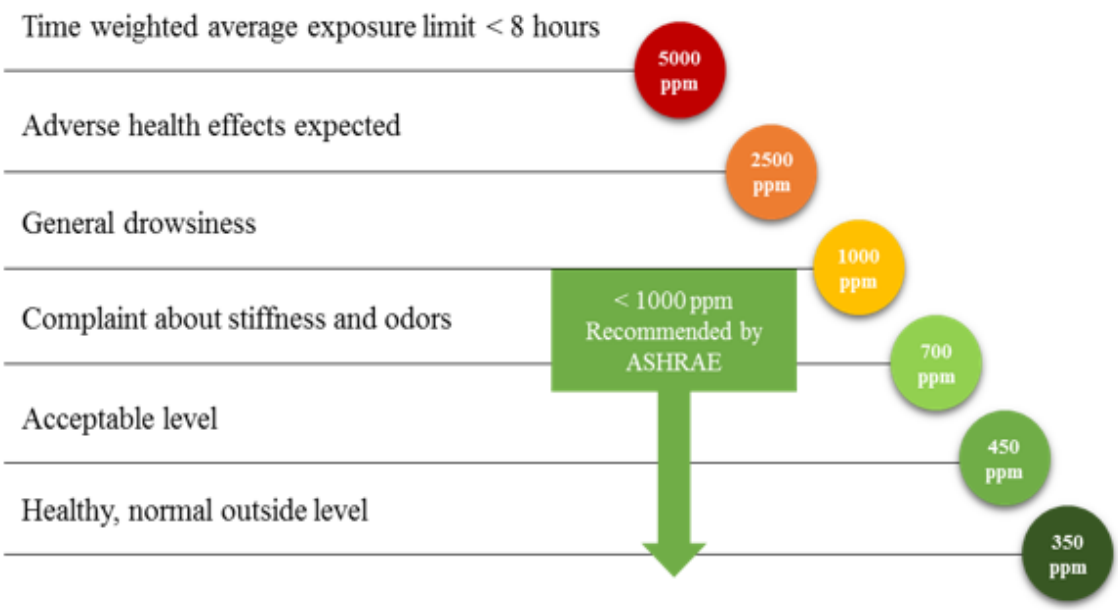

Figure 1.1. Expected CO_2 Effects on Human Health
(Source: Schell and Int-Hout, 2001)

Ventilation can be defined that changing the air in a closed environment, removing polluted air, and controlling the amount of fresh air. It can be performed naturally, mechanically and with combined (hybrid) systems. Natural ventilation can be achieved with the processes include pressure and temperature gradient. These type of ventilation does not require any mechanical components, such as fans. Mechanical ventilation can be performed with the aid of mechanical components, such as fans, blowers, etc. It is also known as forced or induced ventilation system. Hybrid ventilation systems use both natural and mechanical processes. Supply-only ventilations systems create positive pressure inside the building and thus exhaust is naturally done through the air leakage or air outlets. The opposite situation can also be considered. Exhaust air can be evacuated from the space with an exhaust-only ventilation device that creates vacuum in the space. Then supply air naturally provided to the space through the air openings or air leakage.

Some of the main purposes of ventilation are: to maintain the amount of sufficient oxygen in the environment, to limit the carbon dioxide level, to limit the heat build-up due to machinery and humans in an environment, to sustain the temperature and humidity conditions and the comfort level of the air flow rate, to remove dust and toxic gases from the environment, to prevent the multiplication of harmful microorganisms, to reduce the risk of fire and explosion, to prevent the unwanted air currents in the environment.

Electrical energy consumption has started to increase with the industry shifting to mechanical ventilation systems. Ventilation and air conditioning systems with heat or energy recovery have therefore started to become more common. Heat recovery in ventilation devices can be defined that waste heat on the exhausted air is being recovered by using different kind of air-to-air heat exchangers (i.e. cross-flow, counter-flow plate heat exchangers, rotary heat exchangers). In winter, energy on the exhaust air is transferred into the fresh air, and energy on the fresh air is transferred into the exhaust air with these kind of heat recovery systems in summer. By means of the heat recovery ventilation systems, which is also schematically illustrated in Figure 1.2, the energy consumption of cooling and heating systems in ventilation needed spaces can visibly decrease.

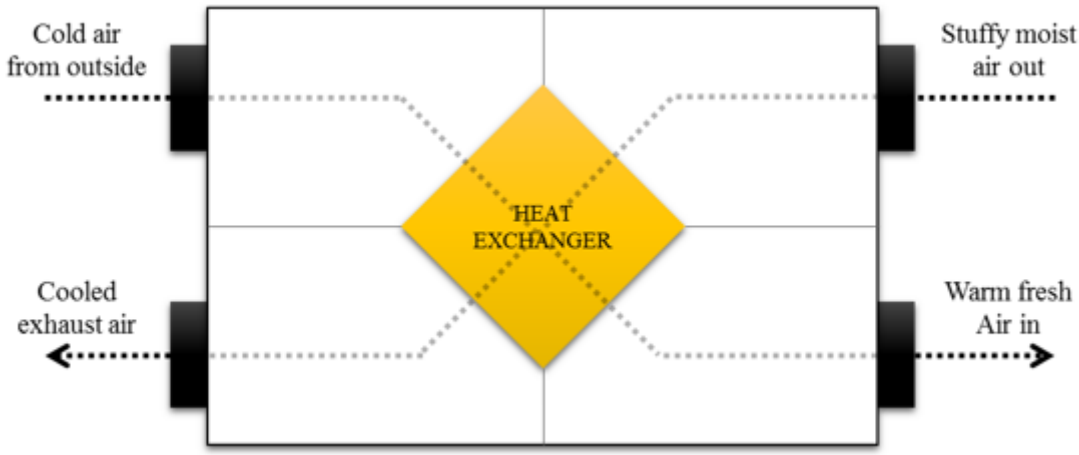

Figure 1.2. A Simple Scheme of a Heat Recovery Ventilation Unit

Rotary heat exchangers known as a type of regenerative heat exchangers are widely used in commercial type heat recovery ventilation devices. The most important uses of rotary heat exchangers are in residential buildings, hotels, shopping malls and airports, workplaces for comfort ventilation; or for industrial ventilation in food, drying or automotive industries.

In this study, the effect of the rotational speed of the rotary heat exchanger in a ventilation system on its thermal efficiency is investigated. The rotor speed effect is experimented for different the air velocities passing through the rotor at different ambient temperatures. Simultaneously, these experimental studies are compared with the mathematical model results according to the literature research.

1.1. Indoor Air Quality (IAQ)

Nowadays, respiratory diseases such as asthma due to the inhalation of polluted air; and excessive health problems such as flushing, watering, headache, dizziness, tiredness, resentment, and drowsiness occur in eyes depending on the exposure to polluted air. There are different factors which demonstrate the Indoor Environmental Quality (IEQ); indoor air quality, thermal comfort, acoustic comfort, vibration, smell and visual comfort. (Toksoy et al., 2015)

Indoor air quality is a concept related to the levels of pollutants in various indoor environments. It may affect human health and the performance of occupants in the spaces.

The lower level of air pollution, the higher air quality will be. Proper ventilation should be used to achieve indoor air quality in spaces. According to EPA (2018), healthy indoor air quality is defined as the air quality within and around buildings and structures. The concept of "green buildings", where indoor air quality is absolutely considered, is therefore becoming more widespread today.

The internal air pollution problems began with the discovery of fire. Because of the smoke as a result of fire, holes were made in the ceilings to remove it from the area. It has been found that the indoor workers of the Egyptian pyramids, who could not get fresh air, felt more disturbed than the outside workers in the same manner. During the Roman period, floor heating was discovered in order to heat without the effects of smoke. In the 16th century in England, measures were taken to reduce the effect of polluted air in the buildings; and smoke and dirty air was exhausted using high ceilings of at least 3 meters as well as the use of high-aspect ratio windows. In the 18th century, investigation of the effects of carbon dioxide on air pollution and human health started with Lavoisier's exploration of carbon dioxide.

In addition to air pollutants, relative humidity is an important factor related indoor air quality. As can be seen from Figure 1.3, the most suitable relative humidity range for human health is 40-60% (Arundel, 1986). Moisture level can lead to some complaints in humans such as the low humidity can cause the nasal mucosa to dry out.

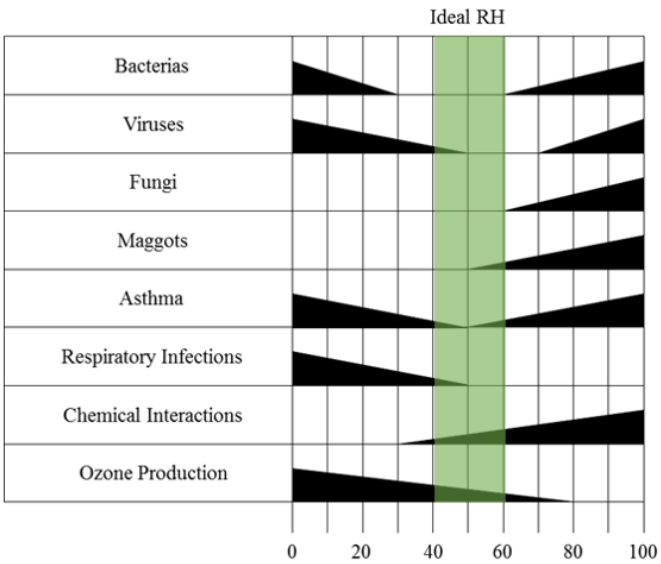

Figure 1.3. Some Elements Affected by Relative Humidity
(Source: Arundel, 1986)

1.2. Heat and Energy Recovery Ventilation

Energy is the ability to do work in the broadest sense. Energy efficiency is defined as the reduction of the share of energy input in production and the lower energy consumption of the same production by the U.S. Department of Energy Office (2004). In the Energy Efficiency Law which has been published in the Official Journal of the Republic of Turkey (2007), it has been also defined as the reduction of energy consumption without decreasing the life standard and service quality in the buildings and the production quality and quantity in industrial enterprise.

There are three different types of heat and energy recovery applications. One is process-to-process heat or energy recovery by which the exhaust air stream temperature can be observed as high as 870 °C. Other heat recovery applications are process-to-comfort and comfort-to-comfort. Process-to-comfort applications are generally observed as a heat recovery system in order to reuse the industrial waste heat sources for residential areas, such as hot water treatment systems. In comfort-to-comfort applications, there is latent and sensible heat transfers from a warmer air stream to a cooler air stream. Thus latent heat transfer can be observed in these kind of applications (ASHRAE, 2012) and additionally, moisture transfer may not be always in the same direction as heat transfer.

In HVAC sector, energy efficiency has become more important with the developments in ventilation and air conditioning. Especially in the US and Europe, the process of deciding on procurement and services of ventilation components have been hampered by the energy efficiency fact with the legal regulations and directives. These studies in Turkey will become inevitable and national policies started being shaped.

Accordingly, ventilation systems are essential for energy efficiency and energy savings. Installation plans, sealing, insulation, low pressure loss, high efficiency ventilation components usage such as electronically commutated (EC) fans which allow users to proportionally arrange fan speed, control strategies, coils and filter cleaning, heat recovery etc. are very important components for energy efficiency in ventilation systems. Installation plans, sealing and insulations must be optimized to decrease pressure loss of the whole system while its heat transfer between the surroundings is minimized. EC fans can be preferred to provide only demanded quantity of air flow to spaces while keeping the energy consumption lower than AC fans. Coil and filter cleanliness has also great

importance on the energy saving issue, thus control systems should be installed to the ventilation systems to detect fouling situations on time.

In terms of ensuring energy saving, the devices that can be controlled proportionally and that adjust the working level for the demand have become important when continuously operated and on/off type devices have been withering away. Demand controlled ventilation can be defined as supplying the right amount of fresh air at the right temperature to the spaces. It can be done by pressure transmitters, humidity sensors, temperature sensors, humidity-temperature sensors, CO_2 sensors, IAQ (Indoor Air Quality) sensors individually or with the combination of some of these control components according to the demands.

Beside above facts, heat recovery has critical part on bidirectional ventilation devices in order to regain the waste heat on the exhaust air stream. An air-to-air heat exchanger is used to provide heat transfer between these two air streams. Depending on the inlet conditions, the heat exchangers efficiency can reach up to 90-95%. By means of the heat recovery, cooling loads in the summer and heating loads in the winter are reduced in all the places where ventilation is required, and a great amount of energy saving is ensured.

1.3. Air-to-Air Heat Recovery Methods

Air-to-air heat recovery devices provide energy savings, clean air and improved climate control by reducing heating and cooling loads. They transfer fresh air that is needed by the environment through a heat exchanger, which can recover heat of the polluted exhaust air taken from inside where the temperature is higher. Common types of air-to-air heat recovery methods can be titled as follows.

- Plate type heat exchangers (Recuperative heat recovery)
- Rotary heat exchangers (Regenerative heat recovery)
- Heat recovery with run-around coils
- Heat recovery with heat pipe
- Heat recovery with heat pump systems (DX Cycle)

Figure 1.4 shows heat exchanger types. The pressure drop of the cross-flow heat exchangers are lower than those of the rotary and counter-flow types while their efficiency is lower than the others.

Figure 1.4. Air-to-Air Heat Exchanger Types – Cross-flow, Counter-flow, Rotary Type

1.3.1. Plate Type Heat Exchangers (Recuperative Heat Recovery)

Plate type heat exchangers have exhaust and supply air streams channels and they are separated from each other completely in a leak-proof manner. Figure 1.5 shows flow directions and transitions between the plates. The distance between the plates can range from 2.5 mm to 12.5 mm (ASHRAE, 2012). Heat is transferred from hot air to cold air by the heat exchanger with its thermal efficiency depending on the speed of the air passing through the exchanger.

According to air flow direction, there are two different types of plate heat exchangers: cross-flow, in which the air flows are perpendicular to each other, and counter-flow, in which the air flows are parallel to each other. In addition to these heat exchangers, they are combined to increase the efficiency and named as the combi type air to air heat exchangers. There is a difference in efficiency and pressure drop between counter-flow and cross-flow exchangers. Since the pressure drop of cross-flow heat exchangers is lower than counter-flow, fan energy consumption is lower. However, the thermal efficiency is higher in counter-flow heat exchangers.

Commonly used plate type heat exchangers are capable of only sensible heat transfer. The plate material is either plastic or aluminum. Cellulosic plates can also be used to perform moisture transfer between the air streams, i.e. recuperative energy recovery.

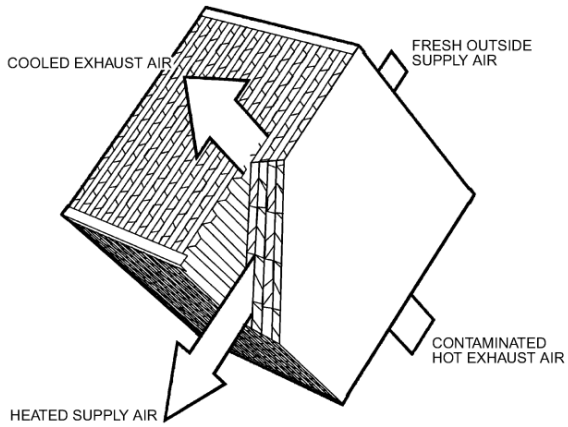

Figure 1.5. Airflow through the Cross-flow Heat Exchanger Channels
(Source: ASHRAE, 2012)

The heat exchangers, which are used in very acidic environments, can be provided with high corrosion resistance properties by using epoxy coating on their heat transfer surfaces.

1.3.2. Rotary Heat Exchangers (Regenerative Heat Recovery)

Rotary heat exchangers or thermal wheels have a rotating cylinder. This cylinder, which is an air permeable matrix, does not allow air flow in the radial direction; allowing air to pass through this matrix via flow passages which are parallel to its axis. It is shown schematically in Figure 1.6. Typical thermal efficiency of these kind of heat exchangers are in the range of 50-85% according to ASHRAE (2012).

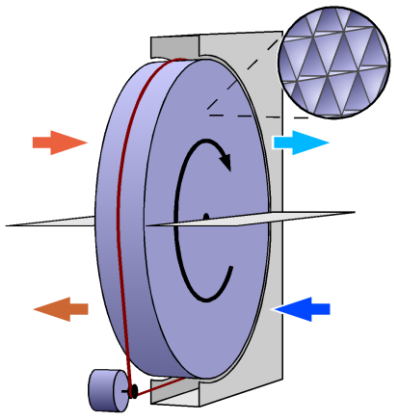

Figure 1.6. Rotary Heat Exchanger Airflow Directions

The rotary heat exchanger is divided into half equal parts. Exhaust stream and supply air stream are individually ducted to this parts. The exchanger then collects the heat of the hot air, and transfers it to the cold air stream depending on its rotation movement. The rotor matrix rotates at a standard rotational speed determined by the supplier with a drive motor with the appropriate torque. Thermal wheels can transfer only sensible heat or both sensible and latent heat at the same time according to their specifications. If the heat exchanger is capable of transferring humidity between the air flows, it's called a "hygroscopic wheel". In addition, ceramic matrix materials can be used in rotor heat recovery exchangers which in heat transfers at elevated temperatures.

There are three types of rotary heat exchangers.

- Condensation rotors: to recover heat or cold from the return air,
- Enthalpy rotors: feature a hygroscopic surface to provide moisture transfer, capable of doing sensible and latent heat transfer,
- Sorption rotors: coated with a strongly hygroscopic zeolite in order to increase heat transfer and moisture in warm and humid regions.

Because of the matrix volume and rotational movement of rotary heat exchanger, a small amount of air can be carried to opposing side. The purge section is used to prevent this situation in supply air stream interest. This kind of leakage is named as carryover leakage. With the purge section shown in Figure 1.7, polluted air inside the matrix is directed back to the exhaust air stream and discharged from the system.

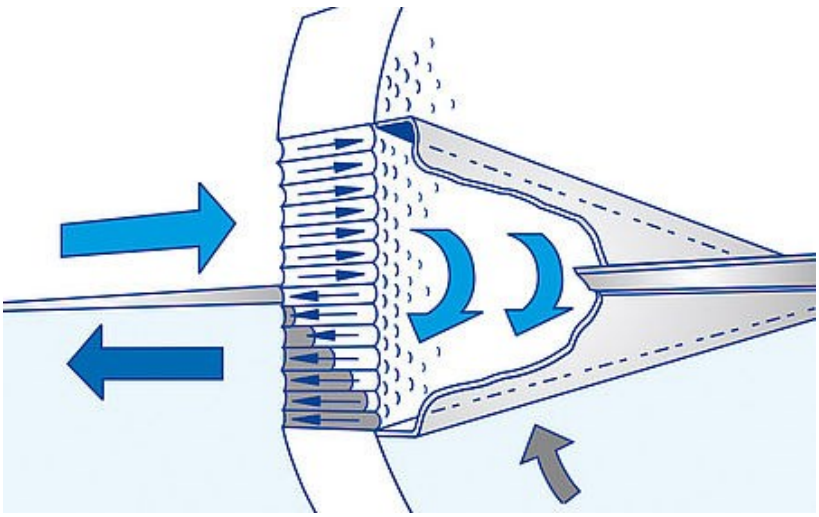

Figure 1.7. Purge Section on the Rotary Heat Exchanger

The matrix of the rotary heat exchangers is usually made of aluminum foils, but this foil can be also coated with silica gel to increase the total heat transfer (sensible + latent heat) loads of the rotors of the hygroscopic type. This will increase the strength of moisture absorption of the matrix and the moisture transfer efficiency increases. Regeneration of the materials such as silica gel is effected automatically when the rotor rotates. Some suppliers are also inhibiting bacterial retention of matrix by using zeolite coatings as silica gel does not have selective adsorption capability. Additionally, epoxy coating to the rotor surface can be done in order to provide high corrosion protection.

1.3.3. Heat Recovery with Run-Around Coils

Run-Around Coils are used to obtain heat transfer between two separate air streams by means of a heat carrier fluid in the coils, either within a device or, if appropriate, through separated air ducts. A fin and tube heat exchangers (coils) placed in the exhaust and supply air streams and a fluid, such as water or water-glycol, are circulated in the coils by a pump. Run-around coils are widely demanded in hygienic ventilation devices which are commonly used for hospitals. One of the most important thing in hygienic ventilation devices is to prevent any air leakage by the exhaust to the supply air stream.

For the most cost-effective operation, on mass-balance between the air streams and without condensation, typical effectiveness values range from 45 to 65%. The highest effectiveness does not necessarily give the greatest net life-cycle cost saving (ASHRAE, 2012).

The basic run-around coil circuit is schematically shown in Figure 1.8. The components are the supply air stream coil, the exhaust air stream coil, the pump, the expansion tank, the 3-way valve and the control elements. In these systems, there is sensible heat transfer and there is not any phase change by the fluid. 3-way valve is used to prevent frosting on exhaust air stream in winter conditions and to maintain the supply air temperature as demanded. Furthermore, expansion tanks are added to the system in order to ensure the expansion and contraction of the heat carrier fluid in healthy way.

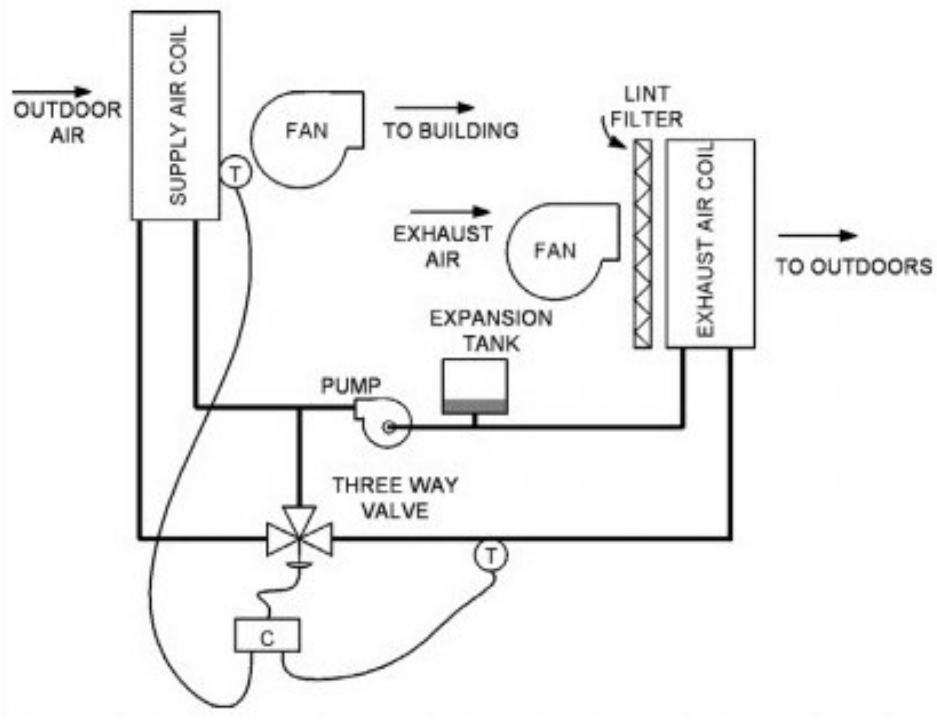

Figure 1.8. Run-around Coil Circuit
(Source: ASHRAE, 2012)

1.3.4. Heat Recovery with Heat Pipe

In heat pipe heat recovery systems, a structure, which is very similar to a fin and tube coil, is used. However, in this kind of coils each tube is independent of one another and tubes are not connected each other. Half of the coil operates as an evaporator and the other half as a condenser. Figure 1.9 shows the example of a heat pipe coil.

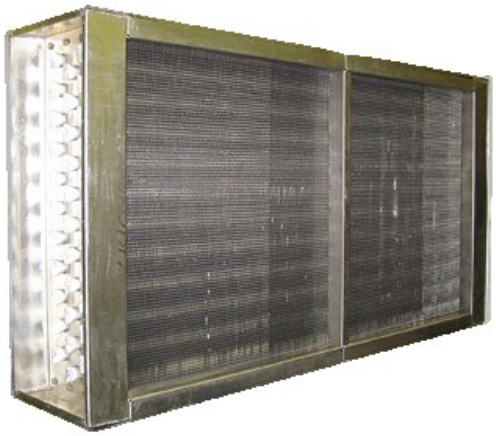

Figure 1.9. Heat Pipe Coil

Special refrigerants are used as heat transfer fluids in heat pipe systems. Hot air passes through the evaporator section of the coil and cold air passes through the condenser section. As the refrigerant warms and evaporates in half of the evaporator, the internal vapor pressure gradient pushes the vapor refrigerant into the condenser and the end of the tube. At the condenser, the liquid refrigerant conceals the latent energy while condensing, thereby heating the low temperature air flow.

Different heat transfer fluids are used in heat pipes according to usage temperature ranges. For example, while refrigerants such as R134a are suitable for heat recovery in ventilation systems, substances such as sodium and potassium can be used in heat pipes for heat transfer between very high temperatures such as 600-1200 °C.

1.3.5. Heat Recovery with Heat Pump Systems

The common use of a heat pump system, which has been shown in Figure 1.10, is as an auxiliary system to a ventilation device with a heat recovery exchanger. The aim is usually to bring the supply air temperature to the ambient temperature, to the comfort conditions or to the desired temperature at desired air flow rates. Transferring the waste heat on exhaust to the supply air with the refrigeration cycle has an appropriate capacity. Furthermore, warm air over evaporator also increases the efficiency of compressors in these kind of systems.

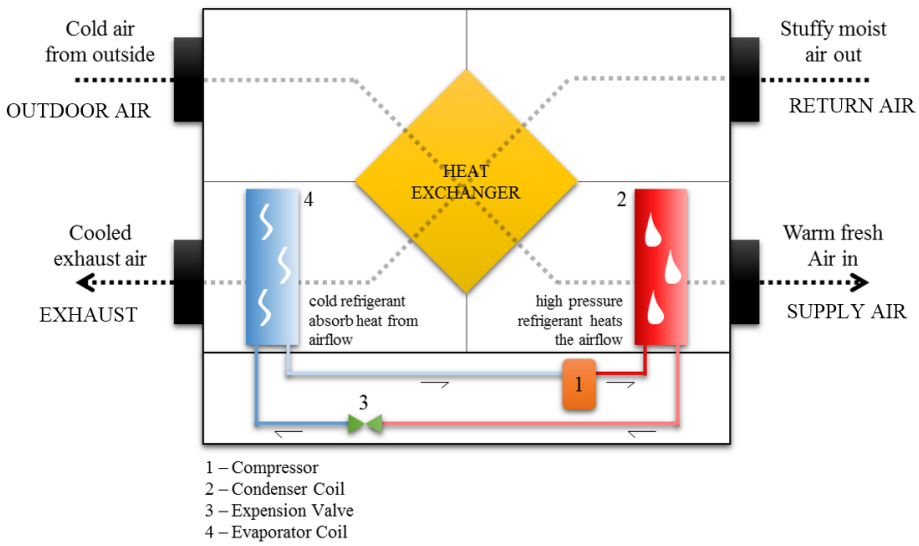

Figure 1.10. Heat Recovery Ventilation with Heat Pump

CHAPTER 2

LITERATURE SURVEY

Coppage and London (1953) proposed the effectiveness calculations with number of transfer units (NTUs) method similar to that employed for recuperative plate type heat exchangers, in which study thermal design method for counter-flow heat exchangers was firstly used, to analyze the rotary heat exchangers for the first time. The advantages of the rotary wheels were also explained and the mathematical difficulties of this analysis are defined in this study. In behalf of that development, the following dimensionless parameters was proposed to be used in the function of rotary heat exchanger efficiency.

$$\varepsilon_a = f\{NTU,\ C^*,\ C_r^*, (UA)^*\} \tag{2.1}$$

The relation between the effectiveness of recuperative plate counter-flow heat exchanger was given by the Equation (2.2a) and (2.2b) with respect to the C^* value. These equations are used to begin the mathematical approach of this study.

$$\varepsilon_o = \frac{1 - e^{[-NTU(1-C^*)]}}{1 - C^* e^{[-NTU(1-C^*)]}} \qquad C^* < 1 \tag{2.2a}$$

$$\varepsilon_o = \frac{NTU}{1 + NTU} \qquad C^* = 1 \tag{2.2b}$$

The first empirically correlated effectiveness of rotary heat exchanger was developed by Lambertsone (1957).

$$\varepsilon_a = \varepsilon_o \left[1 - \frac{1}{9(C_r^*)^2}\right] \tag{2.3}$$

This correlation should be considered as valid for $C_{min}/C_{max} \geq 0.7$ and $C_r/C_{min} \geq 2$.

Razelos (1979) developed a mathematical model which describes the performance of the periodic-flow regenerative heat exchanger. Cyclic periodic operation and the starting-up periods of the regenerator can be determined by this method. Equation (2.4) was also derived and proposed by the researcher in order to get effectiveness values of regenerative heat exchanger.

$$\varepsilon_a = \frac{1 - e^{\left\{e_r\left(C^{*2}-1\right)/[2C^*(1-e_r)]\right\}}}{1 - C^* e^{\left\{e_r\left(C^{*2}-1\right)/[2C^*(1-e_r)]\right\}}} \tag{2.4}$$

where NTU_m, $C^*_{r_m}$ and ε_r parameters can be defined as follows in Equation (2.5), (2.6).and (2.7).

$$NTU_m = \frac{2NTUC^*_r}{1 + C^*_r} \tag{2.5}$$

$$C^*_{r_m} = \frac{2C^*_r C^*}{1 + C^*} \tag{2.6}$$

$$\varepsilon_r = \frac{NTU_m}{1 + NTU_m}\left[1 - \frac{1}{9\left(C^*_{r_m}\right)^{1.93}}\right] \tag{2.7}$$

Kays and London (1984) then studied the relations between rotary heat exchanger speed and its efficiency by considering the heat capacity ratio of rotary heat exchanger (C^*_r) as a function of rotational speed. This ratio is used to develop a simple empirical equation given below for the systems which have thermal efficiency below 90% by modifying the Equation (2.3).

$$\varepsilon_a = \varepsilon_o\left[1 - \frac{1}{9(C^*_r)^{1.93}}\right] \tag{2.8}$$

Worsøe-Schmidt (1988) found an empirical expression which is the relation between the effectiveness of rotary heat exchangers and plate type counter-flow heat exchangers. It was also defined as relevant for NTU range of 0.5 to 5. Equation (2.9) was proposed to obtain effectiveness values of rotary heat exchangers.

$$\varepsilon_a = \varepsilon_o \left\{ 1 - \frac{0.114\left[1 - e^{(-NTU)}\right]}{C^{*0.44} C_r^{*1.93}} \right\} \tag{2.9}$$

Yılmaz and Cihan (1993) developed equations for the heat transfer on a constant wall temperature in developed flow in arbitrary cross section ducts. The comparison between the results of the calculations and theoretically-calculated values are available in literature for circular, rectangular, triangular, elliptical and parallel plate ducts. The following equation is used in this thesis to calculate Nusselt number for thermally developed flow.

$$Nu_d = Nu_\infty + \frac{1.615\Phi/(z^*/\varphi)^{1/3}}{\left[1 + 1.88\left(\frac{z^* Nu_\infty^3}{\varphi \Phi^3}\right) + 3.93\left(\frac{z^* Nu_\infty^3}{\varphi \Phi^3}\right)^{4/3}\right]^{1/2}} \tag{2.10}$$

Candar (1995) studied the dimension optimization of a rotary heat exchanger and produced the related exchanger. Experiments were performed on the rotary heat exchanger in order to obtain its effectiveness with respect to the air velocities due to the air passing through itself. The experimental results were also compared with the calculated data. As a result, a good agreement between the experimental and mathematical results was obtained.

Yılmaz, Büyükalaca and Candar (1996) proposed a mathematical model to calculate pressure drop of the rotary heat exchanger with regar to the airflow rate. In this study, tests were performed also to show whether the rotational speed also affects pressure drop of the exchanger.

TS EN 308 (1997) standard provided information how the experiments of a heat recovery ventilation unit should be performed. The inlet conditions, which should be considered during the thermodynamic tests, were given in this standard with the thermal efficiency equation. The equation is defined as the ratio of the temperature difference between supply air and outdoor air to the temperature difference between indoor air and outdoor air as shown in following equation.

$$\eta_t = \frac{t_{2,2} - t_{2,1}}{t_{1,1} - t_{2,1}} \tag{2.11}$$

Doğruyol (1997) studied the influence of rotational speed within 2 and 7 rpm. Tests were performed to the laboratory-made rotary heat exchanger. That exchanger had been tested in a uni-directional duct system in which supply air outlet was led directly to return air inlet after being conditioned by using a heating coil. According to the comparison between experimental and calculated results, an acceptable agreement was found by researcher. However, Doğruyol suggested that tests for lower rotational speeds than 2 rpm should also be performed.

Büyükalaca, Yılmaz and Atalay (1998) develop a new equation to estimate effectiveness of rotary heat exchanger by using their numerical, mathematical and experimental studies. In that study, it was seen that the previous mathematical model was not appropriate with their experimental and numerical analyses. Hence, they have developed the following empirical correction factor for rotational speed which is shown in Equation (2.12) by using their experimental results.

$$\varphi_r = \frac{0.24C_r^*}{\left[1 + 0.02{C_r^*}^{1.82} + (0.24C_r^*)^3\right]^{1/3}} \tag{2.12}$$

Yılmaz and Yılmaz (1999) studied the optimization of dimensions of rotary heat exchangers. They also proposed an algorithm for the calculations of pressure drop and thermal effectiveness of a rotary heat exchanger by using Equation (2.12). In this study, the proposed algorithm is used to obtain NTU values in order to obtain the thermal effectiveness of recuperative plate counter-flow heat exchanger with the Equation (2.2a) or (2.2b).

Yılmaz, Büyükalaca and Yılmaz (2000) studied a Nusselt number to be used both in developed and developing flows. Equation (2.13) was modified to be directly used for developing flow and Equation (2.14) was found from that research.

$$Nu_o = \frac{0.6774}{f{z^*}^{1/2}Pr^{1/6}} \tag{2.13}$$

$$Nu = (Nu_d^4 + Nu_o^4)^{1/4} \tag{2.14}$$

In that study, they have also given an algorithm for the pressure drop of a rotary heat exchanger calculations.

The thermal efficiency of a rotary heat exchanger was studied by Büyükalaca and Yılmaz (2002). They carried out experiments besides the numerical and the mathematical studies to obtain a relation between the rotational speed of a heat exchanger and its thermal efficiency. They also developed an equation that can be used even for very small rotational speeds according to the results of their numerical study and experiments. Equation (2.15) was proposed for effectiveness calculation.

$$\varepsilon_a = \frac{C_r^*}{\left[1 + 3\left({C_r^*}/{\varepsilon_o}\right)^2 + \left({C_r^*}/{\varepsilon_o}\right)^4\right]^{1/4}} \tag{2.15}$$

Zhang and Niu (2002) studied the performance comparison of desiccant wheels for air dehumidification and enthalpy recovery. Effects of the rotational speed of a rotary heat exchanger, NTUs, and the specific area on its performance were investigated. In that study, it was observed that effectiveness of rotary heat exchanger started to decrease at higher speeds after the critical rotational speed.

De Antonellis et al. (2014) performed experiments in order to obtain thermal effectiveness values of a rotary heat exchanger. Two different units, which provide two air streams separately at accurate controlled conditions of temperature, humidity and volumetric airflow of each. The thermal effectiveness analysis was done by using an enthalpy type rotary heat exchanger within a relative humidity range which provides moisture transfer also.

Guo-Yan (2014) numerically and experimentally studied the heat transfer and the pressure drop of a compact cross-corrugated plate heat exchangers. Fluid dynamics simulations were also performed out to study the performance of recuperators. In that study, an air-to-air plate heat exchanger consisted of plates with corrugated channel geometry. Guo-Yan proposed the following equations in order to calculate the arc length of a unitary cell which is shown in Figure 3.1 in next chapter.

$$l_{arc} = \int_0^{W_c} \sqrt{1 + f'^2(x)}dx \tag{2.16}$$

$$f(x) = \frac{H_c}{2} \sin\left(\frac{2\pi\, x}{W_c}\right) \tag{2.17}$$

Seo, Lee and Kim (2018) investigated the effectiveness correlations of rotary type heat exchangers with their rotational speed. The approximate solutions were done by assuming the physical properties constant and the heat transfer coefficients the same. With that study, the thermal effectiveness correlation was proposed as follows.

$$\varepsilon_a = \varepsilon_o \sqrt{\sum_{n=1,3,5,\ldots}^{\infty} \frac{8}{(2\varepsilon_o/C_r^*)^2 + (n\pi)^2}} \tag{2.18}$$

where n has been accepted as 8.

CHAPTER 3

EXPERIMENTAL APPROACH

The experiments have been carried out by using Eneko EnergyLab®, where the performance tests of the heat recovery ventilation devices of Eneko Havalandırma A.Ş. are performed.

It has been aimed to observe the performance changes of the rotary heat exchanger in a commercial ventilation device due to some important parameters, such as inlet air temperatures, air velocity and rotational speed of the rotary heat exchanger. The laboratory provides to control the internal and external conditions easily in order to simulate the actual working conditions. Figure 3.1 shows the positioning of the heat recovery ventilation device in the laboratory.

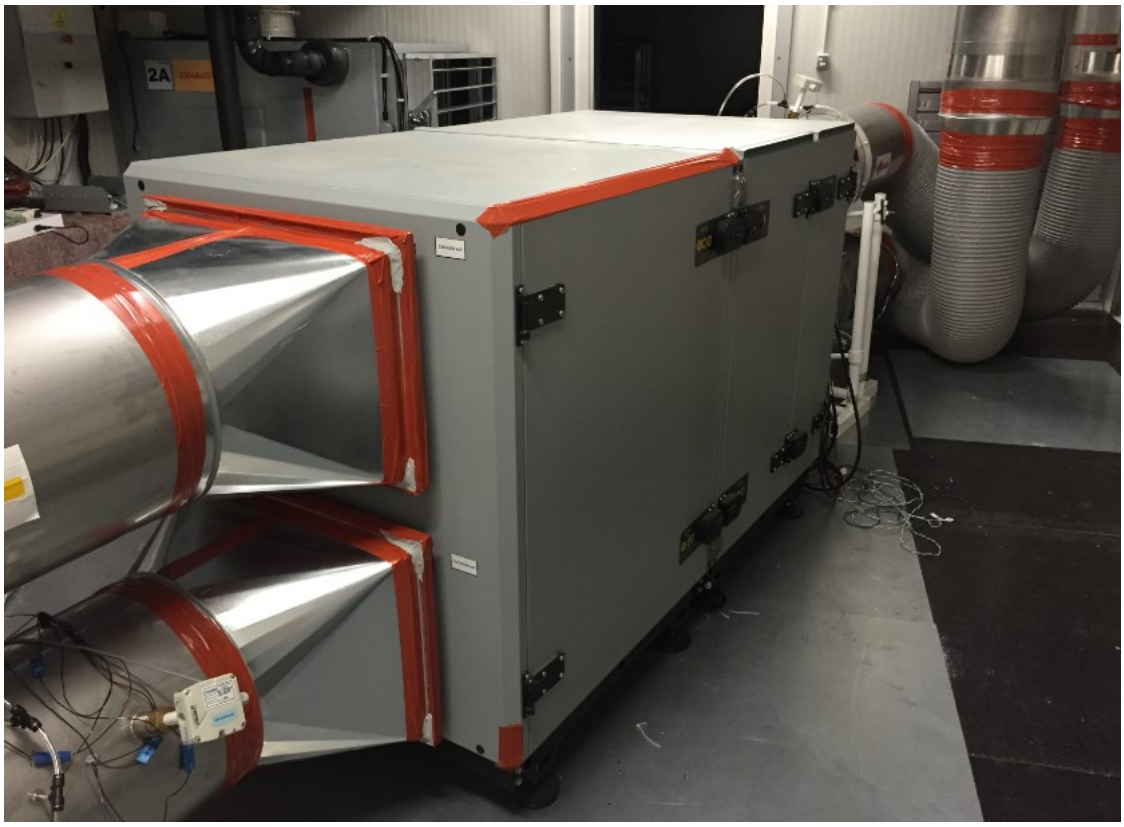

Figure 3.1. Heat Recovery Ventilation Unit in Eneko EnergyLab® (Courtesy of Eneko A.Ş)

The laboratory had been designed for the testing of ventilation devices with airflow capacities up to 10000 m³/h. There are two separate chambers. One of these is used to provide outdoor conditions and the other is used for indoor conditions.

3.1. Description of the Test Unit

As a test device, one of the commercial type heat recovery ventilation devices of Eneko Havalandırma A.Ş. is chosen. Figure 3.2 shows the image of test device. This device is a heat recovery ventilation device which has the maximum airflow of 6000 m³/h and it provides external static pressure up to 320 Pa. External static pressure, which is also known as 'useful static pressure', can be defined as the pressure provided by device fans in order to meet the pressure drop of ventilation channels (and for all external pressure drops, such as dampers) due to the actual air volume flow.

Figure 3.2. Heat Recovery Ventilation Device (Courtesy of Eneko A.Ş)

Since the device is generally used for equal mass flow rates for both air streams, it has the same model radial plug fans on each air stream which provide the same capacities. EC fans have been selected for easy control of fan speeds. All device components, their locations within the device and the name of airflow streams are shown on the device in Figure 3.3.

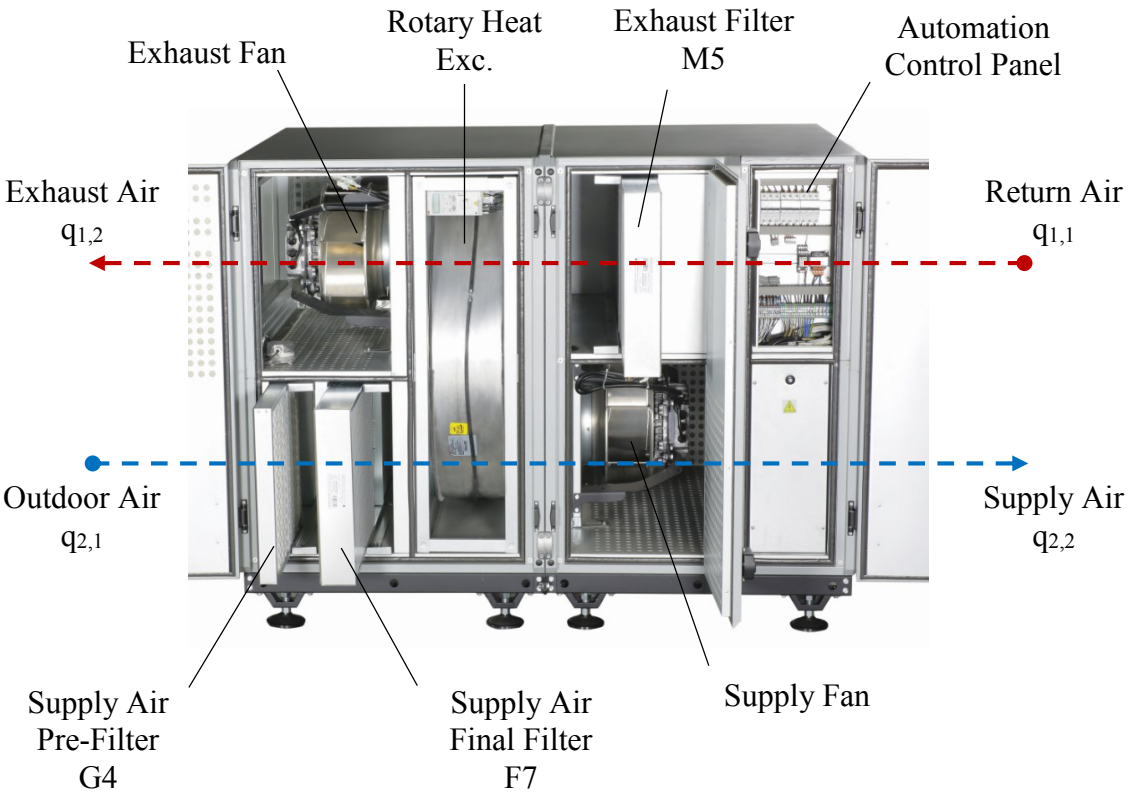

Figure 3.3. Components of the Heat Recovery Ventilation Device (Courtesy of Eneko A.Ş)

The fans are located on the both air stream outlets of the device. There are filters at the suction sides of air streams, just before the heat exchanger, in order to protect the ventilation components such as fans and heat exchanger from dust, particles or larger substances that may come from the suction channels. Beside the protection of ventilation components, another important task is to filter the fresh air which will be obtained from outdoor environment with respect to the indoor air quality aspects due to its specifications.

The airflow directions of the device are shown schematically in Figure 3.3, the suction of supply air stream ($q_{2,1}$ - outdoor air) is made from the outdoor room and the air passing through the exchanger matrix is given to the indoor room ($q_{2,2}$ - supply air). Similarly, the suction of exhaust air stream ($q_{1,1}$ - return air) is taken from the indoor chamber to the outdoor chamber ($q_{2,1}$ – exhaust air) after being passed through the exchanger matrix.

The casing of the test device has been manufactured from 0.8 mm thick sheet metal. The device panels in double-wall construction, which is also known as sandwich

panel, are also insulated with a 70 kg/m³density and 50 mm thick rock wool. For this reason, it is assumed that there is negligible amount of heat transfer between the device and its surroundings for the tests and calculations.

Tests have been carried out on the ventilation device with enthalpy rotor which is able to do latent heat transfer together with sensible heat transfer. However, only the thermal effectiveness, which is about sensitive heat transfer, has been investigated in this study. For the investigation conditions of this study, which have been given in Table 3.2, moisture transfer level can be assumed as negligible.

The specifications of this rotary heat exchanger have been given in Section 3.4. Air leaks between the air streams has been minimized using sweeper sealing around the radial periphery of the rotor and on the mid profile metal of the rotor housing where the two air streams have been separated. In addition, the gaps between the rotor housing and the device have been either sealed or filled with silicone.

The drive motors are supplied as standard with the rotary heat exchangers by their suppliers. However, difficulties have been encountered in reaching to the desired rotational speeds with regard to torque deficit with the standard motor. The gearbox on the drive motor can decrease the rotational speed to 3 rpm, because the torque of the motor is not enough to rotate the rotor at lower speeds. In addition, the maximum speed cannot be exceeded on 12 rpm. Therefore, two separate drive motors and suitable gearboxes have been supplied for low and high speeds and reached revolutions between 0.2 and 30 rpm. The drive motor and gearbox used in the experiments are illustrated in Figure 3.4. Figure 3.5 shows the belt-pulley system that provides the rotational movement to the rotary heat exchanger. A suitable frequency convertor has been used to arrange this speed range for both drive motors.

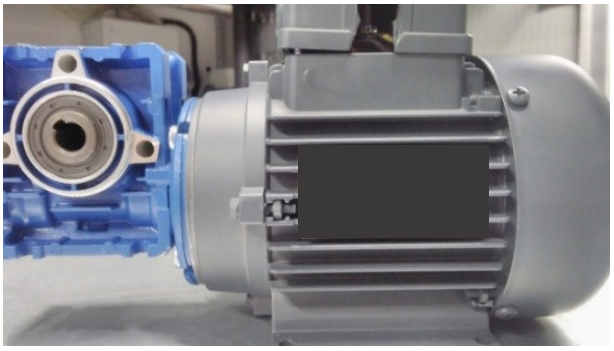

Figure 3.4. Electric Motor and Speed Reducer (Gearbox)

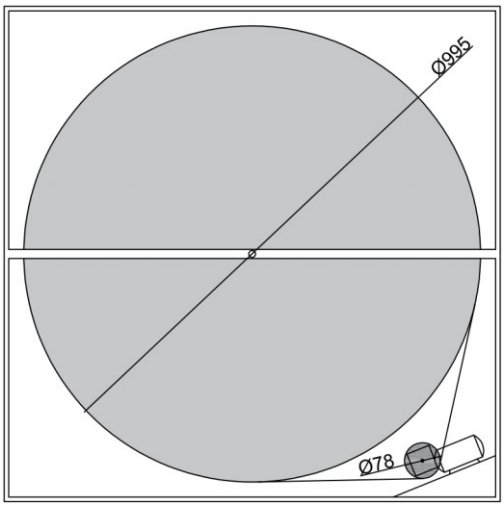

Figure 3.5. Rotary Heat Exchanger (Rotary Wheel) – Electric Motor Pulley and Belt System

3.2. Description of Experiment Rig (Laboratory)

Eneko EnergyLab® (Figure 3.6), designed by the company engineers in 2014, has been established as a state of the art laboratory which has similar specifications with the independent testing laboratories in Europe. The performance tests of the ventilation devices of the company are performed by using this laboratory and the results are shared with the customers on device catalogues as the technical specifications.

Figure 3.6. Eneko EnergyLab® Laboratory (Courtesy of Eneko A.Ş)

Eneko EnergyLab® includes; one laboratory with two chambers, one control room where the internal and external conditions of these chambers are sustained with an automation system, a mechanical installation area with its own cooling system, pumps and accumulation tanks. In order to minimize the heat, transfer between the laboratory and the outside environment, sandwich panels with 20 cm thick foam insulation are used on the inner and outer walls, special doors, ceiling and also floor.

The damper and auxiliary fan boxes shown in Figure 3.7 in the laboratory are designed for the purpose of overcoming the pressure drop on the measurement ducts and the flexible ducts, which are used to connect the device to the duct system of the laboratory, by using the auxiliary fans. The dampers on these boxes can be proportionally opened and closed to obtain desired pressure drop on these air ducts. In substance, auxiliary boxes are used to arrange external static pressure of the ventilation device.

In addition, venturi tubes are used on these ducts, on which the flexible tubes are connected, in order to measure the volumetric air flow through the duct by differential pressure method. A multiplier factor, which is provided by venturi tube supplier, is used to calculate volumetric airflow.

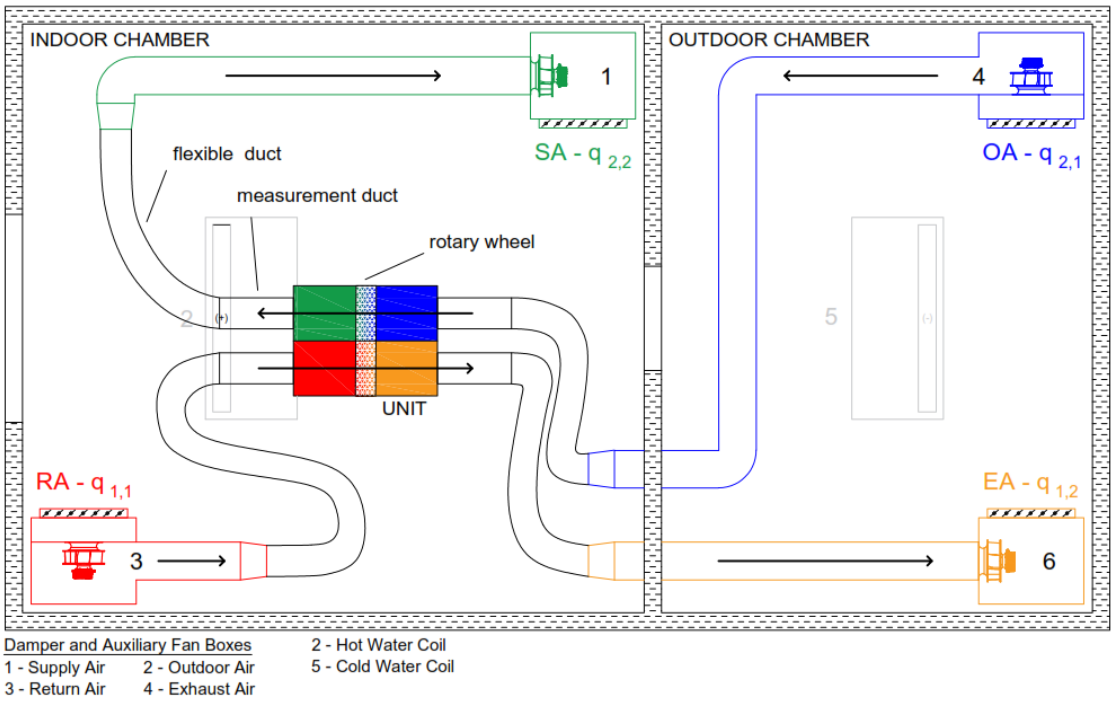

Figure 3.7. Experiment Rig in the Laboratory

The hot and cold water fin and tube coils (see Figure 3.8), which are on each ceiling of the indoor and the outdoor chambers, are used to condition both chambers to desired temperatures by using cold and hot water obtained from the chiller system in the mechanical installation section. This system also meets the need to have a stable temperature for these chambers with the accuracy of ± 0.5 K during the tests.

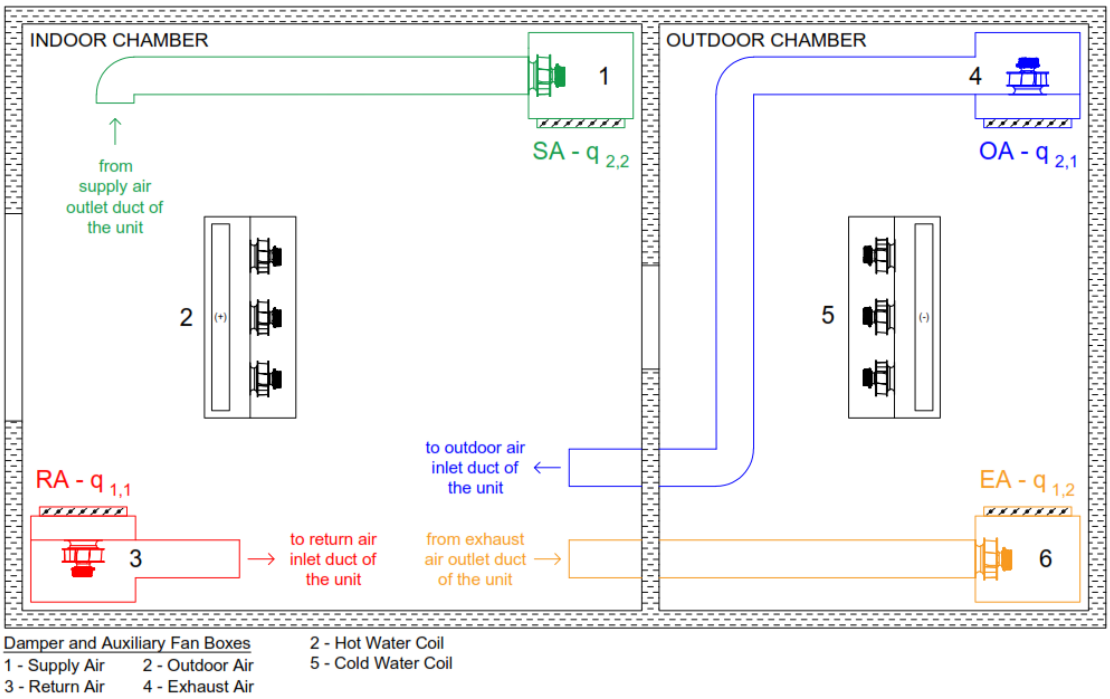

Figure 3.8. Conditioning System in Eneko EnergyLab®

The device is tested according to TS EN 308:1997 standard. Regarding to this standard, the location where the device is installed must be between 17-27 °C. For this reason, the device is located in the indoor chamber where the temperature is maintained within 20-25 °C.

3.3. Measurement System

The dry-bulb temperature, relative humidity, static pressure and volumetric air flow are measured at the inlets and outlets of the ventilation device. Schematically the measurement points are shown in Figure 3.9.

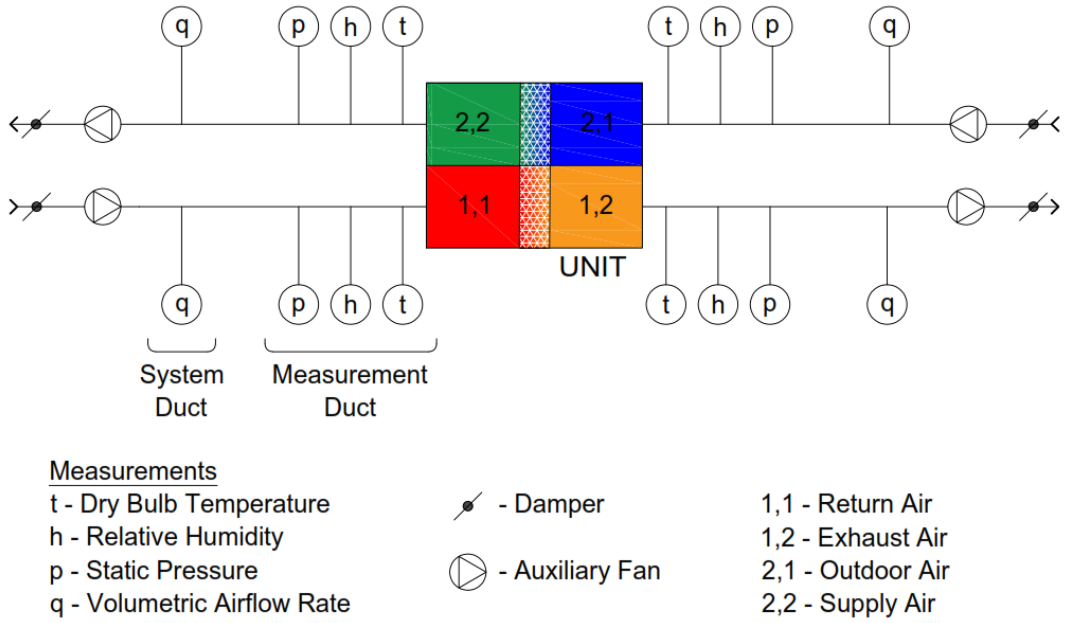

Figure 3.9. Measurement Points on Experiment Rig

One of the measurement ducts is shown in Figure 3.10. For each duct, thermocouples locations are calculated with regard to the channel diameter as suggested in TS EN 308:1997, it can also be seen in Figure 3.11. For each duct there are seven K-type thermocouples on the same cross-section. The average temperature values of these seven thermocouples are taken and the dry-bulb temperature of each channel is obtained.

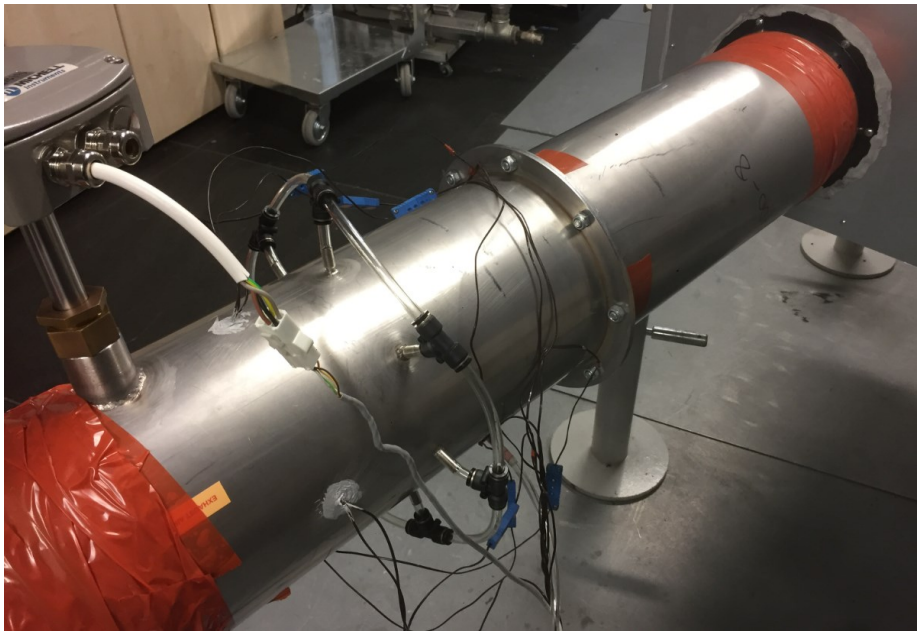

Figure 3.10. Measurement Duct (Courtesy of Eneko A.Ş)

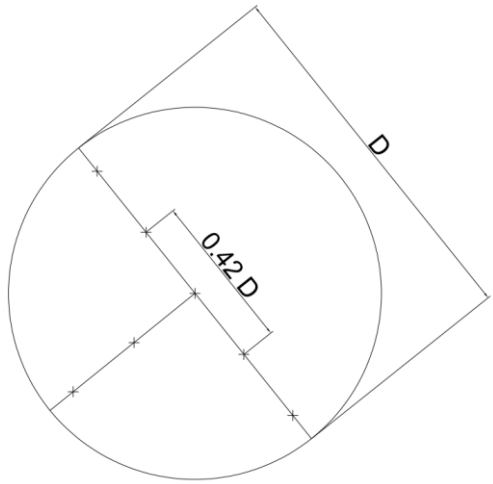

Figure 3.11. Thermocouple Locations in Measurement Ducts (shown with 'x')

By using the measured temperatures, the thermal efficiency of the rotary heat exchanger and equally the device is calculated by the Equation (3.1). According to the related standard the formula is stated only as the temperature difference ratio when the tests are considered to be performed on balanced mass flow rates when the specific heat capacity assumed same for each air stream (TS EN 308:1997).

$$\eta_t = \frac{m_2 C_{p,2}\left(t_{2,2} - t_{2,1}\right)}{m_1 C_{p,1}\left(t_{1,1} - t_{2,1}\right)} \xrightarrow{m_1 C_{p,1} = m_2 C_{p,2}} \eta_t = \frac{t_{2,2} - t_{2,1}}{t_{1,1} - t_{2,1}} \tag{3.1}$$

On each measurement duct, channel type sensors measuring relative humidity between 0-100% are used. The accuracy of the sensors is ± 0.4%. Relative humidity measurement has also an importance in this study to minimize the condensation on the rotary heat exchanger.

In order to calculate the external static pressure of the device, static pressure measurement is performed on each blowing and suction measurement channel. It is equal to the difference between the static pressures at each inlet and outlet streams. Measurement point of each channel include six measuring holes at the same perimeter. These holes are connected to the one common tube in order to be averaged and this tube is directed to a micromanometer with the accuracy of ± 0.25% for static pressure measurement.

By means of the pressure difference measured in these tubes, the airflow of the air is calculated on the basis of the relationship between the fluid velocity and the differential pressure. One of the venturi tubes is shown in Figure 3.12.

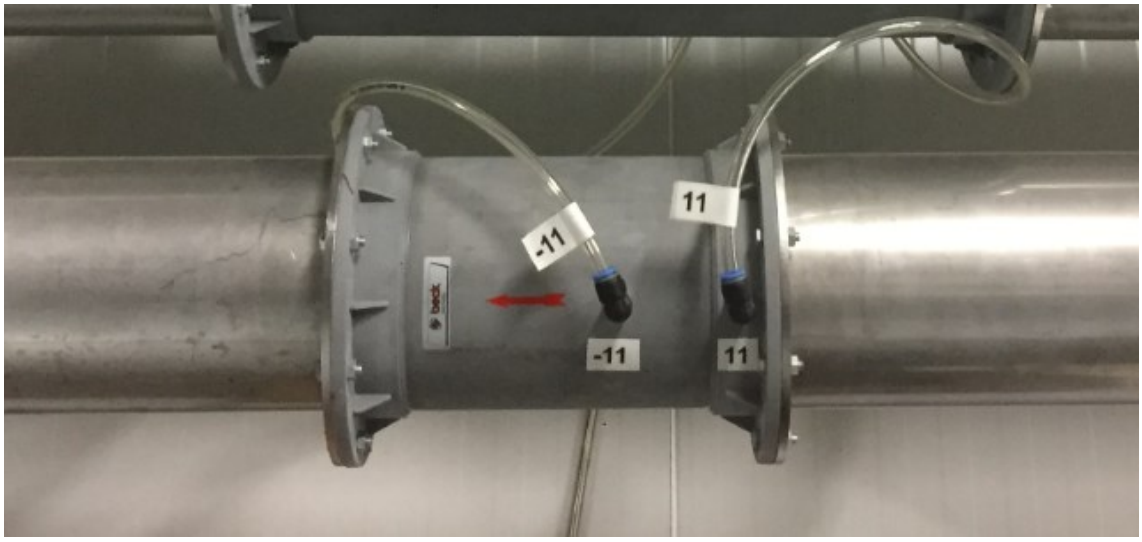

Figure 3.12. Venturi Tube

In addition, energy consumptions of each electricity consuming component (supply fans, exhaust fans and third party electricity consuming components such as drive motors of rotary heat exchanger or compressors) are also measured. Then the efficiency calculations such as COP of the devices can also be performed. For this purpose, energy analyzers are used in the laboratory.

Ambient pressure measurement, temperature measurement with thermocouples, and relative humidity measurement points are connected to direct data acquisition devices. This kind of measurements are performed by being read, evaluated, computed and sent to the computer via the data collecting device with 36 inputs, whose calibrations are periodically done. Energy analyzers and digital micromanometers for static pressure measurement are connected to the measuring computer via MODBUS connection. These kind of measurement information is taken directly from the devices by the computer.

Furthermore, in order to measure and create the pressure drop curves of rotary heat exchanger, holes are opened on the device just before and after the rotary heat exchanger as seen on Figure 3.13. Static pressure measurements over these points are also made using a micromanometer and recorded on a computer. Pressure drop for each air

stream has been calculated by getting the difference between measured inlet and outlet static pressures. During these tests, the indoor chamber temperature and the outdoor temperature are kept constant respectively 25 and 5 °C.

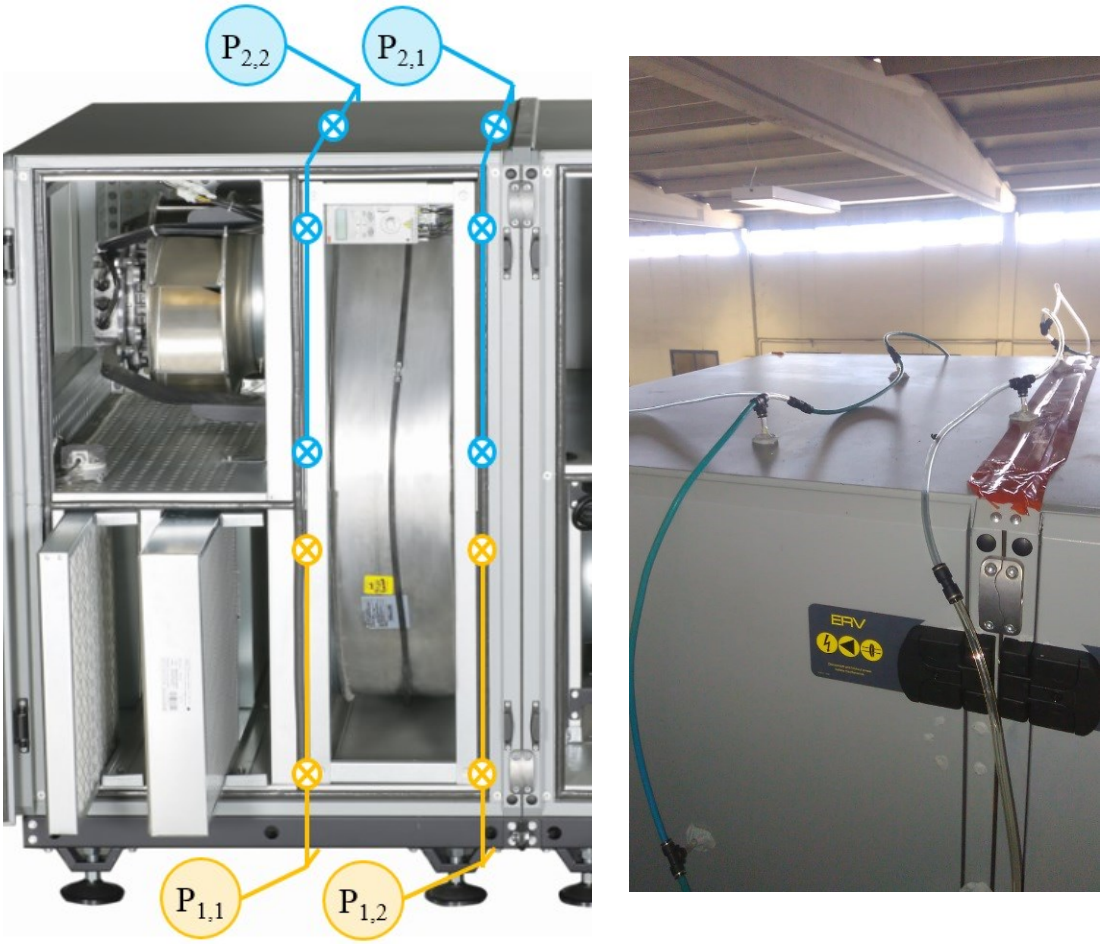

Figure 3.13. Static Pressure Measurement Points on the Test Device (Courtesy of Eneko A.Ş)

3.4. The Rotary Heat Exchanger

As mentioned on previous sections, material of the rotary heat exchanger is aluminum and its type is enthalpy which has hygroscopic properties. All dimension and properties of the rotary heat exchanger are given in Table 3.1. The width, height and depth of the frame for this diameter exchanger are respectively 1080, 1080 and 290 mm. The weight of the rotor formed by the wrapping of aluminum plates is 71 kg. Matrix weight is 38 kg, it can be also calculated by porosity (void fraction) and the exchanger volume. Corrugated wave form aluminum foil is used to produce the exchanger and it can be easily

seen in Figure 3.14. The cell dimensions of matrix are measured by caliper and they are also given in Figure 3.15. There is no purge section on this rotary heat exchanger and it has standard brush type sealing at the edges of moving parts in order to minimize air leakages.

Table 3.1. Physical and Thermodynamic Properties of the Heat Exchanger

Rotor Diameter [mm]	995
Rotor Width [mm]	200
Wave Height of Corrugated Plate of Rotor Matrix [mm]	1.9
Wave Length of Cross Section of Air Channel in the Rotor Matrix [mm]	4.3
Wall Thickness [mm]	0.08
Porosity	91%
Rotor Weight [kg]	38
Hydraulic Diameter of Unitary Cell [mm]	1.53
Density of Matrix Material [kg/m^3]	2707
Specific Heat Capacity of Matrix Material [J/kg.K]	897
Total Heat Transfer Surface Area of Exchanger Matrix [m^2]	360

Figure 3.14. Heat Exchanger Matrix

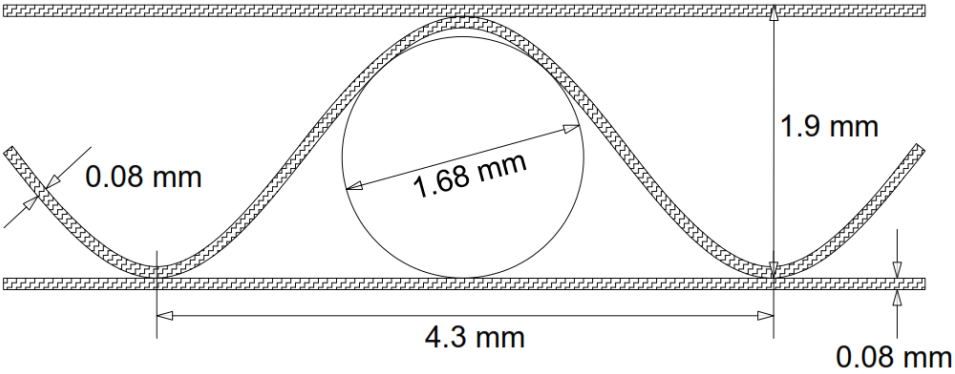

Figure 3.15. Heat Exchanger Matrix Dimensions

Rotary heat exchanger is supplied from Klingenburg Company. Its model is RRU-E-C1-1080/1080/-995. The performance values of this rotary heat exchanger is also obtained from the exchanger selection software of Klingenburg with the version number of 4.6, 05/2017. The mentioned selection software is also shown in Figure 3.16.

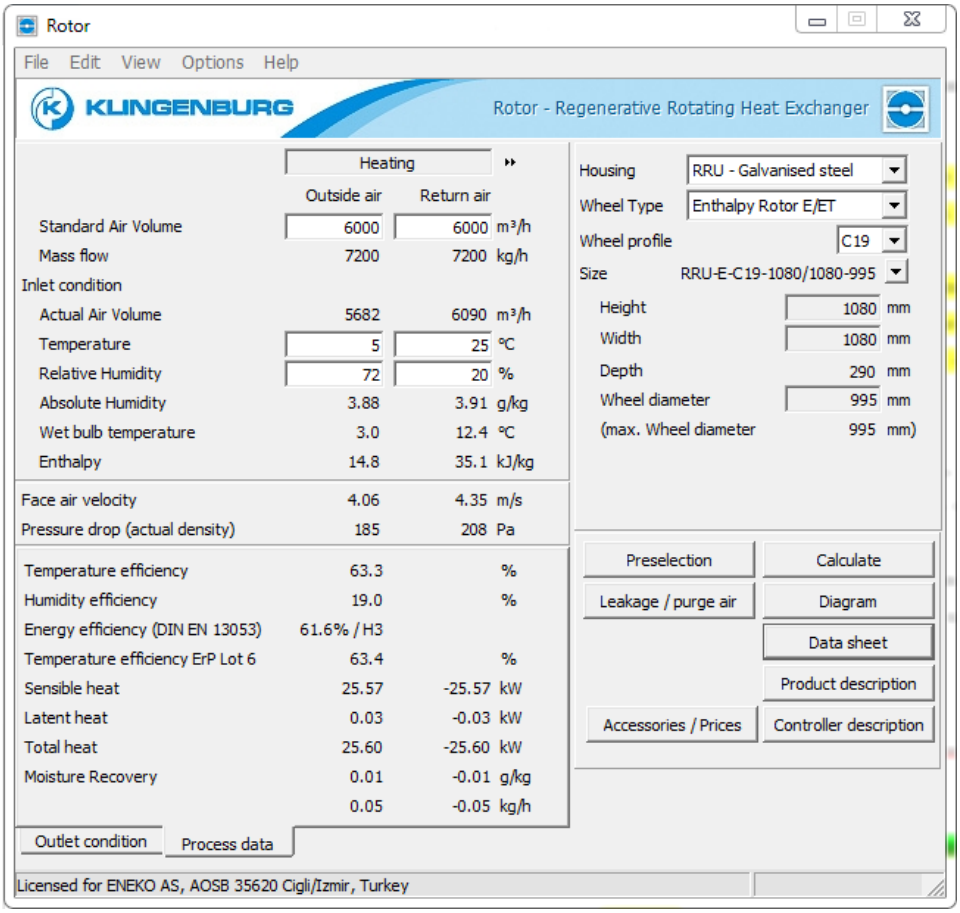

Figure 3.16. Klingenburg Rotor Selection Software

3.5. Experiment Parameters

The following tests have been carried out to investigate the relationship of pressure drop and thermal efficiency individually with the rotational speed of the rotary heat exchanger inside of the test device.

Pressure drop tests are the tests for different rotational speed at different volumetric airflow rates under the conditions of that indoor chamber temperature and outdoor chamber temperature have been kept respectively at 25 °C and 5 °C.

For pressure drop tests, the volumetric airflow rate has been changed by means of the velocity of the air passing through the rotary heat exchanger. The minimum airflow rate of the laboratory is 100 m³/h. According to this boundary, measurements are made from the rotational speed range of 0.2 rpm to 30 rpm at different air volume flow rates within the range of 100 to 7500 m³/h.

Thermodynamic tests are the tests on which the effect of rotational speed of rotary heat exchanger on its thermal efficiency is observed for different volumetric flow rates and at the different indoor and outdoor chamber temperatures.

Table 3.2. List of the Experimental Measurement Points

Meas. No	Rotor Speed rpm	Volumetric Airflow Rate					
		1000 m³/h	2000 m³/h	3000 m³/h	4000 m³/h	5000 m³/h	6000 m³/h
1	0.2	During the experiments each volumetric airflow rate maintained at each following indoor and outdoor temperature and rotational speed has been changed within the given range.					
2	0.5						
3	0.7						
4	1.0						
5	1.2						
6	1.5						
7	2.2						
8	2.7						
9	4.3						
10	6.7						
11	10						
12	12						
13	15						
14	20						
15	30						

Meas. No	Outdoor Air Temp. °C	Return Air Temp. °C
a	0	25
b	5	25
c	10	25
d	15	25
e	5	20

For thermodynamic tests, measurements have been taken at the points given in Table 3.2. These tests have been performed in the laboratory where the indoor and outdoor conditions can be kept constant at the temperatures of a, b, c, d, and e points given in this table. Subsequently, each volumetric flow rate has been fixed for both air streams of the device and the rotation speed of rotary heat exchanger has been changed as given in measurement numbers in Table 3.2.

CHAPTER 4

MATHEMATICAL MODEL

In this section, how the thermal effectiveness of the rotary heat exchanger is calculated with respect to the other variables, such as rotational speed, volumetric flow rate (due to the velocity of air passing through the rotor matrix and the front face area) and inlet temperatures. Additionally, pressure drop of the heat exchanger is calculated in order to analyses if there is any relation between this parameter and the rotational speed of the heat exchanger.

4.1. Dimensionless Parameters

In order to calculate the equations for pressure drop and thermal effectiveness value of the defined rotary heat exchanger, some dimensionless parameters should be estimated with respect to the constant specifications of the rotary heat exchanger.

Figure 4.1 shows the important dimension values of the rotary heat exchanger. These values are tabulated on Table 3.1 in the Chapter 3.

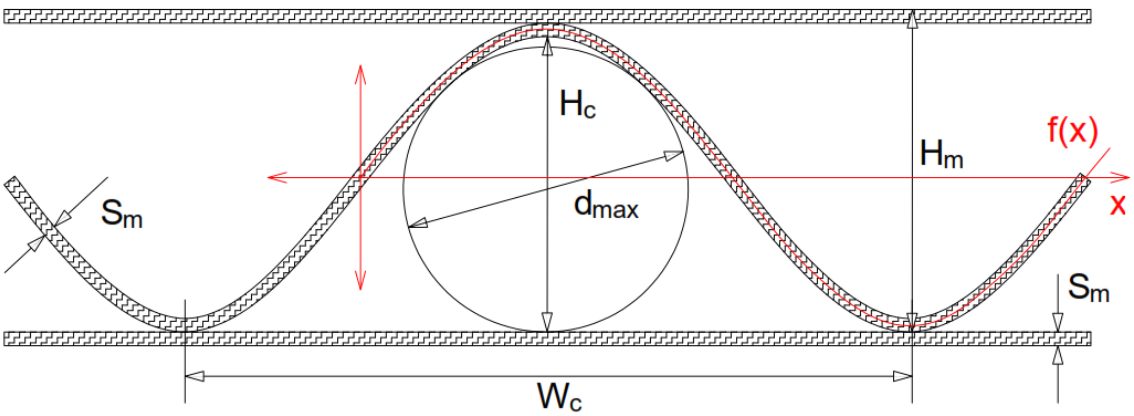

Figure 4.1. Dimension Parameters of a Matrix of Rotary Heat Exchanger

Hydraulic equivalent (d_h) diameter can be calculated with Equation (4.1) where A_c and P_c are respectively the cross-section area and the periphery of a unitary cell.

$$d_h = \frac{4A_c}{P_c} \tag{4.1}$$

l_{arc} is the arc length of a unitary cell and is estimated with the equation used in the study of Guo-Yan et al. (2014) which is also known as a formula for the calculation of the arc length of sinusoidal equations. It can be calculated as follows.

$$l_{arc} = \int_0^{W_c} \sqrt{1 + f'^2(x)dx} \tag{4.2}$$

where, $f(x)$ is the sinusoidal curve function which is assumed as similar with the matrix walls and is also shown in Figure 4.1. This function is modified as,

$$f(x) = \frac{H_c}{2}\sin\left(\frac{2\pi\, x}{W_c}\right) + \frac{H_c}{2} \qquad H_c = H_m - 2S_m \tag{4.3}$$

$$A_c = \int_0^{W_c} f(x)dx \tag{4.4}$$

$$P_c = l_{arc} + W_c \tag{4.5}$$

By using the equations above hydraulic equivalent diameter formula becomes Equation (4.1) as given below.

$$d_h = \frac{4A_c}{l_{arc} + W_c} \tag{4.6}$$

Parameter of n can be found by using following formula,

$$n = \frac{A_c}{A_h} = \frac{P_c}{P_h} \tag{4.7}$$

where A_h and P_h respectively indicate the cross-sectional area and periphery of the equivalent hydraulic diameter. A_c and P_c denote the both for unitary cell. In this study

cross-sectional area is used to calculate n parameter and equivalent one can be found with the equation given below.

$$A_h = \frac{\pi d_h^2}{4} \tag{4.8}$$

d^* is defined as a **dimensionless diameter** of a unitary cell of rotary heat exchanger matrix. It is calculated by the following equation.

$$d^* = \frac{d_h}{d_{max}} \tag{4.9}$$

where d_{max} is the circle, which is inscribed into a unitary cell, is estimated as 1.68 by iterative method. Thus parameters of d_h, d^* and n are as follows.

$$d_h = 1.50\,mm \quad d_{max} = 1.68\,mm \quad \rightarrow \quad d^* = 0.89 \quad n = 2.13 \tag{4.10}$$

x^* and z^* are respectively **dimensionless duct length** and **dimensionless coordinate** and they are calculated with the Equation (4.11).

$$x^* = L/(d_h Re) \qquad z^* = L/(d_h RePr) \tag{4.11}$$

Re and Pr are respectively Reynold and Prandtl numbers. Reynold number can be calculated as given below. given for outdoor and return air temperatures in Equation (4.12).

$$Re = \frac{u d_h}{v} \tag{4.12}$$

where, u is the actual air velocity through the matrix channels. It is calculated by considering the porosity of the rotary heat exchanger. u_f is the velocity which is calculated by neglecting the porosity of the rotary heat exchanger. They are defined as,

$$u = \frac{\dot{M}}{\rho(A_r/2)\,\sigma} \qquad u_f = \frac{\dot{M}}{\rho(A_r/2)} \qquad A_r = \frac{\pi D_r^2}{4} \tag{4.13}$$

Furthermore, density, specific heat capacity, kinematic viscosity, thermal conductivity and Prandtl number of air can be estimated with regard to temperature in °C by using the formulae in between the Equation 4.14a to 4.14e.

$$\rho = 2x10^{-5}T^2 - 4.8x10^{-3}T + 1.2936 \tag{4.14a}$$

$$C_p = -1x10^{-6}T^3 + 6x10^{-4}T^2 + 1x10^{-2}T + 1.005x10^{-3} \tag{4.14b}$$

$$v = 1x10^{-10}T^2 + 9x10^{-8}T + 1x10^{-5} \tag{4.14c}$$

$$\lambda = -4x10^{-8}T^2 + 7.7x10^{-5}T + 24.35x10^{-3} \tag{4.14d}$$

$$Pr = 6x10^{-7}T^2 - 2x10^{-4}T + 0.711 \tag{4.14e}$$

Because of the air channel geometry Yılmaz (1990) suggested a shape factor to be used in pressure drop and thermal effectiveness calculation. The equations were founds as given below.

$$\varphi = 1 + \left\{\frac{\varphi_\infty - 1}{\left[1 + 0.33{d^*}^{2.25}/(n-1)\right]}\right\} \tag{4.15}$$

where φ_∞ is defined as,

$$\varphi_\infty = \frac{3}{8}{d^*}^2(3 - d^*) \tag{4.16}$$

By using the Equation (4.15) and (4.16) and the values in the Equation (4.10) the shape factor for developed flow is found as follows.

$$\varphi_\infty = 0.6269 \qquad \varphi = 0.6954 \tag{4.17}$$

4.2. Calculation of Pressure Drop

Matrix void fraction or porosity is defined either the ratio of the cross-sectional area of the fluid passing to the total surface area of the rotary heat exchanger or the void volume to the total volume of the exchanger. The porosity of the rotary heat exchanger is known and it is shown as follows.

$$\sigma = 0.91 \tag{4.18}$$

Total pressure drop of the rotary heat exchanger consists of frictional and incremental pressure drop ΔP_{fr} and local pressure drop ΔP_l which is related with inlet and outlet of the exchanger.

$$\Delta P_r = \Delta P_{fr} + \Delta P_l \tag{4.19}$$

Local pressure drop ΔP_l can be estimated by using the following equation.

$$\Delta P_l = K_l \frac{\rho u^2}{2} \tag{4.20}$$

where K_l is the pressure drop number which was proposed by White (1994) and Brauer (1971), calculation can be done with the given equation below,

$$K_l = \frac{(3-\sigma)(1-\sigma)^2}{2-\sigma} \qquad \rightarrow \qquad K_l = 0.0155 \tag{4.21}$$

Total pressure is also calculated by Equation (4.22).

$$\Delta P_r = \Delta P_r^* \frac{\rho u^2}{2} \tag{4.22}$$

where ΔP^* is dimensionless pressure drop and is estimated with,

$$\Delta P_r^* = \Delta P_{fr}^* + K \tag{4.23}$$

ΔP_{fr}^{*} is the dimensionless pressure drop and it includes the frictional pressure loss and the pressure loss depending on the velocity profile development in the developing section of the duct. It can be defined as (Yılmaz, 1990).

$$\Delta P_{fr}^{*} = 64\varphi z^{*} + \frac{13.766x^{*0.5}}{\left[1 + 13.95\varphi x^{*0.5} + \left(\frac{13.766}{K}\right)^{3} x^{*1.5}\right]^{1/3}} \tag{4.24}$$

where K is additional pressure drop coefficient and is defined as,

.

$$K = \frac{1.33}{1 + (1.33/K_{\infty} - 1)/\left[1 + 0.74d^{*2}/(n-1)\right]} \tag{4.25}$$

$$K_{\infty} = \frac{12}{5}(3 - d^{*})^{2}\left[\frac{9(3 - d^{*})}{7(7 - 3d^{*})} - \frac{1}{5 - 2d^{*}}\right] \tag{4.26}$$

Equation (4.21) and (4.22) is calculated and they are found as,

$$K = 0.9718 \qquad\qquad K_{\infty} = 3.3754 \tag{4.27}$$

By using the the calculated shape factor (φ) and K values in the Equation (4.24) and then it becomes,

$$\Delta P_{fr}^{*} = 51.65z^{*} + \frac{13.766x^{*0.5}}{\left[1 + 11.259x^{*0.5} + 338.63x^{*1.5}\right]^{1/3}} \tag{4.28}$$

Finally, total pressure drop of the rotary heat exchanger can be calculated by using the following formula for all given volumetric flow rates in Table 4.2,

$$\Delta P_{r} = \left(\Delta P_{fr}^{*} + K_{l}\right)\frac{\rho u^{2}}{2} \tag{4.29}$$

All values at outdoor and indoor air conditions are compared with experimental results in Chapter 5.

4.3. Calculation of Thermal Effectiveness

In this section, it is purposed to show how NTU values can be obtained with respect to the volumetric airflows and the inlet temperature conditions, which are also given on the Table 3.2 in Chapter 3. Thermal effectiveness of rotary heat exchanger can be generally estimated by using the thermal effectiveness of recuperative plate type (counter-flow) heat exchangers. In this study six different equations are used to calculate thermal effectiveness of the rotary heat exchanger (ε_o) according to the literature survey in Chapter 2.

4.3.1. Calculation of NTU and ε_o

In general, the thermal effectiveness of the heat exchanger is given by the following equation.

$$\varepsilon_a = \frac{Q}{Q_{max}} \tag{4.30}$$

Q is the actual heat transfer of the rotary heat recovery exchanger in Equation (4.30). Q_{max} is the maximum heat transfer that can be obtained theoretically. Both heat transfers are calculated by the following formulas.

$$Q = C_i \left| T_{i,2} - T_{i,1} \right| \tag{4.31}$$

$$Q_{max} = C_{min} \left(T_{1,1} - T_{2,1} \right) \tag{4.32}$$

The subscripts refer to the air streams. For the first indices, '1' indicates that the air stream is related with the fresh air stream, '2' is with exhaust air stream. The second indices of the subscript refer to inlet (1) and outlet (2). In Equation (4.31), C_i letters show the thermal capacities and are calculated by the following equation. In this equation, M_i and Cp denote the mass flow rate and specific heat capacity of the air, respectively. C_{min} indicates the lowest of the thermal capacities.

$$C_i = M_i Cp_i \tag{4.33}$$

For the thermal effectiveness of a rotary heat exchanger, Yılmaz, Büyükalaca ve Candar (1996) suggested to use the Equation (4.34).

$$\varepsilon_a = \varepsilon_o \varphi_r \varphi_c \tag{4.34}$$

In this equation ε_o indicates the effectiveness of a recuperative (plate type) heat exchanger, φ_r and φ_c indicates the correction factors related with the rotational speed of rotary heat exchanger and purge section. These parameters are developed by Kays and London (1984). Since there is no purge section in the exchanger used, φ_c is assumed as ineffective, equal to 1, and the equation becomes,

$$\varepsilon_a = \varepsilon_o \varphi_r \tag{4.35}$$

In order to calculate thermal effectiveness of a recuperative heat exchanger, Kays ve London (1984) suggested Equation (4.36a) and (4.36b) which are given below.

$$\varepsilon_o = \frac{1 - e^{[-NTU(1-C^*)]}}{1 - C^* e^{[-NTU(1-C^*)]}} \qquad C^* < 1 \tag{4.36a}$$

$$\varepsilon_o = \frac{NTU}{1 + NTU} \qquad C^* = 1 \tag{4.36b}$$

According to the Equation (4.36a) and (4.36b), the thermal effectiveness of the heat exchanger depends on two parameters, expressed as the heat capacity ratio and the NTUs, respectively and these two parameters are calculated as follows. C_{min} and C_{max} are defined as the smallest and the largest of the heat capacities.

$$C^* = \frac{C_{min}}{C_{max}} \tag{4.37}$$

$$NTU = \frac{UA}{C_{min}} \tag{4.38}$$

where UA is determined as follows and it is used in the Equation (4.38) for NTU calculation.

$$\frac{1}{UA} = \frac{1}{h_1 Ar_1} + \frac{1}{h_2 Ar_2} \tag{4.39}$$

1 and 2 subscript letters indicated cold and hot fluids respectively. h is the heat transfer coefficient between the solid matrix surface and airflow and they can be easily calculated by using Nusselt number in the Equation (4.40). Ar refers to the heat transfer surface area of the rotary heat exchanger and they are both equal.

$$h = Nu \frac{\lambda}{d_h} \tag{4.40}$$

In this equation λ is thermal conduciveness and Nu is the Nusselt number can be calculated with the Equation (4.41) as follows. This equation was proposed by Yılmaz et al. (2000) for both developing and developed flow regimes.

$$Nu = (Nu_d^4 + Nu_o^4)^{1/4} \tag{4.41}$$

where Nu_o is Nusselt number for developing flow, which was proposed by Yılmaz et al. (2000) and Nu_d is Nusselt number for thermally developed flow which was found by Yılmaz and Cihan (1993) and is calculated with the following equations (4.42) to (4.47).

$$Nu_d = Nu_\infty + \frac{1.615\Phi/(z^*/\varphi)^{1/3}}{\left[1 + 1.88\left(\frac{z^* Nu_\infty^3}{\varphi \Phi^3}\right) + 3.93\left(\frac{z^* Nu_\infty^3}{\varphi \Phi^3}\right)^{4/3}\right]^{1/2}} \tag{4.42}$$

Nu_∞ is a Nusselt number and can be calculated as follow for the given conditions of dimensionless coordinate z^* which is defined in Equation (4.11).

$$Nu_\infty = 3.657\phi \qquad z^* \to \infty \tag{4.43}$$

ϕ is a factor related to heat transfer and it is calculated as follows with the other parameters, ϕ_∞, $\Delta\phi$, $\Delta\phi_{max}$. (Yılmaz and Cihan, 1993)

$$\phi = 1 + \frac{\phi_\infty - 1}{1 + {}^{1}/_{(n-1)}} + \Delta\phi \tag{4.44}$$

$$\phi_\infty = 0.5155 \frac{d^{*2}}{3 - d^*} \tag{4.45}$$

$$\Delta\phi = \Delta\phi_{max} \frac{0.95(n-1)^{0.5}}{1 + 0.038(n-1)^3} \tag{4.46}$$

$$\Delta\phi_{max} = \frac{7.10^{-3} d^{*8}}{\left(1 + 10d^{*-28}\right)\left(1 + 64.10^{-8} d^{*28}\right)^{1/2}} \tag{4.47}$$

Other heat transfer factor (Φ) is calculated with the following equations in Nusselt number estimation (Yılmaz and Cihan, 1994).

$$\Phi = 1 + \frac{\left[3(d^*/2)^{7/8}/(1 + d^*)\right] - 1}{1 + 0.25/(n-1)} \tag{4.48}$$

By using d^* and n values from the Eqn (4.10), heat transfer factors and Nu_∞ number are calculated as given below.

$$\Phi = 0.8212 \qquad \varphi_\infty = 0.1936 \qquad \phi = 0.5761 \qquad Nu_\infty = 2.1067 \tag{4.49}$$

Nusselt number for thermally developing flow is given by Yılmaz et al. (2000) with following sorted equations.

$$f = \left(1 + \frac{0.105}{Pr + \sqrt{Pr}/3} + \frac{0.0468}{Pr}\right)^{1/6} \tag{4.50}$$

$$Nu_o = \frac{0.6774}{f z^{*1/2} Pr^{1/6}} \tag{4.51}$$

where f is the function which was formulated by using the data of Merk (1959) and Gauler (1972). As known, Prandtl number is assumed constant at 0.70, thus f value is estimated as 1.027 from the Equation (4.51).

Finally using the results from Equation (4.42) and (4.51) into the Equation (4.41) in order to obtain Nusselt number which is used in Equation (4.40) for heat transfer coefficient calculation.

After the heat transfer calculations, NTU values are obtained from the Equation (4.38). Then the thermal effectiveness can get with the Equation (4.36a) or (4.36b) depending on the C^* ratio.

4.3.2. Calculation of Thermal Effectiveness of the Exchanger

C_r^* is the capacity ratio of heat capacity of solid matrix to lowest heat capacity as shown below.

$$C_r^* = C_r / C_{min} \tag{4.52}$$

Heat capacity of solid matrix can be calculated with the equation below.

$$C_r = M_r C_{pr} N \qquad\qquad M_r = V_r \rho_r \tag{4.53}$$

here M_r is weight of the rotary heat exchanger matrix and C_{pr} is its heat capacity. N is the rotational speed of rotary heat exchanger in the units of rev/s.

The following equation, Equation (4.54) was proposed by the Razelos (1979) in order to get effectiveness values of regenerative heat exchanger. The Equation (2.5), (2.6) and (2.7) can be used for the following formula.

$$\varepsilon_a = \frac{1 - e^{\left\{e_r\left(C^{*2}-1\right)/[2C^*(1-e_r)]\right\}}}{1 - C^* e^{\{e_r(C^{*2}-1)/[2C^*(1-e_r)]\}}} \tag{4.54}$$

Kays and London (1984) also suggested to calculate this thermal effectiveness of

rotary heat exchangers factor as follows.

$$\varepsilon_a = \varepsilon_o \left[1 - \frac{1}{9(C_r^*)^{1.93}}\right] \tag{4.55}$$

Another effectiveness formula is also suggested as follows by Worsøe-Schmidt (1988),

$$\varepsilon_a = \varepsilon_o \left\{1 - \frac{0.114\left[1 - e^{(-NTU)}\right]}{C^{*0.44} C_r^{*1.93}}\right\} \tag{4.56}$$

Moreover, another rotational speed correction factor in order to get more convenient results is developed for lower speed by the experimental and mathematical studies of Büyükalaca, Yılmaz and Atalay (1998). It is given in Equation (2.12), is used to define the effectiveness formula as follows.

$$\varepsilon_a = \varepsilon_o \frac{0.24\, C_r^*}{\left[1 + 0.02 C_r^{*1.82} + (0.24 C_r^*)^3\right]^{1/3}} \tag{4.57}$$

Büyükalaca and Yılmaz (2002) also developed an equation that can be used even for very small rotational speeds. It is given below.

$$\varepsilon_a = \frac{C_r^*}{\left[1 + 3\left({C_r^*}/{\varepsilon_o}\right)^2 + \left({C_r^*}/{\varepsilon_o}\right)^4\right]^{1/4}} \tag{4.58}$$

Finally, Seo, Lee and Kim (2018) found an equation to calculate thermal effectiveness of rotary heat exchanger by correcting the effectiveness of recuperative type heat exchangers. The equation is defined as,

$$\varepsilon_a = \varepsilon_o \sqrt{\sum_{n=1,3,5,\ldots}^{\infty} \frac{8}{(2\varepsilon_o/C_r^*)^2 + (n\pi)^2}} \tag{4.59}$$

4.4. Computer Codes

For this study MATLAB is used to solve mathematical model analysis with the codes developed by us. The codes are given in Appendix A and Appendix B. The thermal effectiveness calculations begin with the interface shown in Figure 4.2. Default values are embedded with respect to the parameter given for this study as in Table 3.1 and Table 3.2. They can be changed by the user with demanded values.

Furthermore, in Appendices C and D, examples about thermal effectiveness and pressure drop calculations for the points given bellow have been done with regard to the related sequences used in MATLAB.

- Thermal effectiveness calculation in Appendix C
  Outdoor Air Temperature = 5 °C
  Return Air Temperature = 25 °C
  Volumetric Airflow Rates for both Air Stream = 1000 m^3/h
- Pressure drop calculation in Appendix D
  Outdoor Air Temperature = 5 °C
  Return Air Temperature = 25 °C
  Volumetric Airflow Rates for both Air Stream = 6000 m^3/h

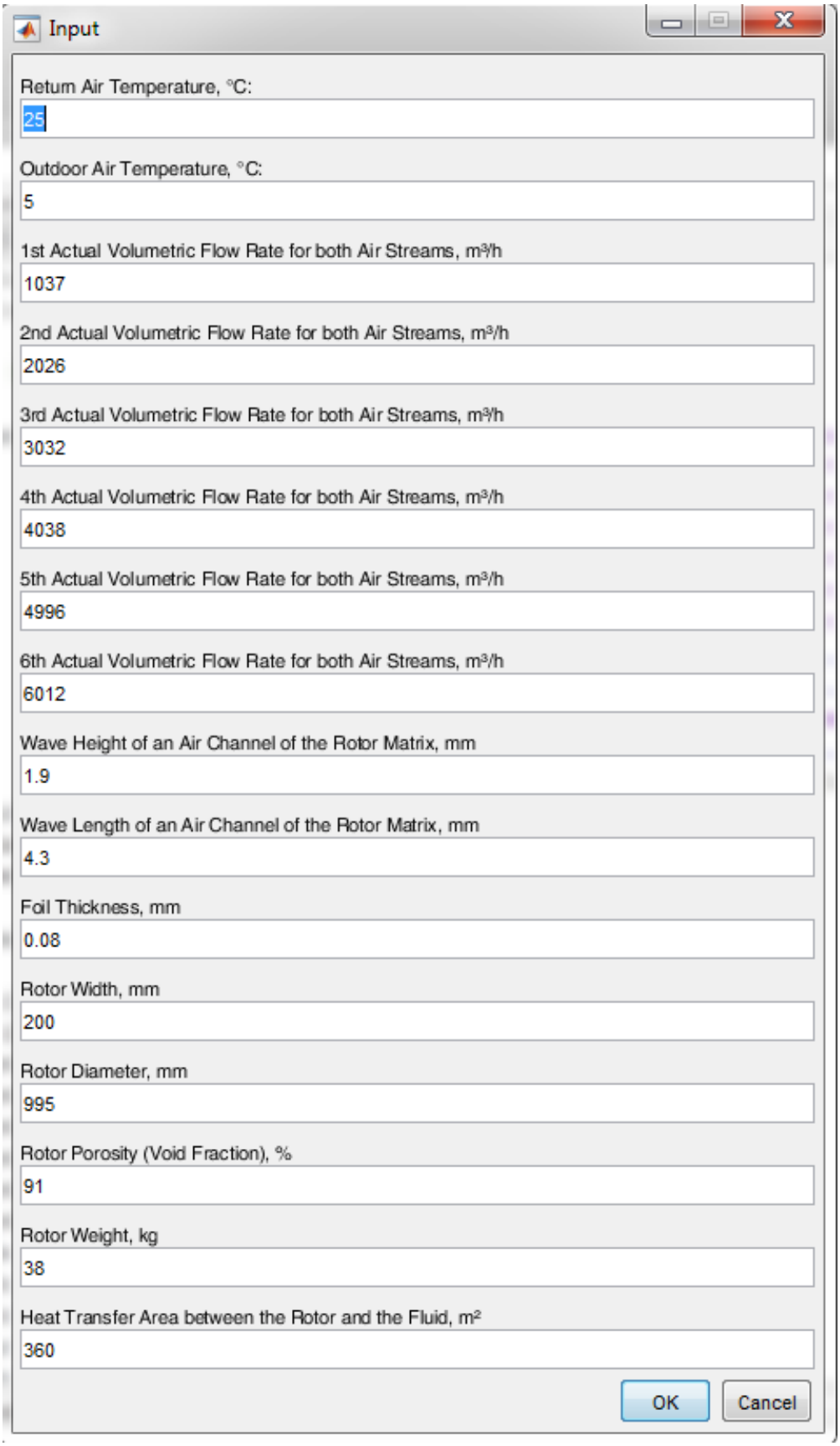

Figure 4.2. Interface of MATLAB Parameter Input

CHAPTER 5

RESULTS

In this chapter, test results have been given and been compared with the equation which has a good agreement with experimental results. As mentioned, Eneko EnergyLab® has been used to provide a simulation for actual indoor and outdoor environments and the standards required for related ventilation device tests have been obeyed. Mathematical model simulations have been made with the proposed equations on the literature. Consequently, mathematical model and experimental results have been compared.

5.1. Experimental Results

5.1.1. Rotational Speed vs. Pressure Drop

Graphs on the Figure 5.1 and Figure 5.2 show the measured volumetric airflow rates and pressure drop curves of respectively supply air stream and exhaust air stream. Each curve shows pressure drop and airflow relation at different rotational speeds. Supplier data has been also obtained and has been added to these graphs with respect of the conditions of each air stream. Additionally mathematical results have also been calculated as mentioned in the Chapter 4 and they have been all shown in these graphs in order to make a comparison.

Finally, in a view of the rotational speed range of this study, the results show that rotational speed does not have an impact on the pressure loss of the rotary heat exchanger.

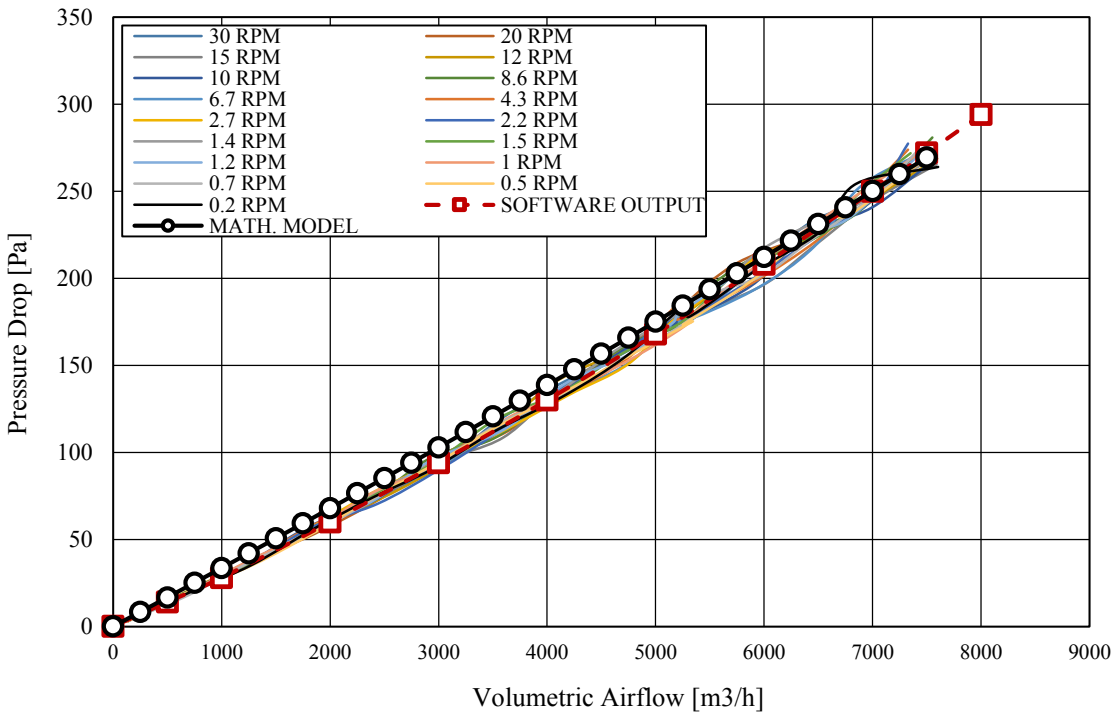

Figure 5.1. Static Pressure Drop of Rotary Heat Exchanger with Respect to the Rotational Speed at Different Airflow Rates (Supply Stream)

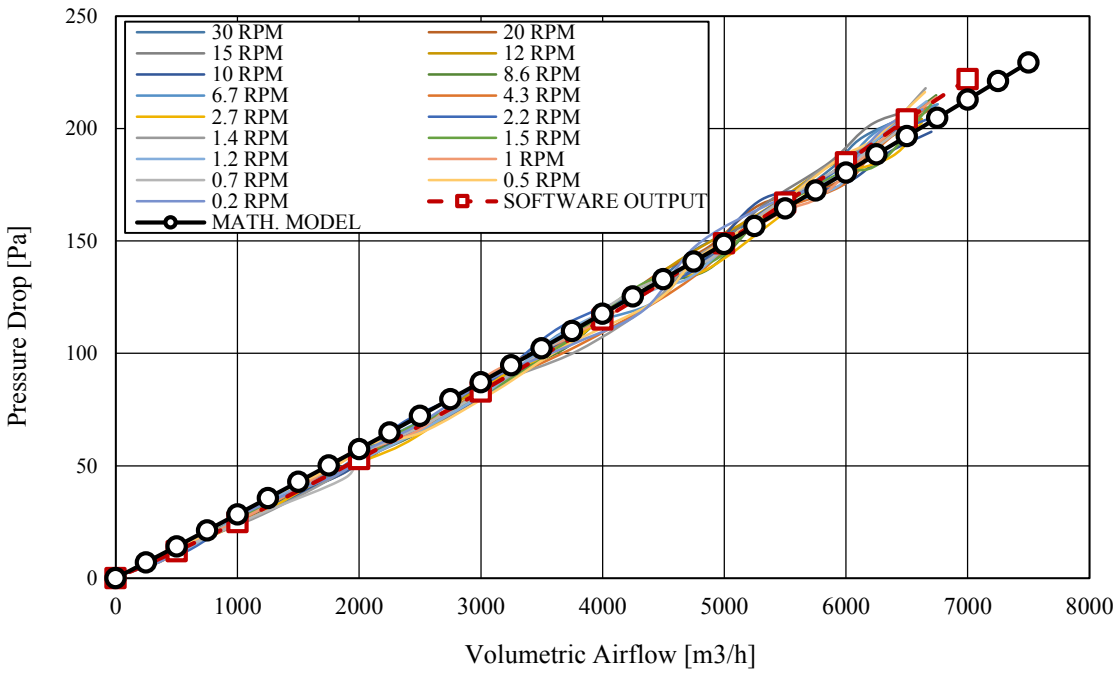

Figure 5.2. Static Pressure Drop of Rotary Heat Exchanger with Respect to the Rotational Speed at Different Airflow Rates (Exhaust Air Stream)

5.1.2. Rotational Speed vs. Thermal Efficiency

The test device has been operated at volumetric airflows and inlet temperatures and indicated in Table 3.2 and the following graphs (Figure 5.3 to 5.7) have been obtained. During all measurements, the absolute humidity of the indoor and outdoor simulation chamber has been kept constant in order to minimize latent heat transfer with regard to the condensation temperature of return air for the given conditions.

In the graphs in Figure 5.3 to 5.7, the experimental results have been given for the averaged volumetric air flow rates and rotational speeds varying according to the indoor and outdoor temperatures indicated by the letters a, b, c, d, e in Table 3.2 respectively. The averages of measured airflow rate for each measurement point of various rpm values under the indoor and outdoor temperatures indicated by the letters a, b, c, d and e in Table 3.2 are given in Table 5.1.

Table 5.1. Volumetric Airflow Rates of Experimental Test Points for each Rotational Speed Given in Table 3.1

Conditions			Volumetric Airflow Rate					
No	Outdoor Temp.	Indoor Temp.						
	°C	°C	m^3/h					
a	0	25	1037	2028	3034	4042	4997	6016
b	5	25	1100	2123	3048	4069	4848	5975
c	10	25	1037	2030	3036	4046	4999	6015
d	15	25	1036	2026	3032	4038	4996	6014
e	5	20	1036	2025	3034	4036	4998	5998
Average			*1049*	*2046*	*3036*	*4046*	*4967*	*6003*

It is observed that there is a common behavior on the relation between the thermal efficiency of the device and rotational speed of its exchanger for various volumetric airflow rates (air velocities). As expected, the thermal efficiency of the device drops as the volumetric airflow, depends on the air velocity, increases as seen in all the graphs in Figure 5.3 to 5.7. As can be seen from these graphs, it has been determined that the rotational speed in each volumetric airflow does not affect the efficiency after a critical value. In this study, critical rotational speed has been defined as the maximum rotational speed after which the thermal efficiency cannot be affected.

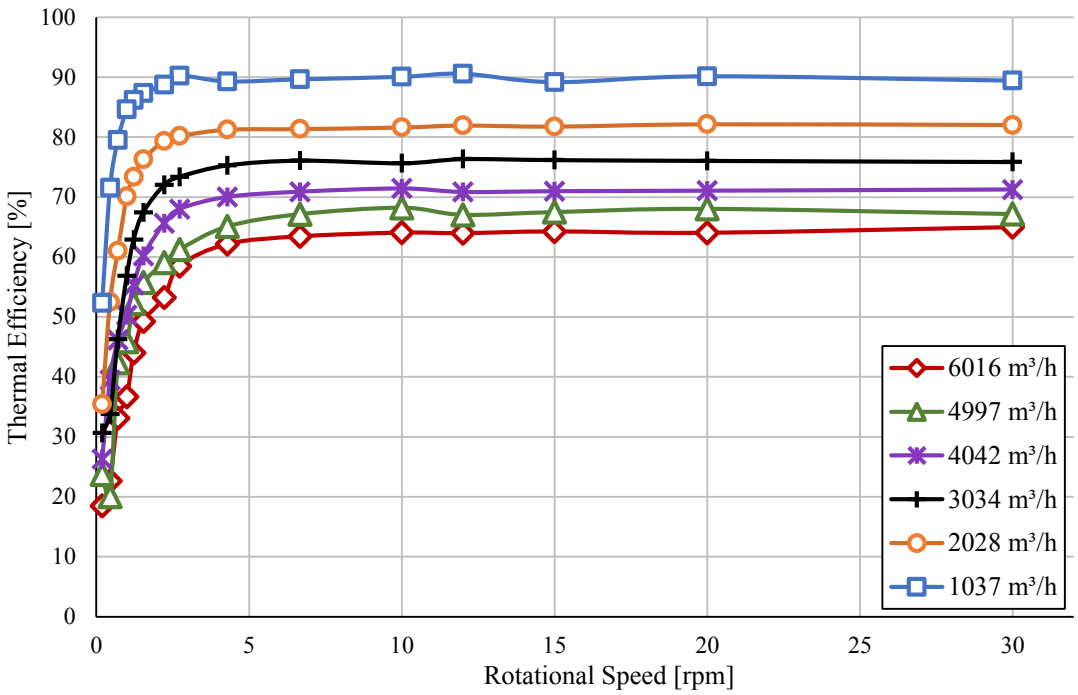

Figure 5.3. Thermal Efficiency for 'a' Conditions on Table 5.1 (Outdoor Air Temperature: 0 °C – Return Air Temperature 25 °C)

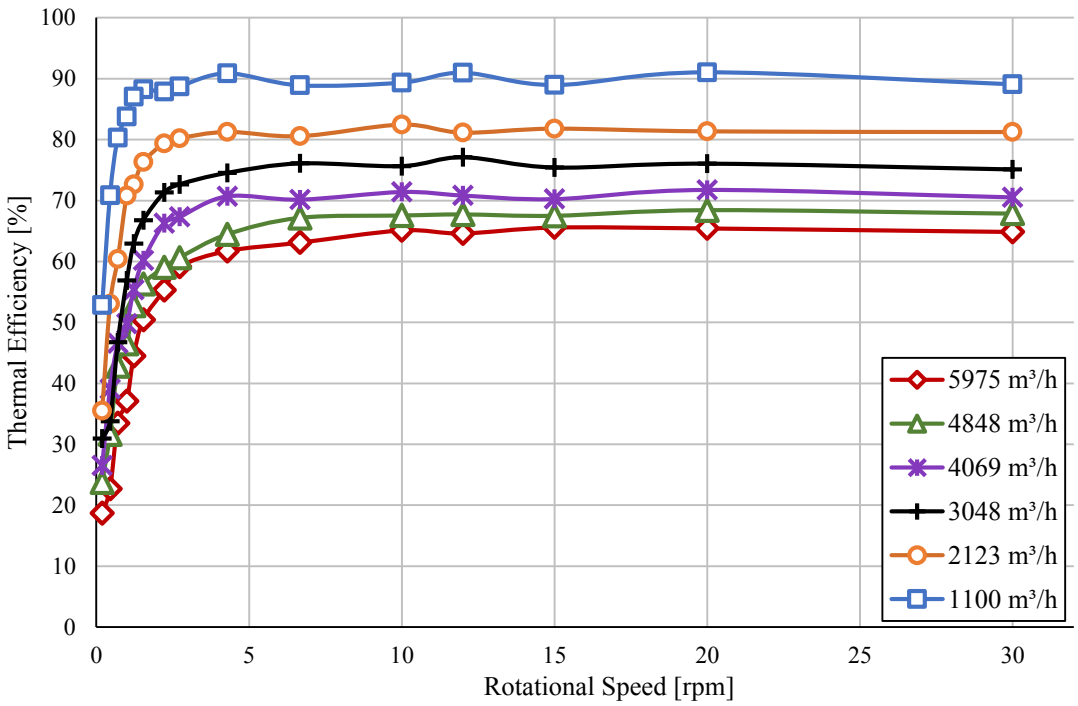

Figure 5.4. Thermal Efficiency for 'b' Conditions on Table 5.1 (Outdoor Air Temperature: 5 °C – Return Air Temperature 25 °C)

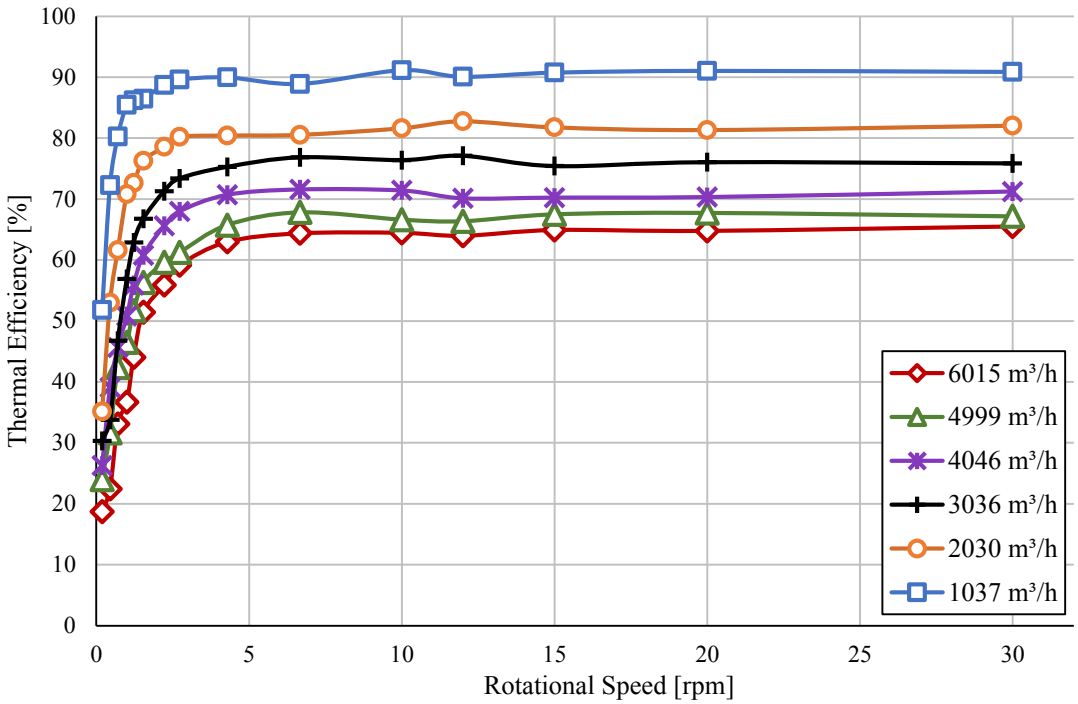

Figure 5.5. Thermal Efficiency for 'c' Conditions on Table 5.1 (Outdoor Air Temperature: 10 °C – Return Air Temperature 25 °C)

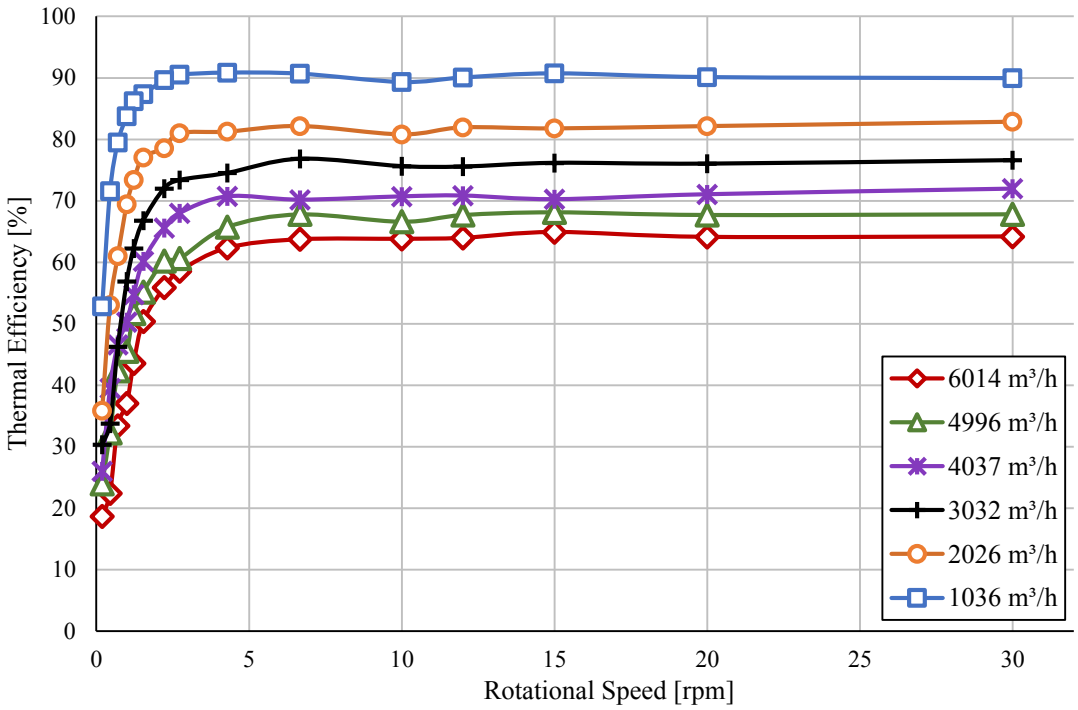

Figure 5.6. Thermal Efficiency for 'd' Conditions on Table 5.1 (Outdoor Air Temperature: 15 °C – Return Air Temperature 25 °C)

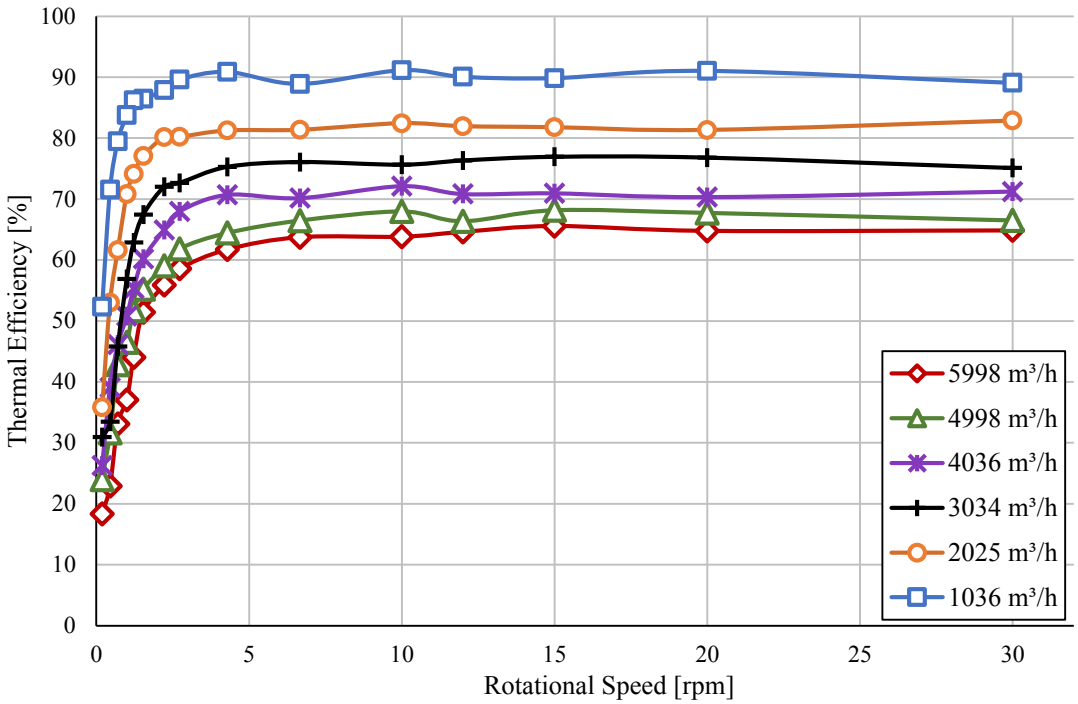

Figure 5.7. Thermal Efficiency for 'e' Conditions on Table 5.1 (Outdoor Air Temperature: 5 °C – Return Air Temperature 20 °C)

As an example, a typical behavior for all test results has been explained for Figure 5.3 as follows. At the volumetric airflow rate of 1037 m³/h, which is also represents the air velocity of 0.74 m/s when considering the cross-sectional area of the rotary heat exchanger, the thermal efficiency of the device is 89.7%. Higher rotational speeds than 2.2 rpm, it has been observed that the thermal efficiency remains constant at this value. Similar behavior has been observed on each curve as mentioned. On these curves, it has been also seen that the critical rotational speed increases while the volumetric airflow rate increases. For each indoor and outdoor conditions similar behavior has been experienced.

Additionally, the thermal efficiency values which have been obtained from the selection software of the exchanger for the volumetric airflows given in Table 5.1 have been also illustrated in Figure 5.8 with the comparison of the experimental results in Figure 5.3. Experimental results are slightly higher than the data provided by the supplier of the heat exchanger.

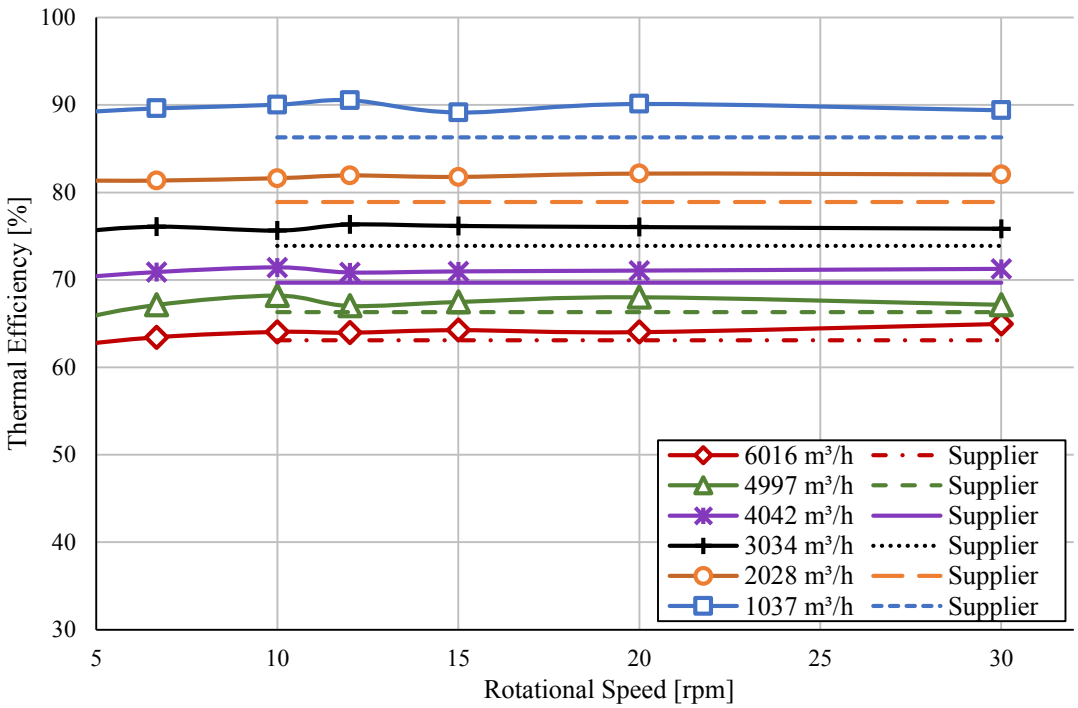

Figure 5.8. Thermal Efficiency Comparison between Experimental Results and Supplier Software Data for 'a' Conditions on Table 5.1 (Outdoor Air Temperature: 0 °C – Return Air Temperature 25 °C)

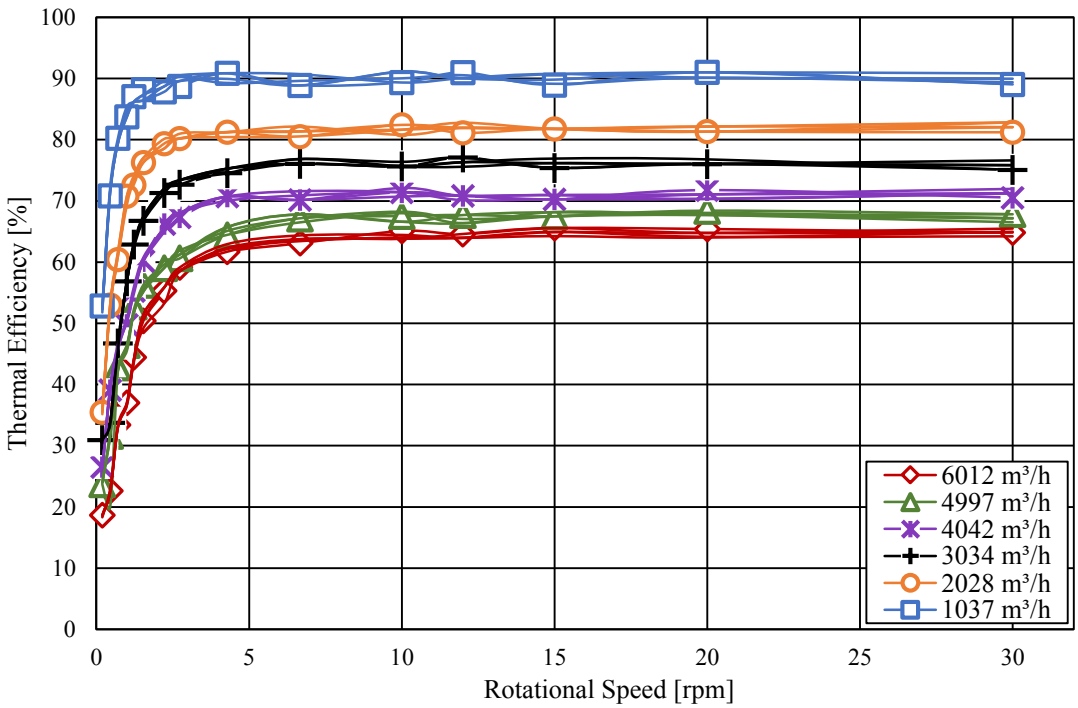

Figure 5.9. Thermal Efficiencies for all Temperature Conditions and Averaged Volumetric Airflow Rates on Table 5.1

Effectiveness is mainly related with the parameters of NTU, heat capacity ratios (C^*, C_r^*). These parameters also depend on heat capacities, Prandtl Number, Nusselt Number. However, the change on these parameters are very low within the range of the temperatures of 0 to 25 °C. On the Figures 5.10(a) to 5.10(c), the ratio of each parameter at actual temperature to its value at 0 °C are shown. As seen from these graphs, thermal parameters have not any significant change within the given temperature range. Thus, thermal effectiveness cannot be affected from the temperature difference on exchanger inlets. This proposal has been also seen from the graph given on Figure 5.9.

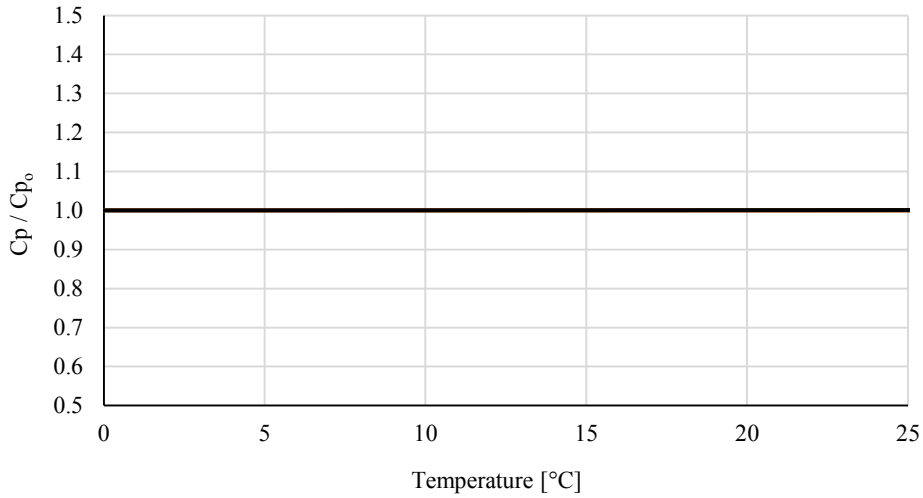

(a)

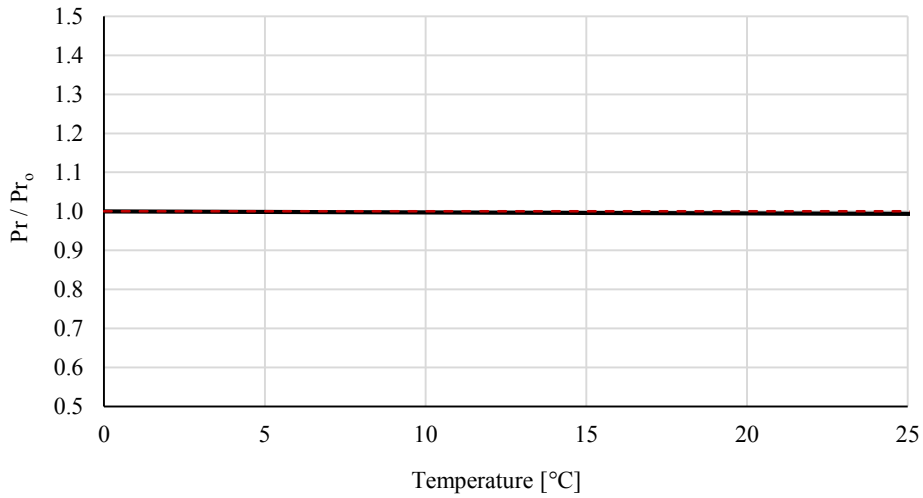

(b)

Figure 5.10. The Variation Ratio of Cp (a), Pr (b), and Nu (c) Parameters

(cont. on next page)

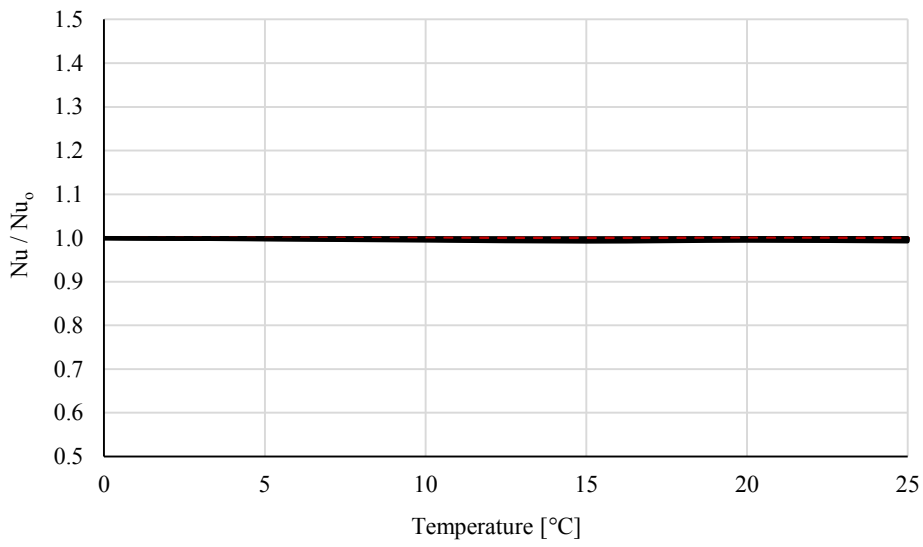

(c)

Figure 5.10. **(cont.)**

5.2. Mathematical Model Results

In this section, thermal effectiveness values for the indoor and outdoor conditions and also for the volumetric air flowrates, which are given in Table 5.1, have been calculated. The equations and algorithms given in Chapter 4 have been used for the mathematical model simulation. All algorithms have been also coded in MATLAB and an application has been created. The codes are given in Appendix A and Appendix B for respectively pressure drop and thermal effectiveness calculations of rotary heat exchanger. Differences between the proposed thermal effectiveness equations (Equation 4.54 to 4.59) have been obtained due to the experimental indoor and outdoor temperatures and six different volumetric air flow.

With this mathematical model study, the most approximate effectiveness equation according to the experimental results has been determined. Figure 5.11 and Figure 5.12 show the comparison between the equations and the experimental results respectively for the volumetric airflow rates of 1100 m³/h and 5975 m³/h. The proposed researchers of these equations are reminded as follows.

- Equation 4.54 – Razelos (1979)

- Equation 4.55 – Kays and London (1984)
- Equation 4.56 – Worsøe-Schmidt (1988)
- Equation 4.57 – Büyükalaca, Yılmaz and Atalay (1998)
- Equation 4.58 – Büyükalaca and Yılmaz (2002)
- Equation 4.59 – Seo, Lee and Kim (2018)

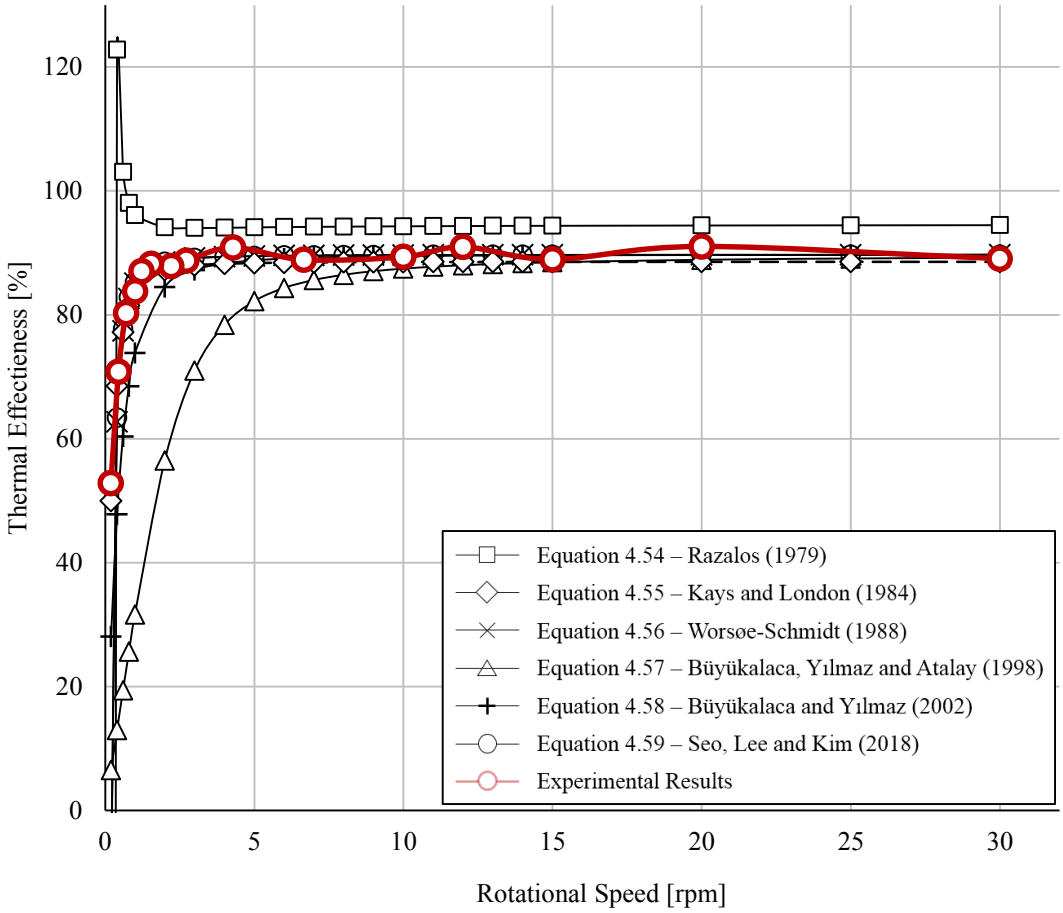

Figure 5.11. Comparison of the Calculated Results with the Experimental Results (Outdoor Air Temperature: 5 °C – Return Air Temperature 25 °C – 1100 m³/h)

As seen from the Figure 5.11 and Figure 5.12 the experimental results seem coherent with the proposed equation of Seo et al. (2018). In a logical manner, it is known that the efficiency or effectiveness cannot be higher than 100%. Thus, for this study Equation (4.54) has not been fitted with the experimental results. For lower rotational speeds of rotary heat exchanger than 2 rpm, the effectiveness has been calculated higher

than 100% at the airflow rate of 1100 m³/h (see Figure 5.11). Additionally, it is also known that there would not be any heat transfer if the rotor stops. Therefore, the effectiveness should be decreased depending on a decline of rotational speed until they are all zero. The effectiveness values, which have been obtained from Equation (4.55) and (4.56) for lower rotational speeds than 2 rpm are below 0%, are below 0%. This situation shows that these two equations are not suitable for lower rotational speeds than 2 rpm for this study. The proposed equation of Büyükalaca et al. (Equation 4.57) has not been provided approximate results with the experimental results, because it has given significantly low results for lower rotational speed than 10 rpm and 30 rpm as seen respectively on Figure 5.11 and Figure 5.12. The proposed equation of Büyükalaca and Yılmaz (2002) has similarities with the experimental results but the results become significantly different while the airflow rate increases.

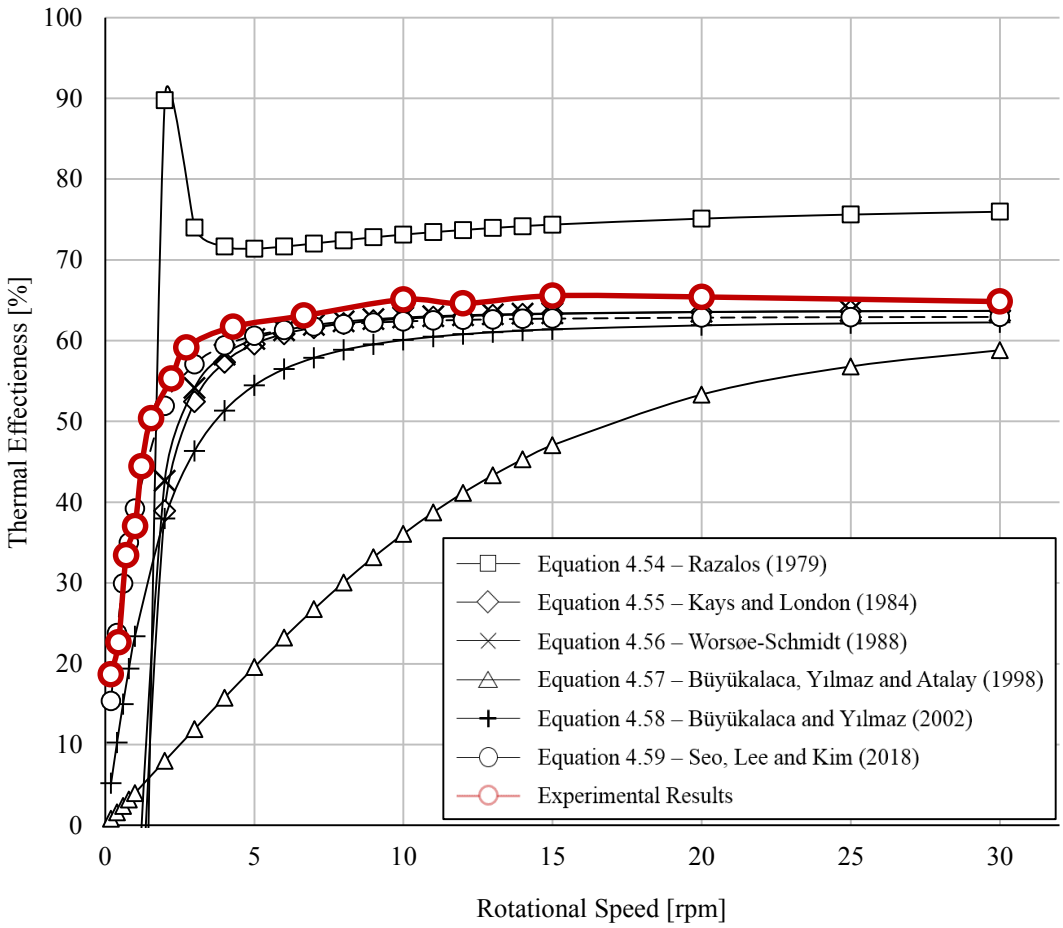

Figure 5.12. Comparison of the Calculated Results with the Experimental Results (Outdoor Air Temperature: 5 °C – Return Air Temperature 25 °C – 5975 m³/h)

The comparison between the experimental results and the calculated results have been plotted within the figures 5.13 to 5.17. Since the good agreement has been found between these results Equation (4.59), which was proposed by Seo et al. (2018), has been used. Although the experimental results seem slightly higher than the calculated results, the behavior of each curve for same volumetric airflow is essentially same. For the same experimental conditions and airflow values, the mathematic model related with Equation (4.59) has been solved with MATLAB. Consequently, each measurement point has been calculated with respect to this decision. According to the related graphs on the following five figures, it has been proved that there is a good agreement between the experimental and mathematical model results for the rotary heat exchanger used for this study.

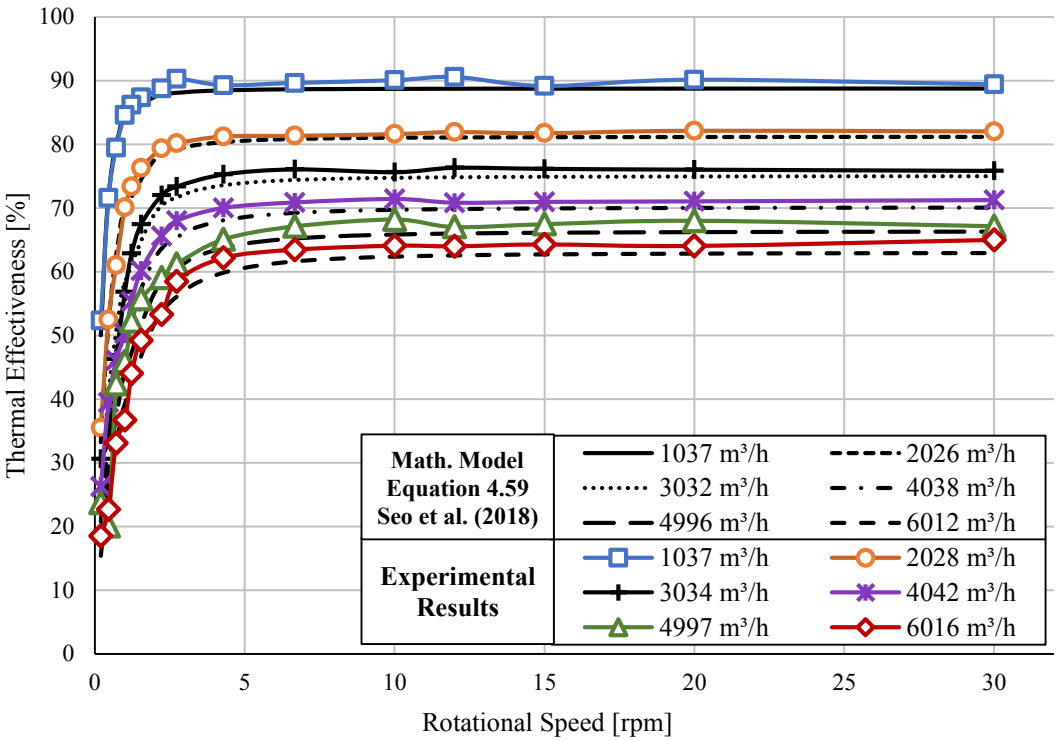

Figure 5.13. Comparison of the Calculated Results with the Experimental Results (Outdoor Temperature: 0 °C, Return Air Temperature: 25 °C)

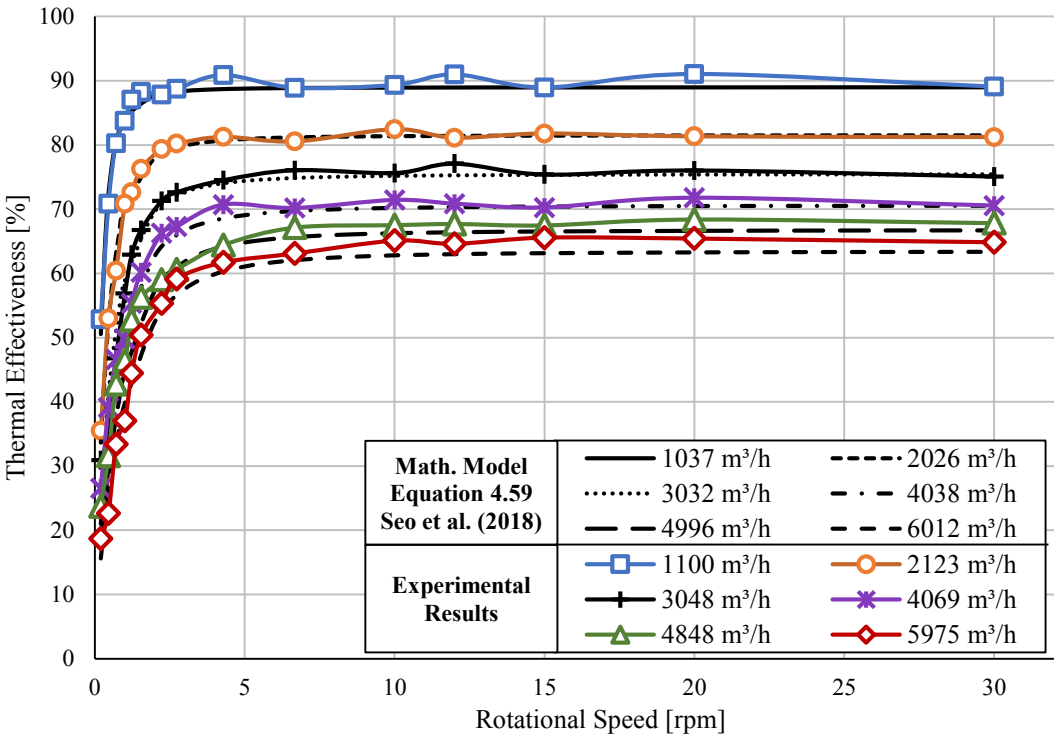

Figure 5.14. Comparison of the Calculated Results with the Experimental Results (Outdoor Temperature: 5 °C, Return Air Temperature: 25 °C)

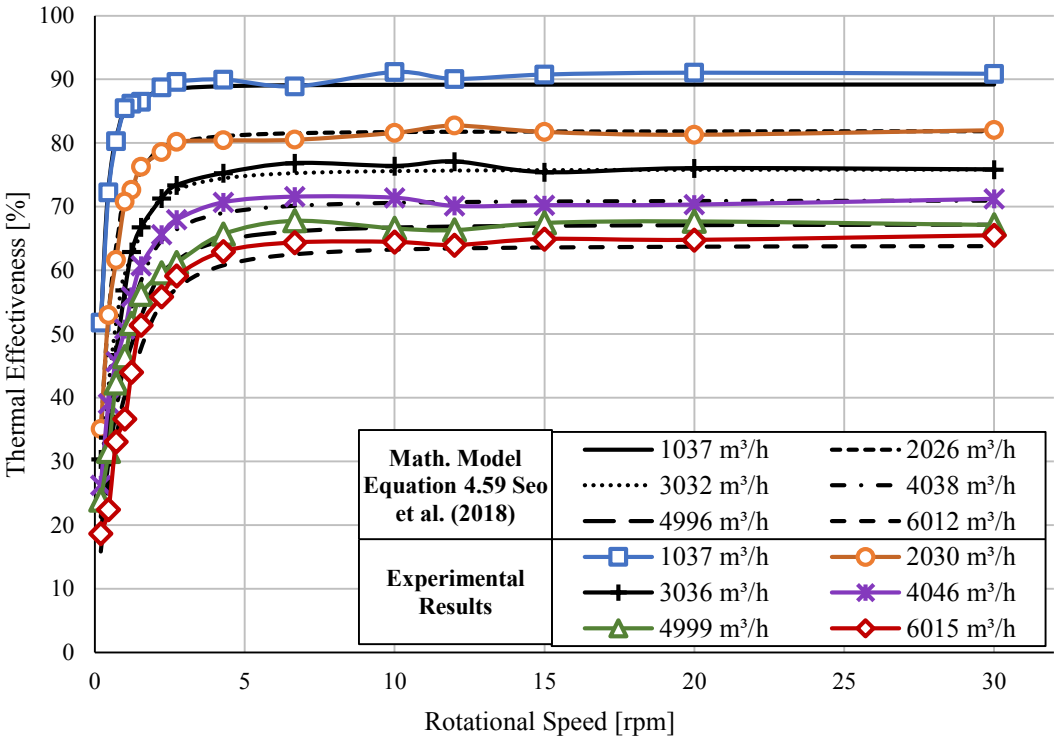

Figure 5.15. Comparison of the Calculated Results with the Experimental Results (Outdoor Temperature: 10 °C, Return Air Temperature: 25 °C)

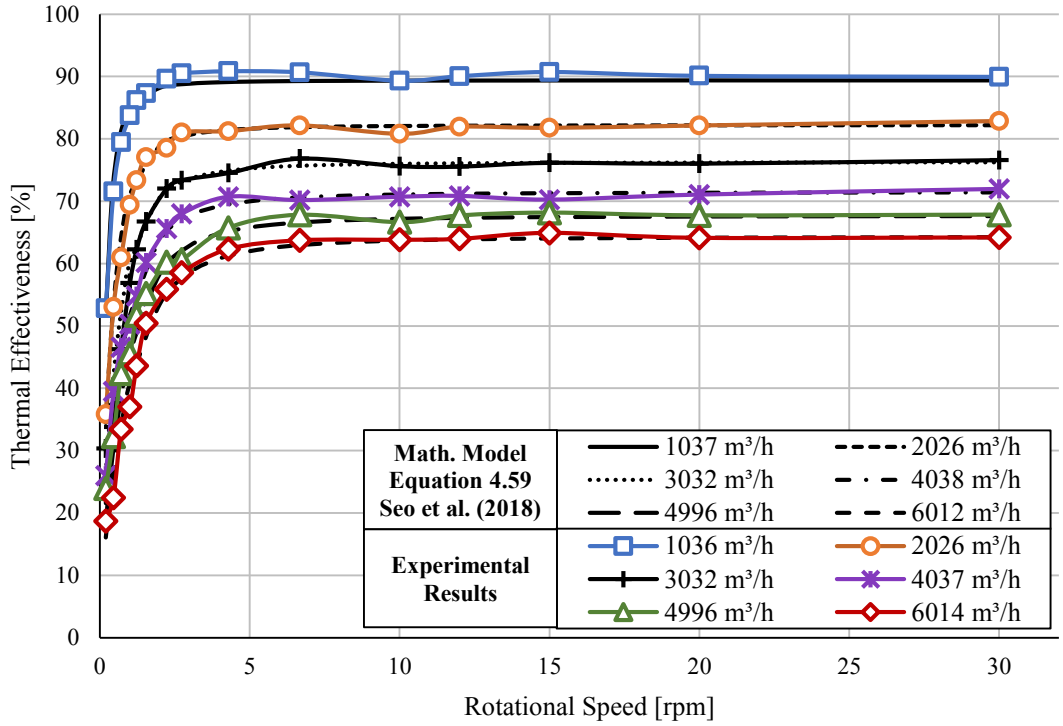

Figure 5.16. Comparison of the Calculated Results with the Experimental Results (Outdoor Temperature: 15 °C, Return Air Temperature: 25 °C)

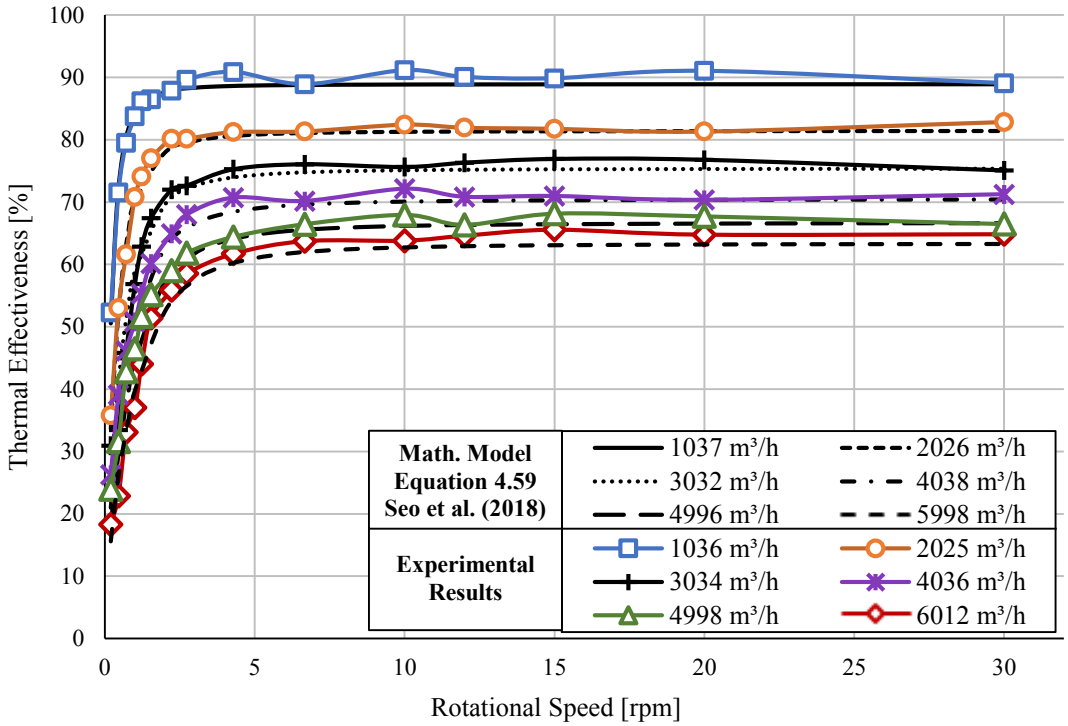

Figure 5.17. Comparison of the Calculated Results with the Experimental Results (Outdoor Temperature: 5 °C, Return Air Temperature: 20 °C)

On Figure 5.18, the efficiency values, which were obtained from the selection software of rotary heat exchanger provider, Klingenburg Company, have been compared with the mathematical model results and the experimental results for same conditions. The graph on this figure shows the variation of thermal effectiveness due to the volumetric airflow rate at constant rotational speed of 10 rpm.

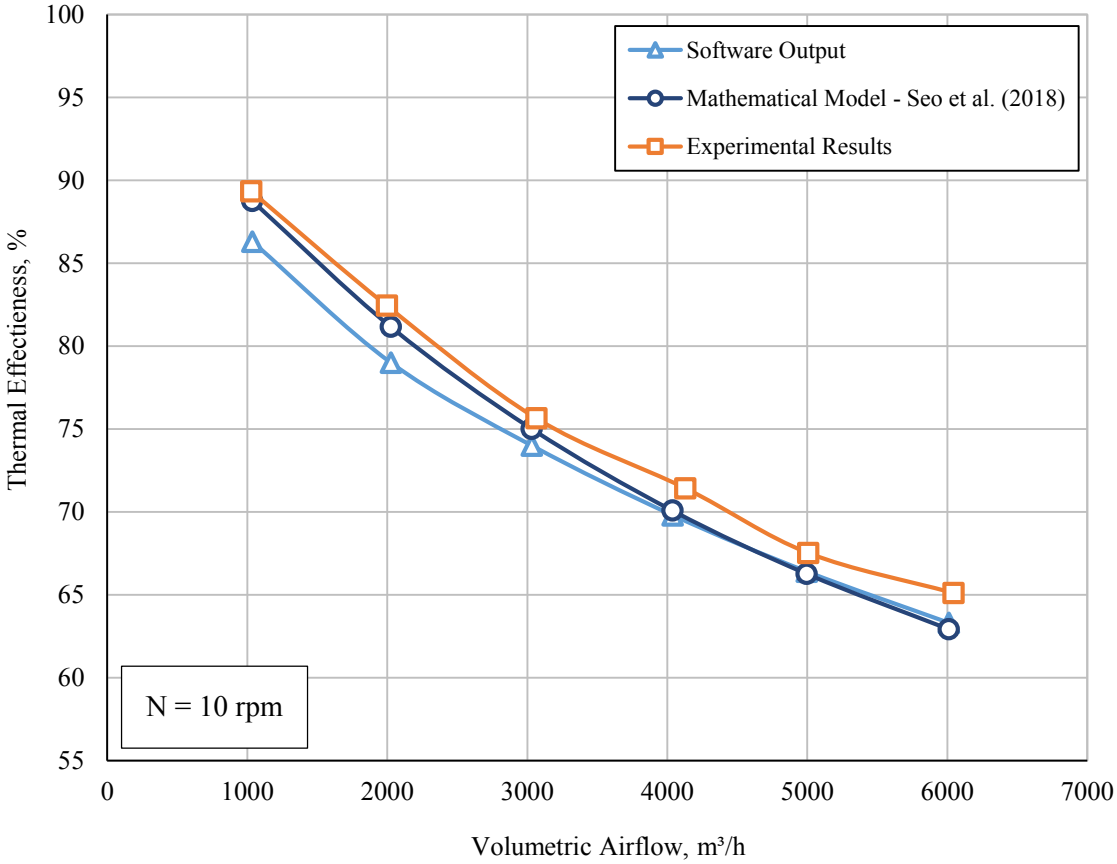

Figure 5.18. Comparison between the Software Output, the Experimental and the Calculated Results

On Figure 5.19, shows the comparison between the thermal efficiency values of the rotary heat exchanger, which have been provided by the supplier for different rotational speeds at the air velocity of 4-4.5 m/s, with the calculated and experimented results. This figure also shows that there is a conformity between software, calculations and experiments.

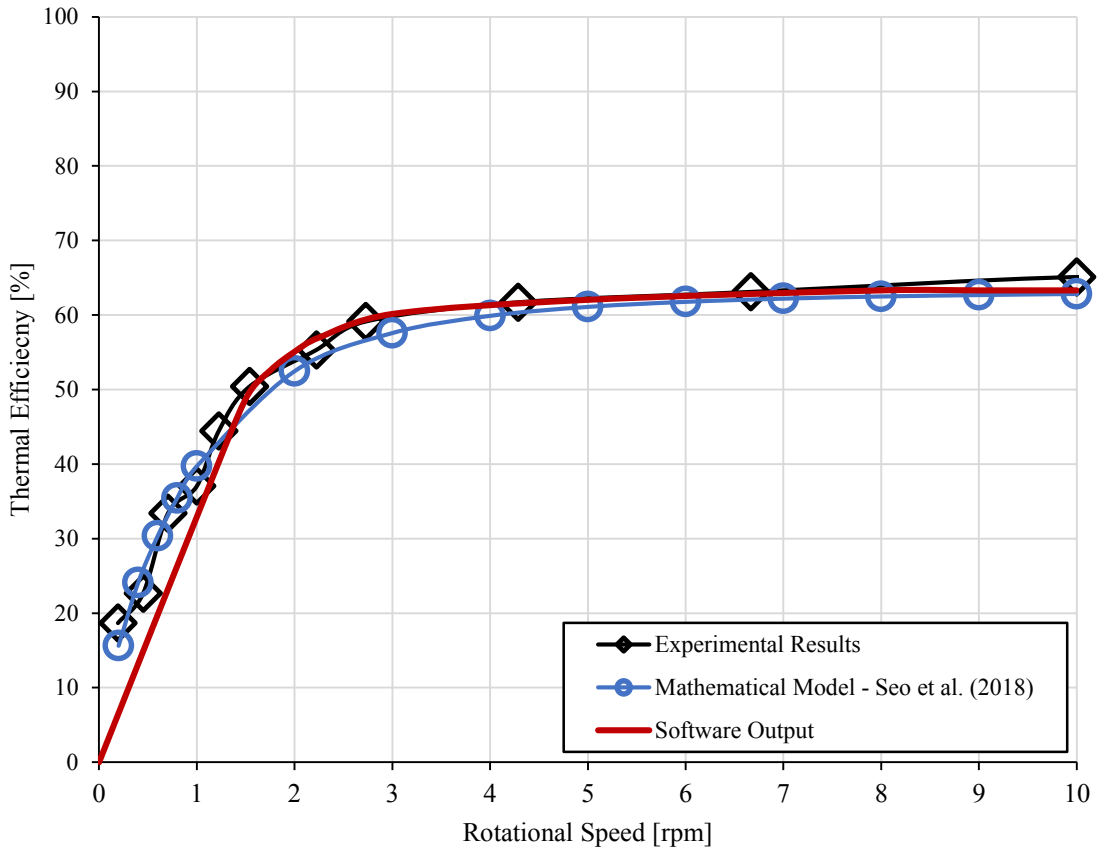

Figure 5.19. The Comparison of Thermal Efficiencies of the Software Output, the Calculated Results and the Experimental Results for Different Rotational Speeds (Source: Klingenburg, 2018)

CHAPTER 6

CONCLUSIONS

The calculated results have been compared with the experimental results and the most approximate method has been defined for this study. Consequently, it has been observed that a good agreement has been found with the experimental results and mathematical results on the Figure 5.13 to 5.17 with Eqn. (4.59), which is the proposal of Seo et al. (2018). The efficiency values which were obtained from the selection software, have been also compared with the mathematical and experimental results. It has been also discerned that the results are accord each other in the Figure 5.18 and 5.19.

All things considered by examining the experimental and the mathematical model studies the followings have been obtained.

- According to the experimental and the mathematical results, there is not any correlation between the rotational speed of a rotary heat exchanger and the pressure drop of itself for this study. Moreover, the mathematical model calculations according to the Chapter 4 are competent with the experimental results and the data provided by supplier.
- It has been determined that the rotational speed has an effect on the thermal efficiency of heat exchanger up to a critical rotational speed. The heat transfers between the matrix of heat exchanger and the fluid increases along with the increment on the rotational speed. This also leads the efficiency of the ventilation device raise at the same time. However, at faster speeds than the critical rotational speed, the heat transfers and relatedly the thermal efficiency cannot be affected because of the fact that the matrix of the heat exchanger cannot stand enough time in the hot or cold fluid region to advance the heat transfer between them.
- The result given above can also be used to analyses critical rotational speed relation with air velocities passing through the heat exchanger. For lower air velocities (< 2 m/s) the critical rotational speed is lower than high air velocities. The increment in air velocity through the heat exchanger requires higher rotational speed for higher thermal efficiencies.

- Considering the indoor and outdoor temperature range of 0 to 25 °C, there are not significant efficiency variations because of the small changes in thermodynamic parameters such as specific heat capacity, the Prandtl number, and the Nusselt number.
- For this study, the data provided by the supplier and the experimental results have practically similar behavior with the mathematical model results which have been obtained by the proposal of Seo, Kim and Lee (2018).

CHAPTER 7

RECOMMENDATIONS FOR FUTURE WORK

During this study, thermal effectiveness and pressure drop of an enthalpy type rotary heat exchanger have been focused with respect to the its rotational speed variation at different indoor and outdoor conditions and airflow. Importantly, the results given in previous chapter should lead the following future work suggestions.

- Leakage values have been neglected during this study. The leakage types and their impact on the thermal effectiveness of rotary heat exchangers should be researched.
- Similar tests should also be carried out at different relative humidity with the consideration of moisture transfer while volumetric airflow rates and inlet temperatures vary also. Adjacent to the enthalpy rotors, sorption rotors may be used in order to evaluate the total effectiveness (can be named as enthalpy efficiency for ventilation devices) depending on the rotational speed of exchanger.
- For the same conditions given in this thesis, tests should be performed to the same type rotary heat exchanger with different dimensions, such as wave length and height of the matrix, length and diameter of the rotary heat exchanger. In order to correlate critical rotational speed with rotor dimensions. The conditions, such as inlet temperatures and airflow rates, then should change to examine if multiple regression is required for critical speed correlations.
- With the purpose of observing the impact of difference between indoor and outdoor temperatures, the lower and upper temperature boundaries should be extended.
- Tests at different indoor and outdoor temperatures and volumetric airflow rates should be performed in order to explore if the pressure drop is independent of rotational speed.
- Frosting and defrosting control scenarios of ventilation devices of rotary heat exchanger itself should be studied at lower outdoor temperature than 0 °C and high indoor relative humidity by changing the rotational speed.

- Same kind of rotary heat exchangers with different dimensions should be tested in order to see if the appropriate equation, which is Equation (4.59) proposed by Seo et al. (2018), would provide a good agreement with their experimental results too.
- As given on the Chapter 5, experimental efficiency curves are slightly higher than the supplier's data. It should be investigated if the fan heat can affect the thermal efficiency of rotary type heat recovery ventilation devices.

CHAPTER 8

REFERENCES

ASHRAE, ASHRAE Handbook - Heating, Ventilating, and Air-Conditioning Systems and Equipment (SI Edition), American Society of Heating, Refrigerating and Air-Conditioning Engineers, (2012).

Arundel, A.V., Sterling, E.M., Biggin J.H., & Sterling, T. D., Indirect Health Effects of Relative Humidity in Indoor Environments, Environmental Health Perspectives, Vol. 65 (1986), pp. 351-361.

Brauer, H., Grundlagen der Einphasen und Mehrphasenströmungen, Verlag, Sauerländer, (1971), pp. 817-821.

Büyükalaca O., Yilmaz T., Atalay B., Effect of Matrix Speed on Effectiveness of Rotary Type Heat Exchanger, International Conference on Energy Research & Development, Vol.2 (1998), pp. 1063-1072.

Büyükalaca, O., & Yilmaz, T., Influence of Rotational Speed on Efficiency of Rotary-Type Heat Exchanger, Heat and Mass Transfer/Waerme- Und Stoffuebertragung, 38(4–5) (2002), pp. 441–447.

Candar, L., Döner Reküperatif Isı Eşanjörü Geliştirilmesi ve Denenmesi, Çukurova University Institute of Natural and Applied Science, Code No: 936 (1995), Adana.

CCOHS – Canadian Centre of Occupational Health and Safety, The Main Features of Dilution Ventilation, http://www.ccohs.ca/oshanswers/prevention/ventilation/-introduction.html Accessed 2018 May 14.

Coppage, J.E., London, A.L. The Periodic-Flow Regenerator – A Summary of Design Theory. Trans. ASME, 80(1) (1953), pp. 779-787.

De Antonellis, S., Intini, M., Joppolo, C. M., Pedranzini, F., Experimental Analysis and Practical Effectiveness Correlations of Enthalpy Wheels, Energy and Buildings, 84 (2014), 316–323.

Doğruyol, E., Döner Rejeneratif Isı Eşanjöründe Devir Sayısına Bağlı Olarak Verimin Ölçülmesi, MSc Thesis, Çukurova University Institute of Natural and Applied Science, Code No: 1309 (1997), Adana.

EPA, Introduction to Indoor Air Quality: Indoor Air Pollution and Health, https://www.epa.gov/indoor-air-quality-iaq/introduction-indoor-air-quality , Accessed 2018 May 14.

Gauler, K., Wärme-und Stoffübertragung an eine mitbewegte ebene Grenzfläche bei Grenzschichtströmung, PhD Thesis, T. U. Karlsruhe, (1972), Germany

Guo-Yan Z, Shan-Tung T, Hu-Gen M., Numerical and Experimental Study on the Heat Transfer and Pressure Drop of Compact Cross-Corrugated Recuperators, ASME J. Heat Transfer, Vol. 136 (2014), 071801-1.

Kays, W. M., & London, A. L., Compact Heat Exchangers, McGraw-Hill, (1984), New York, USA.

Klingenburg GmbH, Overview Rotary Heat Exchanger [Product Catalogue]. http://www.klingenburg-usa.com/fileadmin/user_upload/germany/Downloads/-ROTOR/klingenburg_QuickGuide_en.pdf Accessed 2018 May 03

Lambertsone T., Performance Factors of a Periodic-flow Heat Exchanger, The NPS Institutional Archive, Thesis and Dissertation Collection, (1957), Monterey, California, USA.

Merk, H.J., Mass transfer in laminar boundary layers calculated by means of a perturbation tube, Appl. Sci. Res., A10 (1959), pp. 237-260.

Official Journal of the Republic of Turkey, Energy Efficiency Law, http://www.resmigazete.gov.tr/eskiler/2007/05/20070502-2.htm, 26510 (2007).

Razelos, P., An Analytic Solution to the Electric Analog Simulation of the Regenerative Heat Exchanger with Time-Varying Fluid Inlet Temperatures. Wärme- Und Stoffübertragung, 12(1) (1979), pp. 59–71.

Schell, M., Int-Hout, D., Demand control ventilation using CO_2, ASHRAE Journal, Vol. 43(2), (2001), 18, New York.

Seo, J. W., Lee, D. Y., & Kim, D. S., A Simple Effectiveness Model for Heat Wheels. International Journal of Heat and Mass Transfer, 120 (2018), pp. 1358–1364.

Toksoy, M., Sofuoğlu, S., Atmaca, İ., Sofuoğlu, A., Kazanasmaz, T., Kara, M., Yüksel, H., Ekren, O., Sayar, İ., Varlık, N., Okullarda İç Hava Kalitesi Eğitimi: Pilot Çalışma İzmir, MMO Makale, (2015), İzmir.

TS EN 308:1997 Türk Standardı, Isi Degistiriciler - Havadan Havaya ve Atik Gazlardan Isi Kazanimi Cihazlarinin Performansinin Tayini Icin Deney Metotlari, (1997).

U.S. Department of Energy Office, Energy Use, Loss and Opportunities Analysis: U.S. Manufacturing and Mining, (2004), 1.

Yilmaz, T., General Equations for Pressure Drop for Laminar Flow in Ducts of Arbitrary Cross Sections, ASME. J. Energy Resour. Technol., 112(4) (1993), pp. 220-223.

Yilmaz, T., Büyükalaca, O. And Candar, L., Calculation of Rotary Heat Exchangers with Various Matrix Geometries, First Trabzon International Energy and Environment Symposium, (1996), Trabzon, Turkey.

Yılmaz, T., Cihan, E., General Equation for Heat Transfer for Laminar Flow in Ducts of Arbitrary Cross-Sections, 36(13) (1993), pp. 3265-3270.

Yılmaz, T. & Yılmaz, A., Döner Rejeneratörlerin Optimum Boyutlandırılması, IV. Ulusal Tesisat Mühendisliği Kongresi ve Sergisi, (1999)

Yilmaz, A., Büyükalaca, O., & Yilmaz, T., Optimum shape and dimensions of ducts for convective heat transfer in laminar flow at constant wall temperature. International Journal of Heat and Mass Transfer, 43(5) (2000), pp. 767–775.

Worksafe, "Local Exhaust Ventilation - Quick Guide", https://worksafe.govt.nz/topic-and-industry/dust-and-fumes/fumes/local-exhaust-ventilation-quick-guide/ Accessed 2018 26 June

White, F.M., Fluid Mechanics, 3rd Edition, McGraw Hill, (1994), pp. 339-340.

Worsøe-Schmidt, P., Effect of fresh air purging on the efficiency of energy recovery from exhaust air in rotary regenerators, International Journal of Refrigeration, 14(4) (1988), pp. 233–239.

Zhang, L. Z., Niu, J. L., Performance Comparisons of Desiccant Wheels for Air Dehumidification and Enthalpy Recovery, Applied Thermal Engineering, 22(12) (2002), pp. 1347–1367.

APPENDIX A

MATLAB CODES FOR THE MATHEMATICAL MODEL SIMULATION OF PRESSURE DROP CALCULATION

```
%PRESSURE DROP CALCULATIONS%

clc
clear all

% HYDRAULIC DIAMETER CALCULATION %

prompt = {'Return Air Temperature, °C:','Outdoor Air Temperature,
°C:',...
    'Minimum Volumetric Flow Rate for both Air Streams, m³/h',...
    'Maximum Volumetric Flow Rate for both Air Streams, m³/h',...
    'Wave Height of an Air Channel of the Rotor Matrix, mm',...
    'Wave Length of an Air Channel of the Rotor Matrix, mm',...
    'Foil Thickness, mm','Rotor Width, mm','Rotor Diameter, mm',...
    'Rotor Porosity (Void Fraction), %'};
title = 'Input';
dims = [1 75];
definput = {'25','5','0','7500','1.9','4.3','0.08','200','995','91'};
answer = inputdlg(prompt,title,dims,definput);

t(1) = str2num(answer{1});
t(2) = str2num(answer{2});
Vmin = str2num(answer{3});
Vmax = str2num(answer{4});
Hw = str2num(answer{5});
Wc = str2num(answer{6});
Sc = str2num(answer{7});
Lr = str2num(answer{8})/1000;
Dr = str2num(answer{9})/1000;
Por = str2num(answer{10})/100;

Hc=Hw-2*Sc; % INSIDE HEIGHT OF AN AIR CHANNEL OF THE ROTOR MATRIX
Ar=pi*Dr^2/4/2; % ROTOR TOTAL CROSS-SECTION AREA FOR ONE AIR STREAM
A=Ar*Por; % NET CROSS-SECTIONAL AREA FOR ONE AIR STREAM
V=Vmin:250:Vmax; %VOLUMETRIC FLOWRATE STEPS

syms temp
rho_air = @(temp) 0.00002*temp^2-0.0048*temp+1.2936; % DENSITY
v_air = @(temp) 0.0000000001*temp^2+0.00000009*temp+0.00001; %
KINEMATIC VISCOSITY
pr_air = @(temp) 0.0000006*temp^2-0.0002*temp+0.711; % PRANDTL NUMBER

% HYDRAULIC DIAMETER %
syms x
scurve = @(x) (Hc./2).*(sin((2.*pi.*x)./Wc))+(Hc./2);
scurve_diff1 = matlabFunction( diff(scurve(x)));
arcl_1=@(x) sqrt(1+ scurve_diff1(x).^2);
```

```
arclength=integral(arcl_1,0,Wc);
Ac=integral(scurve,0,Wc);
Pc=arclength+Wc;
Dh=4*Ac/Pc/1000; % mm to m
n=(Ac/1000000)/((pi*Dh^2)/4); % mm to m

% d_max ITERATION %
syms xd rd
curve=@(xd,rd) (xd-2.15)^2+((0.87*sin(2*pi*(xd-1.075)/4.3)+0.87)-
rd)^2-rd^2;

for rd=0.87:-0.01:0;
    for xd=2.15-rd:0.001:2.15;
        if (curve(xd,rd)>-0.0005)&&(curve(xd,rd)<0.0005);
            d_max=rd*2/1000;
            break
        end
    end
end

Do=Dh/d_max;

% SHAPE FACTOR %
Psi_inf=(3/8)*(Do^2)*(3-Do)
Psi=1+((Psi_inf-1)/(1+0.33*(Do^2.25)/(n-1)))

% PRESSURE DROP NUMBER %
Kl=(3-Por)*(1-Por)^2/(2-Por)

    % VARIABLES for SUPPLY AIR %

    Vm=V.*(1.2./rho_air(t(2)))./(A*3600);
    Re=Vm.*Dh/v_air(t(2));
    xo=Lr./(Dh.*Re);
    zo=Lr./(Dh.*Re.*pr_air(t(2)));

    k_inf_s=12./5.*(3-Do).^2.*(9.*(3-Do)./7./(7-3*Do)-1./(5-2*Do));
    k_s=1.33./(1+(1.33./(k_inf_s-1)./(1+0.74.*Do.^2./(n-1))));

dPf_inf_s=64.*zo.*Psi+13.766.*xo.^0.5./((1+13.95.*Psi.*xo.^0.5+(13.766
./xo).^3.*xo.^1.5).^(1./3));
    dPr_inf_s=dPf_inf_s+k_s;
    dPr_s=dPr_inf_s.*rho_air(t(2)).*Vm.^2/2

    xlswrite('dPr_s.xls', dPr_s)

    % VARIABLES for EXHAUST AIR %

    Vm=V.*(1.2./rho_air(t(1)))./(A*3600);
    Re=Vm.*Dh/v_air(t(1));
    xo=Lr./(Dh.*Re);
    zo=Lr./(Dh.*Re.*pr_air(t(1)));

    k_inf_e=12./5.*(3-Do).^2.*(9.*(3-Do)./7./(7-3*Do)-1./(5-2*Do));
    k_e=1.33./(1+(1.33./(k_inf_e-1)./(1+0.74.*Do.^2./(n-1))));

dPf_inf_e=64.*zo.*Psi+13.766.*xo.^0.5./((1+13.95.*Psi.*xo.^0.5+(13.766
./xo).^3.*xo.^1.5).^(1./3));
```

```
dPr_inf_e=dPf_inf_e+k_e;
dPr_e=dPr_inf_e.*rho_air(t(1)).*(Vm.^2)/2

xlswrite('dPr_e.xls', dPr_e)

% PLOTTING THE PRESSURE DROP CURVES %

figure(1);
plot(V,dPr_e,'b');
xlabel('Volumetric Airflow, m³/h');
ylabel('Pressure Drop, Pa');
xlim([0 9000]);
ylim([0 350]);

figure(2);
plot(V,dPr_s,'b');
xlabel('Volumetric Airflow, m³/h');
ylabel('Pressure Drop, Pa');
xlim([0 9000]);
ylim([0 350]);
```

APPENDIX B

MATLAB CODES FOR THE MATHEMATICAL MODEL SIMULATION OF THERMAL EFFECTIVENESS CALCULATIONS

```
%THERMAL EFFECTIVENESS CALCULATIONS%

clc
clear all

% HYDRAULIC DIAMETER CALCULATION %

prompt = {'Return Air Temperature, °C:','Outdoor Air Temperature,
°C:',...
    '1st Actual Volumetric Flow Rate for both Air Streams, m³/h',...
    '2nd Actual Volumetric Flow Rate for both Air Streams, m³/h',...
    '3rd Actual Volumetric Flow Rate for both Air Streams, m³/h',...
    '4th Actual Volumetric Flow Rate for both Air Streams, m³/h',...
    '5th Actual Volumetric Flow Rate for both Air Streams, m³/h',...
    '6th Actual Volumetric Flow Rate for both Air Streams, m³/h',...
    'Wave Height of an Air Channel of the Rotor Matrix, mm',...
    'Wave Length of an Air Channel of the Rotor Matrix, mm',...
    'Foil Thickness, mm','Rotor Width, mm','Rotor Diameter, mm',...
    'Rotor Porosity (Void Fraction), %','Rotor Weight, kg',...
    'Heat Transfer Area between the Rotor and the Fluid, m²'};
title = 'Input';
dims = [1 75];
definput = {'25','5','1037','2026','3032','4038','4996',...
    '6012','1.9','4.3','0.08','200','995','91','38','360'};
answer = inputdlg(prompt,title,dims,definput);

t(1) = str2num(answer{1});
t(2) = str2num(answer{2});
qv2(1) = str2num(answer{3});
qv2(2) = str2num(answer{4});
qv2(3) = str2num(answer{5});
qv2(4) = str2num(answer{6});
qv2(5) = str2num(answer{7});
qv2(6) = str2num(answer{8});
Hw = str2num(answer{9});
Wc = str2num(answer{10});
Sc = str2num(answer{11});
Lr = str2num(answer{12})/1000;
Dr = str2num(answer{13})/1000;
Por = str2num(answer{14})/100;
Mr = str2num(answer{15})/1000;
Ah = str2num(answer{16})/2;

Hc=Hw-2*Sc; % INSIDE HEIGHT OF AN AIR CHANNEL OF THE ROTOR MATRIX
```

```
Ar=pi*Dr^2/4/2; % ROTOR TOTAL CROSS-SECTION AREA FOR ONE AIR STREAM
A=Ar*Por; % NET CROSS-SECTIONAL AREA FOR ONE AIR STREAM
cp_r=897; % SPECIFIC HEAT CAPACITY OF ALUMINUM (ROTOR)
rho_r=2707; % DENSITY OF ALUMINUM (ROTOR)
Nr=[0.2 0.4 0.6 0.8 1 2 3 4 5 6 7 8 9 10 11 12 13 14 15 20 25 30];

% AIR PROPERTIES %
syms temp mass
rho_air = @(temp) 0.00002*temp^2-0.0048*temp+1.2936; % DENSITY
cp_air = @(temp) 1000*(-
0.000000001*temp^3+0.0000006*temp^2+0.00001*temp+1.005); % SPE. HEAT
CAP.
v_air = @(temp) 0.0000000001*temp^2+0.00000009*temp+0.00001; %
KINEMATIC VISCOSITY
lam_air = @(temp) (-0.00004*temp^2+0.077*temp+24.353)/1000; % THERMAL
CONDUCTIVITY
pr_air = @(temp) 0.0000006*temp^2-0.0002*temp+0.711; % PRANDTL NUMBER
re_air = @(temp,mass) vel_air(temp,mass)*w_rotor/v_air(temp); %
REYNOLD NUMBER

m2=qv2.*rho_air(t(2))/3600; % MASS FLOW RATE of SUPPLY AIR, kg/s
m1=m2; % MASS FLOW RATE of EXHUAST AIR, kg/s
qv1=m1./rho_air(t(1))*3600; % ACTUAL VOLUMETRIC FLOW RATE of EXHUAST
AIR, m³/h

c1=cp_air(t(1)).*m1; % HEAT CAPACITY OF EXHAUST AIR
c2=cp_air(t(2)).*m2; % HEAT CAPACITY OF SUPPLY AIR
c_min=min(c1,c2); % MINIMUM HEAT CAPACITY
c_max=max(c1,c2); % MAXIMUM HEAT CAPACITY
co=c_min./c_max; % RATIO OF MIN/MAX HEAT CAPACITY

% HYDRAULIC DIAMETER %
syms x
scurve = @(x) (Hc./2).*(sin((2.*pi.*x)./Wc))+(Hc./2);
scurve_diff1 = matlabFunction( diff(scurve(x)));
arcl_1=@(x) sqrt(1+ scurve_diff1(x).^2);
arclength=integral(arcl_1,0,Wc);
Ac=integral(scurve,0,Wc);
Pc=arclength+Wc;
Dh=4*Ac/Pc/1000; % mm to m
n=(Ac/1000000)/((pi*Dh^2)/4); % mm to m

% d_max ITERATION %
syms xd rd
curve=@(xd,rd) (xd-2.15)^2+((0.87*sin(2*pi*(xd-1.075)/4.3)+0.87)-
rd)^2-rd^2;

for rd=0.87:-0.01:0;
    for xd=2.15-rd:0.001:2.15;
        if (curve(xd,rd)>-0.0005)&&(curve(xd,rd)<0.0005);
            d_max=rd*2/1000;
            break
        end
    end
end

Do=Dh/d_max;
```

```
% SHAPE FACTOR %
Psi_inf=(3/8)*(Do^2)*(3-Do);
Psi=1+((Psi_inf-1)/(1+0.33*(Do^2.25)/(n-1)));

% HEAT TRANSFER CALCULATIONS - NUSSELT NO CALCULATION %

    % HEAT TRANSFER FACTOR - 1 %
    diff_phi_max = (0.007*Do)/((1+10*Do^-28)*(1+(64.1^-8)*Do^28)^0.5);
    diff_phi = diff_phi_max*(0.95*(n-1)^0.5)/(1+0.038*(n-1)*3);
    phi_inf = 0.5155*Do^2/(3-Do);
    phi = 1+diff_phi+(phi_inf-1)/(1+1/(n-1));

    % NUSSELT INFINITE %
    nu_inf = 3.657*phi;

    % HEAT TRANSFER FACTOR - 2 %
    CPhi=1+(3*((Do/2)^(7/8))/(1+Do)-1)/(1+0.25/(n-1));

% NTU CALCULATION %

% NU & H CALCULATION FOR EXHAUST AIR
Vm1=qv1./(A*3600); % VELOCITY OF EXHAUST AIR
Re1=Vm1.*(Dh/v_air(t(1)));
zo1=Lr./(Dh.*Re1.*pr_air(t(1)));
Nud1=nu_inf+((1.615.*(zo1./Psi).^(1/3))./(1+(1.88.*((zo1.*nu_inf^3)./.
..

(Psi*CPhi^3)))+(3.93.*(zo1.*nu_inf^3)./(Psi*CPhi^3)).^(4/3))).^(1/2);
f1=(1+(0.105/(pr_air(t(1))+pr_air(t(1))/3))+(0.0468/pr_air(t(1))))^(1/
6);
Nuo1=0.6774./(f1.*zo1.^0.5*pr_air(t(1)).^(1/6));
Nu1=(Nud1.^4+Nuo1.^4).^(1/4);
h1=Nu1.*lam_air(t(1))./Dh;

% NU & H CALCULATION FOR SUPPLY AIR
Vm2=qv2./(A*3600); % VELOCITY OF SUPPLY AIR
Re2=Vm2.*(Dh/v_air(t(2))); % VELOCITY OF SUPPLY AIR
zo2=Lr./(Dh.*Re2.*pr_air(t(2))); % VELOCITY OF SUPPLY AIR
Nud2=nu_inf+((1.615.*(zo2./Psi).^(1/3))./(1+(1.88.*((zo2.*nu_inf.^3)./
...

(Psi.*CPhi.^3)))+(3.93.*(zo1.*nu_inf.^3)./(Psi.*CPhi.^3)).^(4/3))).^(1
/2);
f2=(1+(0.105/(pr_air(t(2))+pr_air(t(2))/3))+(0.0468/pr_air(t(2)))).^(1
/6);
Nuo2=0.6774./(f2.*zo2.^0.5*pr_air(t(2))^(1/6));
Nu2=(Nud2.^4+Nuo2.^4).^(1/4);
h2=Nu2.*lam_air(t(2))./Dh;

UA=1./((1./(h1.*Ah))+(1./(h2.*Ah)));
NTU=UA./c_min;

% THERMAL EFFICIENCY OF RECUPERATIVE EXCHANGER %
eps0_1=transpose((1-exp(-NTU.*(1-co)))./(1-co.*exp(-NTU.*(1-co))));
eps0_2=transpose(NTU./(1+NTU));
```

```
% THERMAL EFFICIENCY OF ROTARY HEAT EXCHANGER %

% CAPACITY RATIO OF ROTARY HEAT EXCHANGER

cr=((pi*Dr^2/4)*Lr*(1-Por)*rho_r)*cp_r*(Nr/60);

for i=1:6
   cro(i,:)=cr./c_min(i);
end

% EQN. (4.54)
NTUm=(2.*transpose(NTU).*cro)./(1+cro);
crom=(2.*transpose(co).*cro)./(1+transpose(co));
er=(NTUm./(1+NTUm))./(1-(1./(9.*crom.^1.93)));
epsr_1=(1-exp(er.*(transpose(co).^2-1)./(2.*transpose(co).*(1-
er))))./...
    (1-transpose(co).*exp(er.*(transpose(co).^2-
1)./(2.*transpose(co).*(1-er))));

% EQN. (4.55)
epsr_2=eps0_1.*(1-(1./(9.*cro.^(1.93))));

% EQN. (4.56)
epsr_3=eps0_1.*(1-(0.114.*(1-exp((transpose(-NTU))))./...
    ((transpose(co).^0.44).*(cro.^1.93))));

% EQN. (4.57)
epsr_4=eps0_1.*((0.24.*cro)./((1+0.02.*(cro.^1.82)+...
    (0.24.*cro).^3)).^(1/3));

% EQN. (4.58)
epsr_5=(cro)./(1+3.*((cro)./eps0_1).^2+((cro)./eps0_1).^4).^(1/4);

% EQN. (4.59)
epsr_6f_1=8./(((2.*eps0_1./cro).^2)+(1*pi).^2);
epsr_6f_2=8./(((2.*eps0_1./cro).^2)+(3*pi).^2);
epsr_6f_3=8./(((2.*eps0_1./cro).^2)+(5*pi).^2);
epsr_6f_4=8./(((2.*eps0_1./cro).^2)+(7*pi).^2);
epsr_6f_5=8./(((2.*eps0_1./cro).^2)+(9*pi).^2);
epsr_6f_6=8./(((2.*eps0_1./cro).^2)+(11*pi).^2);
epsr_6f_7=8./(((2.*eps0_1./cro).^2)+(13*pi).^2);
epsr_6f_8=8./(((2.*eps0_1./cro).^2)+(15*pi).^2);

epsr_6f=epsr_6f_1+epsr_6f_2+epsr_6f_3+epsr_6f_4+epsr_6f_5+epsr_6f_6+ep
sr_6f_7+...
    epsr_6f_8;

corr_6=sqrt(epsr_6f);
epsr_6=eps0_1.*corr_6;

figure(1);

plot(Nr,epsr_1(1,:),'b',Nr,epsr_2(1,:),'g',Nr,epsr_3(1,:),'r',Nr,epsr_
4(1,:),...
        'c',Nr,epsr_5(1,:),'m',Nr,epsr_6(1,:),'y');
    xlabel('Rotational Speed, rpm');
    ylabel('Thermal Eff., %');
    ylim([0 1]);
```

```
figure(2);

plot(Nr,epsr_1(2,:),'b',Nr,epsr_2(2,:),'g',Nr,epsr_3(2,:),'r',Nr,epsr_
4(2,:),...
        'c',Nr,epsr_5(2,:),'m',Nr,epsr_6(2,:),'y');
    xlabel('Rotational Speed, rpm');
    ylabel('Thermal Eff., %');
    ylim([0 1]);

figure(3);
    plot(Nr,epsr_1,'b');
    xlabel('Rotational Speed, rpm');
    ylabel('Thermal Eff., %');
    ylim([0 1]);

figure(4);
    plot(Nr,epsr_2,'b');
    xlabel('Rotational Speed, rpm');
    ylabel('Thermal Eff., %');
    ylim([0 1]);

figure(5);
    plot(Nr,epsr_3,'b');
    xlabel('Rotational Speed, rpm');
    ylabel('Thermal Eff., %');
    ylim([0 1]);

figure(6);
    plot(Nr,epsr_4,'b');
    xlabel('Rotational Speed, rpm');
    ylabel('Thermal Eff., %');
    ylim([0 1]);

figure(7);
    plot(Nr,epsr_5,'b');
    xlabel('Rotational Speed, rpm');
    ylabel('Thermal Eff., %');
    ylim([0 1]);

figure(8);
    plot(Nr,epsr_6,'b');
    xlabel('Rotational Speed, rpm');
    ylabel('Thermal Eff., %');
    ylim([0 1]);

xlswrite('epsr_1.xls', epsr_1);
xlswrite('epsr_2.xls', epsr_2);
xlswrite('epsr_3.xls', epsr_3);
xlswrite('epsr_4.xls', epsr_4);
xlswrite('epsr_5.xls', epsr_5);
xlswrite('epsr_6.xls', epsr_6);
xlswrite('cro.xls', cro);
xlswrite('Nr.xls', Nr);
```

APPENDIX C

CALCULATION EXAMPLE OF THERMAL EFFECTIVENESS WITH RESPECT TO THE SEQUENCE ON MATLAB FOR ONE MEASUREMENT POINT

No	Parameter	Eqn.	Sym.	Unit	Equation / Table	Result / Value
1	Wave Height of Corrugated Plate	-	H_m	mm	Table 3.1	1.90
2	Wall thickness of Matrix	-	S_m	mm	Table 3.1	0.08
3	Wave Height of Cross Section of Air Channel in the Rotor Matrix	(4.3)	H_c	mm	$H_c = H_m - 2S_m$	1.74
4	Wave Length of Cross Section of Air Channel in the Rotor Matrix	-	W_c	mm	Table 3.1	4.30
5	The function for sinusoidal line which is assumed as similar with the matrix wall structure	(4.3)	$f(x)$	-	$f(x) = \frac{H_c}{2}\sin\left(\frac{2\pi x}{W_c}\right) + \frac{H_c}{2}$	-
6	First derivative of the function f(x)	(4.3)	f'	-	$f' = \frac{\pi H_c \cos(\frac{2\pi x}{W_c})}{W_c}$	-
7	Arc length of the unitary cell	(4.3)	l_{arc}	mm	$l_{arc} = \int_0^{W_c} \sqrt{1 + f'^2(x)}dx$	5.71
8	Periphery of a unitary cell	(4.5)	P_c	mm	$P_c = l_{arc} + W_c$	10.01
9	Cross-section area of a unitary cell	(4.4)	A_c	mm²	$A_c = \int_0^{W_c} f(x)dx$	3.74
10	Hydraulic Diameter of Air Channel in the Rotor Matrix	(4.1)	d_h	mm	$d_h = \frac{4A_c}{P_c}$	1.50
11	Cross-section area of a unitary cell with respect to the hydraulic diameter	(4.8)	A_h	mm²	$A_h = \frac{\pi d_h^2}{4}$	1.76
12	Parameter of 'n'	(4.7)	n	-	$n = \frac{A_c}{A_h}$	2.13
13	Maximum hydraulic diameter	(4.10)	d_{max}	mm	Calculated by an iterative method with MATLAB	1.68
14	Dimensionless diameter	(4.9)	d^*	-	$d^* = \frac{d_h}{d_{max}}$	0.89
15	Shape Factor (Inf.)	(4.16)	φ_∞	-	$\varphi_\infty = \frac{3}{8}d^{*2}(3 - d^*)$	0.6269
16	Shape Factor	(4.15)	φ	-	$\varphi = 1 + \left\{\frac{\varphi_\infty - 1}{[1 + 0.33d^{*2.25}/(n-1)]}\right\}$	0.6954
17	Heat transfer factor - 1	(4.48)	Φ	-	$\Phi = 1 + \frac{[3(d^*/2)^{7/8}/(1+d^*)] - 1}{1 + 0.25/(n-1)}$	0.8212
18	Max. Differential Heat Transfer Factor - 2	(4.47)	$\Delta\phi_{max}$	-	$\Delta\phi_{max} = \frac{7.10^{-3}d^{*8}}{(1 + 10d^{*-28})(1 + 64.10^{-8}d^{*28})^{1/2}}$	0.0040
19	Differential Heat Transfer Factor - 2	(4.46)	$\Delta\phi$	-	$\Delta\phi = \Delta\phi_{max}\frac{0.95(n-1)^{0.5}}{1 + 0.038(n-1)^3}$	0.0038
20	Heat Transfer Factor - 2 (Inf.)	(4.45)	ϕ_∞	-	$\phi_\infty = 0.5155\frac{d^{*2}}{3 - d^*}$	0.1936
21	Heat Transfer Factor - 2	(4.44)	ϕ	-	$\phi = 1 + \frac{\phi_\infty - 1}{1 + 1/(n-1)} + \Delta\phi$	0.5761
22	Nusselt No (Inf.)	(4.43)	Nu_∞	-	$Nu_\infty = 3.657\phi$	2.1067

No	Parameter	Eqn.	Sym.	Unit	Equation / Table	Result / Value	
23	Air Temp	-	T	°C	***Measured***	***25.0000***	***5.0000***
24	Actual Volumetric Air Flow	-	$\dot{V}$	m³/h	***Measured***	***1110***	***1037***
25	Density, rho	(4.14a)	ρ	kg/m³	$\rho = 1x10^{-5}T^2 - 4.8x10^{-3}T + 1.2936$	1.1861	1.2701
26	Specific Heat Capacity, Vp	(4.14b)	C_p	J/kgK	$C_p = 1x10^{-9}T^3 + 6x10^{-7}T^2 + 1x10^{-5}T + 1.005$	1005.6094	1005.0649
27	Kinematic Viscosity, v	(4.14c)	v	m²/s	$v = 1x10^{-10}T^2 + 9x10^{-8}T + 1x10^{-5}$	1.2313E-05	1.0453E-05
28	Mass Flowrate, M_dot	-	$\dot{M}$	kg/s	$\dot{M} = \dot{V}\rho$	3.6571E-01	3.6586E-01
29	Rotor Diameter	-	D_r	mm	Table 3.1	995	
30	Rotor Cross-section Area, Ar	(4.13)	A_r	m²	$A_r = \frac{\pi D_r^2}{4}$	0.7776	
31	Air Velocity	(4.13)	u_f	m/s	$u_f = \frac{\dot{M}}{\rho(A_r/2)}$	0.7931	0.7409
32	Rotor Porosity	-	σ	%	Table 3.1	0.9100	
33	Air Velocity (wrt Porosity)	(4.14)	u	m/s	$u = \frac{\dot{M}}{\rho(A_r/2)\sigma}$	0.8715	0.8142
34	Prandtl No	(4.13)	Pr	-	$Pr = 6x10^{-7}T^2 - 2x10^{-4}T + 0.711$	7.0638E-01	7.1002E-01
35	Reynolds No	(4.12)	Re	-	$Re = \frac{ud_h}{v}$	105.9	116.5
36	Rotor length	-	L	m	Table 3.1	0.2	
37	Dimensionless coordinate	(4.11)	z^*	-	$z^* = L/(d_h RePr)$	1.7885	1.6169
38	Nusselt number for thermally **developed** flow	(4.42)	Nu_d	-	$Nu_d = Nu_\infty + \frac{1.615\Phi/(z^*/\varphi)^{1/3}}{\left[1 + 1.88\left(\frac{z^* Nu_\infty^3}{\varphi\Phi^3}\right) + 3.93\left(\frac{z^* Nu_\infty^3}{\varphi\Phi^3}\right)^{4/3}\right]^{1/2}}$	2.1078	2.1079
39	-	(4.50)	f	-	$f = \left(1 + \frac{0.105}{Pr + \sqrt{Pr}/3} + \frac{0.0468}{Pr}\right)^{1/6}$	1.0269	1.0268
40	Nusselt number for thermally **developing** flow	(4.51)	Nu_o	-	$Nu_o = \frac{0.6774}{f z^{*1/2} Pr^{1/6}}$	0.5227	0.5493
41	Nusselt No	(4.41)	Nu	-	$Nu = \left(Nu_d^4 + Nu_o^4\right)^{1/4}$	2.1098	2.1103
42	Thermal conduciveness	-	λ	W/mK	$\lambda = -4x10^{-5}T^2 + 7.7x10^{-2}T + 24.353$	0.0263	0.0247
43	Heat transfer coefficient	(4.40)	h	W/m²K	$h = Nu\frac{\lambda}{d_h}$	37.0367	34.9071
44	Heat transfer area	-	Ar	m²	Table 3.1	180.0000	180.0000
45	UA	(4.39)	UA	W/K	$\frac{1}{UA} = \frac{1}{h_1 Ar_1} + \frac{1}{h_2 Ar_2}$	3234.6351	
46	Heat Capacity	(4.33)	C	J/K	$C_i = M_i Cp_i$	367.7656	367.7124
47	NTU	(4.38)	NTU	-	$NTU = \frac{UA}{C_{min}}$	8.7966	
48	Heat capacity ratio	(4.37)	C^*	-	$C^* = \frac{C_{min}}{C_{max}}$	0.9999	
49	Thermal effectiveness of a recuperative heat exchanger	(4.36a)	ε_o	%	$\varepsilon_o = \frac{1 - e^{[-NTU(1-C^*)]}}{1 - C^* e^{[-NTU(1-C^*)]}}$	89.80%	
50	Thermal effectiveness of a recuperative heat exchanger	(4.36b)	ε_o	%	$\varepsilon_o = \frac{NTU}{1 + NTU}$	89.79%	
51	Specific heat capacity of rotary heat exchanger matrix	-	C_{pr}	J/kgK	Table 3.1	897	
52	Density of rotary heat exchanger	-	ρ_r	kg/m³	Table 3.1	2707	
53	Solid volume of rotary heat exchanger	-	V_r	m³	$V_r = \frac{\pi D_r^2}{4} L_r (1 - \sigma)$	0.0140	

No	Parameter	Eqn.	Sym.	Unit	Equation / Table	Result / Value
54	Weight of rotary heat exchanger	-	M_r	kg	$M_r = V_r \rho_r$	37.9
55	Rotational speed	-	N	rpm	$N\ x\ 60$	10.0
56	Heat capacity of rotary heat exchanger matrix	(4.53)	C_r	J/K.rps	$C_r = M_s C_{pr} N$	5664
57	Heat capacity ratio between rotary heat exchanger matrix and Cmin	(4.52)	C_r^*	-	$C_r^* = \frac{C_r}{C_{min}}$	15.4039
58	-	(2.6)	$C_{r_m}^*$	-	$C_{r_m}^* = \frac{2C_r^* C^*}{1 + C^*}$	15.4028
59	-	(2.5)	NTU_m	-	$NTU_m = \frac{2NTUC_r^*}{1 + C_r^*}$	16.5208
60	-	(2.7)	ε_r	-	$\varepsilon_r = \frac{NTU_m}{1 + NTU_m}\left[1 - \frac{1}{9(C_{r_m}^*)^{1.93}}\right]$	0.94
61	**Kays and London (1984)**	**(4.54)**	ε_a	%	$\varepsilon_a = \frac{1 - e^{\{\varepsilon_r(C^{*2}-1)/[2C^*(1-\varepsilon_r)]\}}}{1 - C^* e^{\{\varepsilon_r(C^{*2}-1)/[2C^*(1-\varepsilon_r)]\}}}$	**94.29%**
62	**Kays and London (1984)**	**(4.55)**	ε_a	%	$\varepsilon_a = \varepsilon_o\left[1 - \frac{1}{9(C_r^*)^{1.93}}\right]$	**89.75%**
63	**Worsøe-Schmidt (1988)**	**(4.56)**	ε_a	%	$\varepsilon_a = \varepsilon_o\left\{1 - \frac{0.114[1 - e^{(-NTU)}]}{C^{*0.44} C_r^{*1.93}}\right\}$	**89.75%**
64	**Büyükalaca et al. (1998)**	**(4.57)**	ε_a	%	$\varepsilon_a = \varepsilon_o \frac{0.24\ C_r^*}{[1 + 0.02C_r^{*1.82} + (0.24C_r^*)^3]^{1/3}}$	**87.60%**
66	**Büyükalaca and Yılmaz (2002)**	**(4.58)**	ε_a	%	$\varepsilon_a = \frac{C_r^*}{\left[1 + 3\left(C_r^*/\varepsilon_o\right)^2 + \left(C_r^*/\varepsilon_o\right)^4\right]^{1/4}}$	**89.57%**
67	**Seo, Lee and Kim (2018)**	**(4.59)**	ε_a	%	$\varepsilon_a = \varepsilon_o \sqrt{\sum_{n=1,3,5,\ldots}^{\infty} \frac{8}{(2\varepsilon_o/C_r^*)^2 + (n\pi)^2}}$	**88.95%**

APPENDIX D

CALCULATION EXAMPLE OF PRESSURE DROP WITH RESPECT TO THE SEQUENCE ON MATLAB FOR ONE MEASUREMENT POINT

No	Parameter	Eqn.	Sym.	Unit	Equation / Table	Result / Value
1	Wave Height of Corrugated Plate	-	H_m	mm	Table 3.1	1.90
2	Wall thickness of Matrix	-	S_m	mm	Table 3.1	0.08
3	Wave Height of Cross Section of Air Channel in the Rotor Matrix	(4.3)	H_c	mm	$H_c = H_m - 2S_m$	1.74
4	Wave Length of Cross Section of Air Channel in the Rotor Matrix	-	W_c	mm	Table 3.1	4.30
5	The function for sinusoidal line which is assumed as similar with the matrix wall structure	(4.3)	$f(x)$	-	$f(x) = \frac{H_c}{2}\sin\left(\frac{2\pi x}{W_c}\right) + \frac{H_c}{2}$	-
6	First derivative of the function f(x)	(4.3)	f'	-	$f' = \frac{\pi H_c \cos(\frac{2\pi x}{W_c})}{W_c}$	-
7	Arc length of the unitary cell	(4.3)	l_{arc}	mm	$l_{arc} = \int_0^{W_c} \sqrt{1 + f'^2(x)}dx$	5.71
8	Periphery of a unitary cell	(4.5)	P_c	mm	$P_c = l_{arc} + W_c$	10.01
9	Cross-section area of a unitary cell	(4.4)	A_c	mm²	$A_c = \int_0^{W_c} f(x)dx$	3.74
10	Hydraulic Diameter of Air Channel in the Rotor Matrix	(4.1)	d_h	mm	$d_h = \frac{4A_c}{P_c}$	1.50
11	Cross-section area of a unitary cell with respect to the hydraulic diameter	(4.8)	A_h	mm²	$A_h = \frac{\pi d_h^2}{4}$	1.76
12	Parameter of 'n'	(4.7)	n	-	$n = \frac{A_c}{A_h}$	2.13
13	Maximum hydraulic diameter	(4.10)	d_{max}	mm	Calculated by an iterative method with MATLAB	1.68
14	Dimensionless diameter	(4.9)	d^*	-	$d^* = \frac{d_h}{d_{max}}$	0.89
15	Shape Factor (Inf.)	(4.16)	φ_∞	-	$\varphi_\infty = \frac{3}{8}d^{*2}(3 - d^*)$	0.6269
16	Shape Factor	(4.15)	φ	-	$\varphi = 1 + \left\{\frac{\varphi_\infty - 1}{[1 + 0.33d^{*2.25}/(n-1)]}\right\}$	0.6954
17	K - Infinite	(4.26)	K_∞	-	$K_\infty = \frac{12}{5}(3 - d^*)^2\left[\frac{9(3 - d^*)}{7(7 - 3d^*)} - \frac{1}{5 - 2d^*}\right]$	3.3754
18	Additional pressure drop coefficient	(4.25)	K	-	$K = \frac{1.33}{1 + (1.33/K_\infty - 1)/[1 + 0.74d^{*2}/(n-1)]}$	0.9718

No	Parameter	Eqn.	Sym.	Unit	Equation / Table	Result / Value	
19	Air Temp	-		°C	***Measured***	***25.0000***	***5.0000***
20	Actual Volumetric Air Flow	-		m³/h	***Measured***	***6000***	***6000***
21	Density, rho	(4.14a)	ρ	kg/m³	$\rho = 1x10^{-5}T^2 - 4.8x10^{-3}T + 1.2936$	1.1861	1.2701
22	Specific Heat Capacity, Vp	(4.14b)	C_p	J/kgK	$C_p = 1x10^{-9}T^3 + 6x10^{-7}T^2 + 1x10^{-5}T + 1.005$	1005.6094	1005.0649
23	Kinematic Viscosity, v	(4.14c)	v	m²/s	$v = 1x10^{-10}T^2 + 9x10^{-8}T + 1x10^{-5}$	1.2313E-05	1.0453E-05
24	Prandtl No	(4.13)	Pr	-	$Pr = 6x10^{-7}T^2 - 2x10^{-4}T + 0.711$	7.0638E-01	7.1002E-01
25	Mass Flowrate, M_dot	-	$\dot{M}$	kg/s	$\dot{M} = \dot{V}\rho$	1.9768E+00	2.1168E+00
26	Rotor Diameter	-	D_r	mm	Table 3.1	995	
27	Rotor Cross-section Area, Ar	(4.13)	A_r	m²	$A_r = \frac{\pi D_r^2}{4}$	0.7776	
28	Air Velocity	(4.13)	u_f	m/s	$u_f = \frac{\dot{M}}{\rho(A_r/2)}$	4.2869	4.2869
29	Rotor Porosity	-	σ	%	Table 3.1	0.9100	
30	Air Velocity (wrt Porosity)	(4.14)	u	m/s	$u = \frac{\dot{M}}{\rho(A_r/2)\sigma}$	4.7109	4.7109
31	Reynolds No	(4.12)	Re	-	$Re = \frac{ud_h}{v}$	572.2	674.0
32	Rotor length	-	L	m	Table 3.1	0.2	
33	Dimensionless duct length	(4.11)	x^*	-	$x^* = L/(d_h Re)$	0.2337	0.1984
34	Dimensionless coordinate	(4.11)	z^*	-	$z^* = L/(d_h RePr)$	0.3309	0.2795
36	Dimensionless pressure drop (due to friction)	(4.24)	ΔP_{fr}^*	-	$\Delta P_{fr}^* = 64\varphi z^* + \frac{13.766x^{*0.5}}{\left[1 + 13.95\varphi x^{*0.5} + \left(\frac{13.766}{K}\right)^3 x^{*1.5}\right]^{1/3}}$	15.0573	12.7171
37	Dimensionless pressure drop	(4.23)	ΔP_r^*	-	$\Delta P_r^* = \Delta P_{fr}^* + K$	16.0291	13.6889
38	Total pressure drop	(4.22)	ΔP_r	-	$\Delta P_r = \Delta P_r^* \frac{\rho u^2}{2}$	211.0	192.9